November 2021

Riverine and Estuarine CO2-System Studies on the West Coast of Florida

Christopher S. Moore
University of South Florida

Riverine and Estuarine CO_2-System Studies on the West Coast of Florida

by

Christopher S. Moore

A thesis submitted in partial fulfillment
of the requirements for the degree of
Master of Science
College of Marine Science
University of South Florida

Major Professor: Robert H. Byrne, Ph.D.
Kimberly K. Yates, Ph.D.
Mark E. Luther, Ph.D.

Date of Approval:
November 5th 2021

Keywords: Carbonate, pH, Dissolved inorganic carbon, Total alkalinity, Tampa Bay, Saturation state

Acknowledgements

I would like to thank my advisor, Dr. Robert H. Byrne for his patience, professional guidance, and expertise in creating this work. It has been an unforgettably rewarding experience that I will call upon for years to come. I would also like to thank Dr. Kimberly K. Yates, for her trust, mentorship, and scientific training over the past several years. Kim pushed me to be a better scientist every day through her constant example in the field, the laboratory and in the office. Thanks also to Dr. Mark E. Luther for his scientific expertise and enthusiasm as a professor and advisor. I would like to give a huge thanks to Dr. Sherwood Liu for his generosity with his time and scientific instruction in the laboratory and field. In addition, I would also like to thank him for performing the [Ca^{2+}] analyses for this work. I would like to thank Dr. Rob Masserini for the integral nutrient analyses performed for this this work. Thanks also to the U.S. Geological Survey's Marine Operations staff for their help in preparing and maintaining the vehicles and vessels used for fieldwork in this study. I would also like to thank each of the volunteers: Sean, Scott, Derrick, and Sam who separately joined me on weekends for each river expedition. With little comfort and sleep I greatly appreciated your help and taste for adventure. Lastly, I would like to thank my friends and family for their support and understanding while pursuing this work. Any use of trade, firm, or product names is for descriptive purposes only and does not imply endorsement by the U.S. Government.

Table of Contents

List of Tables

List of Figures

Abstract

Coastal and estuarine acidification impacts ecosystem health and economic resources and has both natural and anthropogenic components (Cai et al., 2021). Riverine input is one of several important factors that can influence acidification in coastal ecosystems. Rivers disgorging into coastal environments can create strong gradients, both spatial and temporal, that make accurate CO_2-system characterization challenging. The work described in this thesis provides a baseline CO_2-system study of four major rivers that flow into Tampa bay with an emphasis on seasonal change. As a second objective, this thesis examines the effects of Hg^{II} additions on CO_2-system measurements in organic-rich estuarine waters. Recent advancements in spectrophotometric techniques using sulfonephthalein indicator dyes were implemented in my work. Measurements of surficial water samples included dissolved inorganic (C_T), total alkalinity (A_T), pH_T (total scale), calcium (Ca^{2+}) and major inorganic nutrients. Water samples were collected either from shore or from a U.S. Geological Survey research vessel. Each river exhibited distinct seasonal variability wherein CO_2-system parameters were strongly influenced by river discharge rates. Major nutrients did not strongly correlate with river discharge, but instead correlated strongly with CO_2 system parameters, C_T, and A_T. Comparisons of seasonal riverine CO_2-system and nutrient measurements with similar measurements in Tampa Bay showed that the rivers' short-term influence on Tampa Bay's CO_2-system was modest. In contrast, the rivers were shown to be a major source of nutrients to the Bay. My examinations of Hg^{II} additions to organic rich estuarine waters showed that Hg^{II} amendments eliminated changes in C_T over time, but had undesirable effects on A_T and pH_T. As a result, for organic rich estuarine waters, alternative sample processing methods should be considered when samples cannot be promptly analyzed. This work provides the first Bay-wide look at the riverine CO_2-system of Tampa

Bay, and reveals the dramatic influence of Hg^{II} on measurements of CO_2-system parameters in organic rich estuarine waters.

Chapter One:
Introduction

Coastal and estuarine ecosystems, and the commercial and recreational industries they support, are particularly vulnerable to the compounding effects of coastal ocean acidification derived from increasing levels of atmospheric CO_2, and acidification that is a consequence of anthropogenic nutrients (Miller et al., 2009; Hall et al., 2020; Galavotti et al., 2021). As a means of understanding the complex and wide-ranging consequences of the multiple factors that underlie acidification in coastal environments (Yates et al., 2007; Goldsmith et al., 2019; Cai et al., 2020), investigations of CO_2-system dynamics are increasingly being undertaken in estuaries and the coastal ocean. Estuaries have complex internal spatial and temporal heterogeneity in carbon processing and fluxes (Hunt et al., 2010; Bauer et al., 2013; Rosenau et al., 2021), creating substantial investigative challenges. A significant component of estuarine heterogeneity is created by variations in the intensity of riverine input (river flow) and variations in the terrestrially-derived concentrations of organic and inorganic forms of carbon and nutrients in rivers (Hopkinson et al., 1998; Cai et al., 2011; Bauer et al., 2013). In the context of changing climate and global hydrology, CO_2-system dynamics at the interface of land and sea is complex and poorly understood (Ward et al., 2017; Bauer et al., 2013).

Most CO_2-system studies to date have investigated the complex interactions taking place either in the open ocean or between the open ocean and estuaries (Jiang et al., 2008; Cai et al., 2011; Johnson et al., 2013; Carstensen and Duarte, 2019; Urbini et al., 2020). Relatively few studies have directly examined riverine CO_2-systems (Cai and Wang, 2013; Dinsmore et al., 2013; Marx et al., 2017; Drake et al., 2017; Liu and Han, 2021). Most estuarine investigations have used combinations of two or more of

the four measurable CO_2-system parameters (total inorganic carbon (C_T), total alkalinity (A_T), partial pressure of carbon dioxide (pCO_2), and pH), to estimate carbon fluxes on a seasonal basis (Frankignoulle et al., 1996, Cai et al., 1999, Raymond and Bauer, 2000, Brasse et al., 2002; Yates et al, 2007). Until recently, standard techniques used for the collection, storage and analysis of pH and CO_2-system parameters were limited to a range of salinity and temperature conditions found in open ocean and coastal settings (Clayton and Byrne, 1993; Dickson et al., 2007). Recently developed procedures for measurements of spectrophotometric pH (Douglas and Byrne, 2017; Müller and Rehder, 2018) and A_T (Hudson-Heck et al., 2021) over a wide range of salinity and temperature conditions have enabled quantitative assessments of CO_2-system behavior over a river-to-sea range of conditions, solely using spectrophotometric procedures.

In this thesis, recent advances in spectrophotometric methods for CO_2-system analysis are used to investigate spatial and temporal differences in the carbon system and nutrient characteristics of four major rivers that flow into Tampa Bay: The Hillsborough River, Alafia River, Little Manatee River, and Manatee River. In addition to these investigations conducted in the field, we also provide a general assessment of the use of Hg^{II} as a preservative for estuarine water samples that are collected and subsequently used for CO_2-system measurements at a later date.

Chapter Two:

Spatial and Temporal Studies of the Carbonate Systems of Four Major Tampa Bay Rivers

2.1 Abstract

Using recent advances in spectrophotometric carbonate system analysis, a spatial and temporal survey of pH_T and carbonate system parameters was conducted in four rivers that provide a majority of the freshwater input to Tampa Bay. The Hillsborough, Alafia, Little Manatee, and Manatee rivers were examined over approximately one year that encompassed periods of low precipitation (November – April) and high precipitation (May – October). Distinctive spatial and temporal variations in carbonate parameter and nutrient concentrations were correlated with changes/variations in riverine flow conditions.

During 2019, each of the four rivers was sampled twice, first during the dry season (February-March) and subsequently during the wet season (August-September). During each season the four rivers were sampled over four consecutive weekends. Carbonate system and nutrient samples from each river were collected using a U.S. Geological Survey (USGS) research vessel. Water temperature and salinity were measured continuously with a thermosalinograph. Spectrophotometric pH_T (total scale) was analyzed promptly in the field, and subsequent measurements of dissolved inorganic carbon (C_T), total alkalinity (A_T), and pH_T were conducted at the USGS Ocean Carbon Laboratory in St. Petersburg Florida. Ca^{2+} measurements were made at the University of South Florida. Macro nutrient samples were analyzed at the University of Tampa.

Seasonal C_T and A_T results showed substantial A_T and C_T correlations with riverine discharge. The strongest correlations, and the lowest A_T and C_T concentrations, were observed in the wet-season during high flow conditions. The ratios of A_T to C_T (A_T/C_T) during the dry season were broadly consistent

between rivers (R^2 = 0.85-0.94) while wet season ratios (high flow conditions) showed more variation (R^2 = 0.55-0.89). River pH_T, which was strongly controlled by A_T/C_T ratios, was elevated in the dry season. The pH_T of the Alafia was the highest of the four rivers in both seasons and substantial differences in average seasonal pH_T were observed for the four rivers: ΔpH = 0.477 (Hillsborough), 0.240 (Alafia), 0.723 (Little Manatee), and 0.572 (Manatee). In response to flow-induced variations in pH_T, C_T and Ca^{2+}, $CaCO_3$ saturation states (Ω) showed strong seasonal variations. Dry/wet season saturation state ratios for the spring-fed Alafia and Hillsborough rivers were 3.5 and 7.1, while ratios for the Little Manatee and Manatee were 17.6 and 14.9. Macro-nutrient results did not exhibit a strong co-variation with discharge rates but, instead, correlated strongly with A_T/C_T ratios and showed distinct seasonal differences that were likely attributable to flow conditions. Inorganic phosphate concentrations were highest for all rivers in the wet-season, and, in contrast, silica was highest for all rivers in the dry season. Nitrate + nitrite showed a complex pattern of seasonality where concentrations were highest on the Alafia in the dry season and highest for the Manatee in the wet season.

Comparisons of riverine C_T and A_T to Tampa Bay measurements made by the EPC-HC and the U.S. Geological Survey, indicated that the rivers lower the Bay's average C_T and A_T concentrations in the wet season while, in the dry season, similarity of river and Bay C_T and A_T concentrations should lead to strong salinity gradients with approximately constant C_T and A_T. Nutrients exhibited contrasting patterns of seasonality. Bay and riverine inorganic phosphate concentrations were substantially similar, while river concentrations of nitrate + nitrite and silica were markedly higher than Bay concentrations.

2.2 Introduction

Between the 1950's and 1980's, Tampa Bay's water quality and seagrass coverage declined due to coastal development, urban expansion, and eutrophication. However, water quality and seagrass abundance has significantly recovered (Sherwood et al., 2016) due to a reduction in nitrogen inputs to the Bay from municipal wastewater treatment and industrial point sources (Greening et al., 2011; Yates et al., 2011; Greening et al., 2015; Sherwood et al., 2016). Water quality data obtained since 1972 at 52 locations in Tampa Bay by the Environmental Protection Commission of Hillsborough County (EPC-HC) have shown an increase in daytime pH that is correlated with an increase in seagrass coverage (Sherwood et al., 2016).

Diurnal variability of pH and CO_2-system parameters in Tampa Bay is strongly influenced by primary productivity and respiration of benthic communities (Yates et al., 2007). Over short time periods, seagrass beds in Tampa Bay can locally elevate pH by up to 0.5 pH units compared to nearby bare sand habitats. Conversely, diurnal respiration in seagrass beds can cause a decrease in pH compared to nearby sand habitats. A large controlling factor in the observed ranges of pH in seagrass beds is the hydrodynamic effect of water mass residence time during periods of intense photosynthesis and respiration (Yates et al., 2016). An analysis of sea level from locations in St. Petersburg and the Sunshine Skyway Bridge by Weisberg and Zhang (2006) showed that flow and circulation in Tampa Bay are primarily controlled by tides, while still exhibiting a two-layer estuarine model with an average outflow of less dense water at the surface and an inflow of denser water at the bottom. Weisberg and Zheng (2006) modeled the Bay's water mass residence time as approximately 100 days. A study by Meyers and Luther (2008) modeled residence time during periods of 156 days and 36 days for low- and high-freshwater inflow and baroclinic circulation, respectively. These residence times were reduced to 53 and 26 days for low and high flow conditions, respectively, when tidal and wind driven signals were removed (Meyers and Luther, 2008).

Relatively long water mass residence times, coupled with effects of seagrass photosynthesis and respiration on overlying seawater pH, results in large scale changes in the chemical signatures of water masses as they flow into the Bay from rivers and exit to the Gulf of Mexico (GOM). The chemical signatures of these processes on this spatial and temporal scale pointed to a need for bay-wide, high-resolution, long-term monitoring of CO_2-system parameters in Tampa Bay (Yates et al., 2007, Yates et al., 2016).

In December 2017, an in-situ ocean carbon system (OCS) was installed at mid water depth on the University of South Florida's Tampa Bay Physical Oceanographic Real Time System (PORTS) Middle Bay station (27.661 N 82.594 W) (Yates et al., 2019). The OCS consists of a Seabird SeapHOx that measures pH, dissolved oxygen (mg/l), temperature (°C), salinity and pressure (dBar), a Pro Oceanus CO_2-Pro CV that measures pCO_2 (ppm), and a Wet Labs PAR sensor that measures photosynthetically active radiation ($\mu M/m^2/sec$). The OCS logs data using a Seabird Stor-X and transmits data to an online platform (tampabay.loboviz.com) with a Seabird LOBO system (Land Ocean Biogeochemical Observatory). Hourly sampling of the OCS in Tampa Bay is concurrent with ancillary sampling by meteorological and current profiling instrumentation. The location and sampling frequency of the OCS enables researchers to capture temporal variability in CO_2-system parameters of Tampa Bay concurrent with real-time comparable CO_2-system measurements anywhere in the Bay (Yates et al., 2019).

Until recently spectrophotometric pH measurements on the total hydrogen ion scale (pH_T) using purified meta-Cresol Purple (mCP) were characterized only in pure water ($S = 0$) and marine waters ($20 \leq S \leq 40$) (Liu et al., 2011). New models for spectrophotometric pH measurement with purified mCP (Douglas and Byrne, 2017; Müller and Rehder, 2018) now provide capabilities for spectrophotometric pH measurements over the full ranges of temperature ($278.15 \leq T \leq 308.15$ K) and salinity ($0 \leq S \leq 40$) commonly found in temperate estuaries (Douglas and Byrne, 2017). This expanded measurement range enables well-calibrated river to sea pH measurements for comprehensive baseline studies in Tampa Bay.

Previous spatial and temporal studies of chemical variability in the Hillsborough River showed large temporal pH variations (Pillsbury and Byrne, 2007). Examination of the Hillsborough River's pH, carbonate alkalinity, and calculated saturation state in conjunction with the chemical characteristics of rainwater and groundwater, indicated that temporal variations were strongly dependent on precipitation (Pillsbury and Byrne, 2007). During the May-June period of low precipitation, river water was supersaturated with respect to $CaCO_3$ due to long contact time with the river's limestone substrate. Conversely, river water was undersaturated with respect to $CaCO_3$ during the August-September period of high precipitation (Pillsbury and Byrne, 2007).

As a substantial extension of previous carbonate system investigations in and around Tampa Bay, using recent advances in spectrophotometric carbonate system analysis, a spatial and temporal survey of pH and carbonate system parameters in the four rivers (Hillsborough, Alafia, Little Manatee, Manatee) that supply the majority of freshwater to Tampa Bay was conducted. The data were examined in the context of Middle Bay pH values over a period of time (~one year) that encompassed low precipitation (November – April) and high precipitation conditions (May – October). The measurements provide a high-quality carbonate system baseline against which acidification impacts attributable to anthropogenic CO_2 can be evaluated. This data also enable assessments of how the carbonate system chemistry of each river is related to the characteristics of its drainage basin and how inorganic carbon and alkalinity influence the seasonal characteristics of water masses that mix into the Bay and exit to the GOM.

2.2.1 Study Areas

Tampa Bay is a shallow subtropical estuary fed by nine named rivers and open to the GOM (Lewis and Estevez, 1988). The Bay receives, on average, about 3.8 billion liters of runoff daily. The four rivers studied (Hillsborough, Alafia, Little Manatee, Manatee) account for 85% of all flow to the Bay (Lewis and Estevez, 1988). Except for the Hillsborough River which flows southwest (Figure 2.1), each

river originates to the east and flows west into the Bay (Boning, 2016). From North to South the rivers' respective floodplains are progressively wider and become tidally influenced over longer distances (Table 2.1). The characteristics of each river's drainage basin are distinctive. The northern rivers (Hillsborough and Alafia) are mostly spring fed and more urbanized, while the southern rivers (Little Manatee and Manatee) are fed by run off and hold more wetlands, forest, and range/farm land (Lewis and Estevez, 1988).

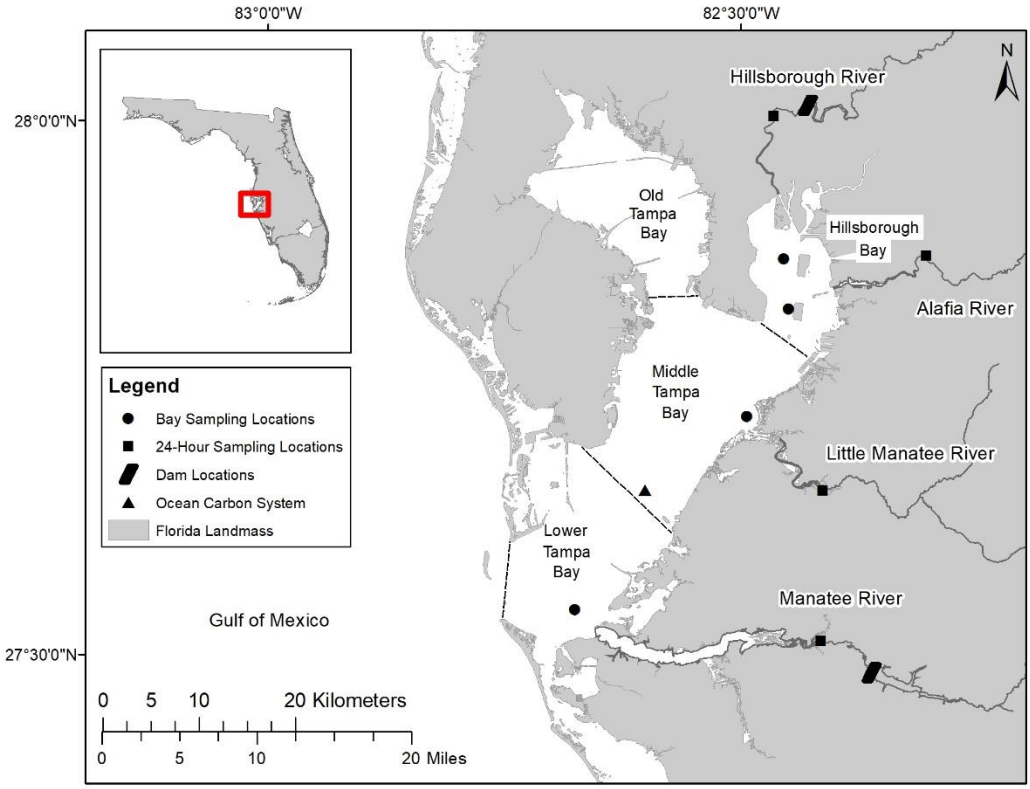

Figure 2.1. A map of Tampa Bay showing the four rivers sampled, sampling locations and notable geographic features.

The Hillsborough River is 54 miles (86.9 km) long and its substrate consists of sand, silt, and limestone rubble. The river is separated into two waterways by a dam just north of Tampa that contains a major water source for the city. The lower waterway is an urbanized stream subjected to tidal influence.

This portion of the river has been polluted to some degree by urban runoff. The upper waterway is largely undeveloped making it pristine and wild. Its headwaters originate in the Green Swamp with a significant contribution of water from Crystal Springs and five major tributaries (Champion and Starks, 2001; Boning, 2016).

The Alafia River is 26 miles (41.8 km) long and its substrate consists of sand and mud. The river is fed by several tributaries that form two prongs consisting of various terrains including farmland, upland hammocks, swamps, residential/urban developments, and active/former phosphate mines. A geologic formation, called Bone Valley, located within the watershed contains quartz and phosphate sand and gravel supports longstanding commercial phosphate mining activities (Lewis and Estevez, 1988, FDEP, 2021). Historically phosphate mining and agriculture runoff have negatively impacted the river's water quality (Boning, 2016 and Duan, 2021).

The Little Manatee River is 41 miles (66 km) long and its substrate consists of sand. Its current is slow, and the water is dark and tannic. The river is fed by several tributaries, and the lower five miles are tidally influenced. This river's ecological condition is best of the four rivers, and it is listed as an Outstanding Florida Water by the state's Department of Environmental Protection (FDEP,1982; Boning, 2016; Scott et al., 2017).

The Manatee River is 58 miles (93.9 km) long and its substrate consists of sand. The river is slow and receives water from several major tributaries fed by runoff and swampy areas. The river is dammed 18 miles (30 km) upriver to provide drinking water for the surrounding municipalities. The lower river is highly developed with homes lining both shores. The upper river drains pastures and agricultural land, resulting in an excess of nutrients entering the waterway (Boning, 2016).

Table 2.1. Average annual discharge, watershed size, tidal influence upstream and the 2019 24-hour average dry season (February-March) and wet season (August-September) discharge rates of four major rivers flowing into Tampa Bay (Lewis and Estevez, 1988; U.S. Geological Survey (USGS) National Water Information System (NWIS) stream gauge stations, 2019).

River	Average Annual discharge (10^9 liters/year)	Watershed (km^2)	Tidal Influence Upstream (km)	Dry Season 24-hr AVG Discharge (ft^3/s)	Wet Season 24-hr AVG Discharge (ft^3/s)
Hillsborough	580	1684	17.7 (Dammed)	312	881
Alafia	425	1088	16.0	232	904
Little Manatee	225	570	24.0	195	1027
Manatee	260	907	30.0 (Dammed)	22	416

2.3 Methods and Materials

2.3.1 Sampling Plan

Over the period of one year each of the four rivers was sampled twice, first during the dry season (February-March) and then in the wet season (August-September). During each season, the four rivers were sampled over four consecutive weekends to capture the state of the Bay's riverine carbonate system. For each river's sampling expedition, a U.S. Geological Survey research vessel was outfitted to sample water while underway and at anchor. During the dry season, the R/V Twin Vee was used and during the wet season the R/V Barge was used (Appendix A1 & A2). Each river was sampled using identical methods and procedures. On each river, the outfitted vessel was launched and driven to the river's mouth during a low tide to capture maximum freshwater outflow. Next, water sampling began at the river's mouth and continued once each hour or when a 5-unit change in salinity was observed as the vessel was driven upstream. During the dry season, once a location exhibiting freshwater conditions was observed (i.e., $S<0.5$), the vessel was anchored, and water sampling continued each hour for 24 hours. During the wet season, the same geographical location as that used in the dry season was sampled, also for 24 hours. Once complete, the vessel was driven on the reciprocal course downstream to the river's mouth while performing the same sampling protocol.

2.3.2 Sample Collection

Measurements collected from each of the four rivers included water temperature, salinity, dissolved inorganic carbon (C_T), total alkalinity (A_T), pH_T (total scale), Calcium (Ca^{2+}) and nutrients including: inorganic nitrogen (NO_3^{2-}+NO_2^-) designated as (N_T), inorganic phosphate ($H_2PO_4^-$ + HPO_4^{2-} + PO_4^{3-}) designated as (P_T), ammonia (NH_3+NH_4^+), and silica ($SiO(OH)_3^-$ + $Si(OH)_4$) designated as (Si_T). Temperature and salinity were continuously measured from a flow-through reservoir while underway or anchored on site (Appendix A3). Water was pumped from 0.3 meters below the water's surface to the onboard reservoir through schedule 80 polyvinyl chloride (PVC) tubing using a submersible pump affixed alongside the boat. The tubing was contained within an aluminum housing to maintain its position while underway. The reservoir was fabricated from a 38-gallon HDX rectangular storage bin containing a thermistor and two water sample ports. Pumped water was returned overboard from two PVC overflow ports. Water was pumped at complete reservoir exchange rate of once every 1.5 minutes, which minimized thermal contamination from any solar radiation absorbed by the reservoir. In-situ temperature was measured using a Seabird Scientific SBE 38 digital oceanographic thermometer located near the inflow port in the reservoir. In-situ salinity of continuously-pumped sample water was measured with an externally mounted Seabird Scientific SBE 45 MicroTSG thermosalinograph (Micro TSG). The sample water was obtained using a Geotech peristaltic pump connected to the MicroTSG port on the reservoir with tubing located behind the reservoir inflow port. Both temperature and salinity sensors were factory calibrated and connected to an AC-powered interface box to report temperature (SBE38) and salinity (SBE45) every ten seconds to a laptop.

Water samples collected for pH_T, C_T, A_T, Ca^{2+}, and nutrient analysis were obtained from the sampling tube port (Appendix A3) where water was pressure filtered using a peristaltic pump and platinum cured silicon tubing. The filtration system consisted of a 142 mm diameter acrylic filter housing (GeoTech™) containing a 0.45 μm cellulose nitrate filter (GeoTech™) to remove particulate sediment and organic material (Appendix A1 & A2).

During each sampling event, water for pH_T was promptly collected in two or three cylindrical 10 cm pathlength glass cells made by Hella Inc. (No. 120-100-20) and set aside in the shade to minimize temperature change for onboard analysis. Next, water was collected for C_T, A_T, and Ca^{2+} analysis in a single 300 mL borosilicate glass bottle with a ground glass neck and stopper (Wheaton™). The water was filtered and poisoned with 100 µL of a 6.5% saturated $HgCl_2$ solution (LabChem™). The bottle was then sealed (at positive pressure) using Apiezon™ M grease on the stopper before being transported to the laboratory for analysis (Dickson et. al., 2007; Yates et al., 2016). Lastly, water was collected for nutrient analysis in a 30 mL acid-washed high-density polyethylene bottle (Nalgene™). Sample water for nutrients was filtered using a sterile 0.22 µm pressure filter (Sterivex™) attached by Luer lock to a 60 mL syringe. Once sealed, the sample was stored on ice in a cooler and transported to the laboratory to be frozen until analysis (Doer et al. 1996). During each river sampling expedition, 10% of C_T, A_T, and nutrient samples were collected as duplicates. All pH_T samples were analyzed as duplicates or triplicates.

2.3.3 Sample Analysis

Spectrophotometric pH_T analysis was performed onboard within 30 minutes of collection using the methods of Clayton and Byrne (1993). Water samples collected in cylindrical glass cells were placed within an aluminum housing (Ocean Optics) connected to an Ocean Optics LS-1 Tungsten light source and an Ocean Optics USB2000 spectrometer. 10 µL of purified mCP indicator dye from Dr. Byrne's laboratory at the University of South Florida's College of Marine Science was administered with a Gilmont GS-1100 Micrometer Syringe. Absorbance measurements were made using the Ocean Optics software package OOIBase 32. The temperatures of pH_T analyses were measured using a Fluke 51 II Handheld Digital Probe Thermometer. pH_T was calculated on the total scale from absorbance measurements using the algorithm of Müller and Rehder (2018). Next, pH_T was corrected for any dye perturbation by back correction from a second dye addition (Clayton and Byrne, 1993). The pH_T was then temperature corrected to 25° Celsius using CO2sys.m (Van Heuven et al., 2011), the K1K2 constants of

Waters, Millero, & Woosley (2014), the KSO_4 constants of Dickson (1990), and the total boron to salinity ratio (B_T/S) constant of Lee (2010). Finally, the average and standard deviation of the replicate pH_T measurements made during each sampling event were calculated. The pH_T precision for all four rivers was 0.013 during the dry season 0.024 during the wet season.

Total inorganic carbon analyses (C_T) were performed in the laboratory using a CM5017 CO_2 carbon coulometer coupled to a CM5330 Acidification Module acidification module (UIC, Inc.) following the methods described by Dickson and Goyet (1994).Each sample (~ 20 mL) was drawn from a newly opened sample bottle using a 60 mL syringe attached to a three-way Luer lock valve and stopper to minimize gas exchange. Sample weight was determined from the difference in the syringe weight before and after the sample was injected through a septum on the stripping chamber of the acidification module, using a Denver Instruments PI-214 analytical balance (± 0.1 mg). Samples were acidified with ~10 mL of 8.5% $H_3PO_4^-$ Analytical grade N_2 gas was used as the carrier gas for CO_2 from acidified samples to the coulometer. The titration endpoint was determined by the coulometer, and C_T was calculated using software from UIC, Inc. Accuracy and precision was determined from analysis of certified reference materials (CRM) from Scripps Institution of Oceanography (Dr. Andrew Dickson, Dickson, 2010). Repeated measurements (N = 97) of CRM Batch 176 yielded a precision of ± 2.53 μmol kg^{-1} (standard deviation of all CRM analysis) and an accuracy of 1.99 ± 1.56 μmol kg^{-1} (Average of the absolute value of the difference between each measured CRM and reported batch concentration).

Total alkalinity analyses (A_T) were performed in the laboratory using the spectrophotometric methods of Yao and Byrne (1998) and Liu et al. (2015). The mass of water sample (~100 g) and acid additions were determined gravimetrically using a Denver Instruments PI-214 analytical balance (± 0.1 mg). Water samples were analyzed in an open square glass cell (Hellma Cells, Inc.) placed within a custom plastic frame connected to an Ocean Optics LS-1 tungsten light source and Ocean Optics USB2000 spectrometer. Bromocresol purple indicator dye (4 mM) was administered by pipette and the sample was titrated using 0.100 N standardized HCl (± 0.0001 N) added with a plastic 10 mL syringe

fitted with a Teflon syringe needle. Absorbance measurements were made using the Ocean Optics software package OOIBase 32. Solution pH_T was measured continuously throughout the titration to an endpoint near pH 4.3 and the total weight of the added acid was determined from the difference in the syringe weight before and after acid addition. At the end of each titration, the solution was purged with a stream of N_2 gas pre-saturated with H_2O. After purging, final absorbance measurements were made, and solution temperature was determined using a Fluke 51 II Handheld Digital Probe Thermometer. A_T was calculated using the equations of Hudson-Heck et al. (2021). Accuracy and precision were determined from analysis of CRMs (Dickson, 2010). Repeated measurements (N = 79) of CRM Batch 176 yielded a precision of ± 0.83 μmol kg^{-1} and an accuracy of 0.55 ± 0.62 μmol kg^{-1}.

The water samples remaining in the borosilicate bottles after C_T and A_T analyses were used for Ca^{2+} analyses. Ca^{2+}concentrations were measured on an Agilent 7500 ICP-MS instrument by Dr. Sherwood Liu at the University of South Florida. Calcium-43 concentrations were measured in Helium (He) gas mode using Indium (In) as an internal standard to reduce polyatomic interferences. Measured Ca^{2+} concentrations along with carbonate concentrations ($[CO_3^{2-}]$) calculated with CO2sys.m from C_T and pH_T measurements were used to calculate $[Ca^{2+}][CO_3^{2-}]$ ion products. The solubility product constants of Mucci (1983) were then used to calculate calcium carbonate ($CaCO_3$) saturation states (Ω). All calculations using CO2sys.m included nutrient concentrations when needed for corrections to in situ conditions.

Nutrient analyses were performed at the University of Tampa under the direction of Dr. R. Masserini. Samples were analyzed for N_T, P_T, Si_T, and ammonia (NH_3+NH_4^+) using the methods of Gordon et al. (2000).

2.4 Results and Discussion

2.4.1 Spatial and Temporal Distributions of Carbonate Parameters

Figures 2.2 and 2.3 show the dry season (Feb. - Mar.) and wet season (Aug. - Sep.) 24-hour collection results for measured total inorganic carbon (C_T) and total alkalinity (A_T). The results for the Hillsborough, Alafia, Little Manatee, and Manatee Rivers are shown from left to right by their geographic position from north to south. Dry season C_T, A_T, and Ca^{2+} results for the Manatee River showed an influence from salinity (Bay water intrusion) and were corrected for this effect as follows: C_T, A_T, and Ca^{2+} data for the Manatee River were plotted as a function of salinity and interpreted as end member mixing between the river and the Bay. Using the procedure and data shown in supplemental information (Appendix A4), the C_T, A_T, and Ca^{2+} data were extrapolated (C_T ($R^2 = 0.74$), A_T ($R^2 = 0.73$), Ca^{2+} ($R^2 = 0.70$)) to the average salinity of the other three rivers during the dry season (S = 0.25). This correction was necessary only for the Manatee River in the dry season.

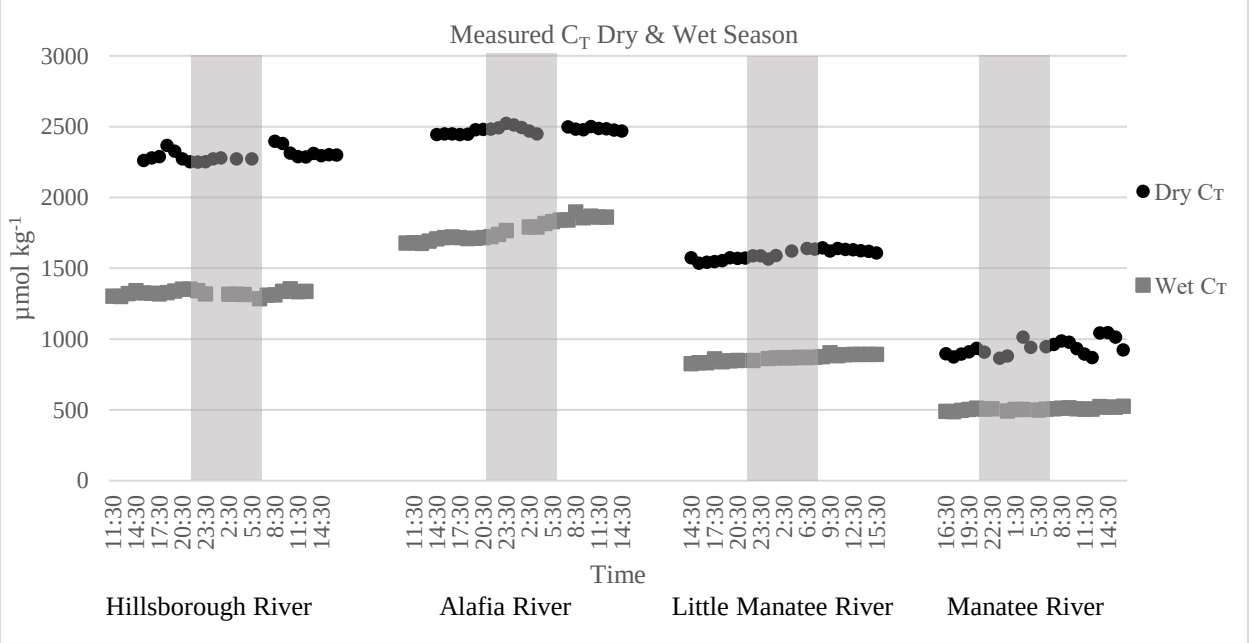

Figure 2.2. Measured total dissolved inorganic carbon (C_T) for each river during the dry and wet seasons. Shaded areas indicate nighttime on each river.

For each river, seasonal C_T and A_T results showed distinct differences whereby dry season concentrations substantially exceeded wet season concentrations (Figures 2.2 and 2.3). Average seasonal concentration ratios (dry/wet) for C_T for the four rivers were 1.73 for the Hillsborough, 1.41 for the Alafia, 1.84 for the Little Manatee, and 1.85 for the Manatee (Table 2.2). The patterns for A_T showed larger seasonal ratios. Seasonal A_T ratios (dry/wet) were 2.09 for the Hillsborough, 1.48 for the Alafia, 2.57 for the Little Manatee, and 3.62 for the Manatee (Table 2.2).

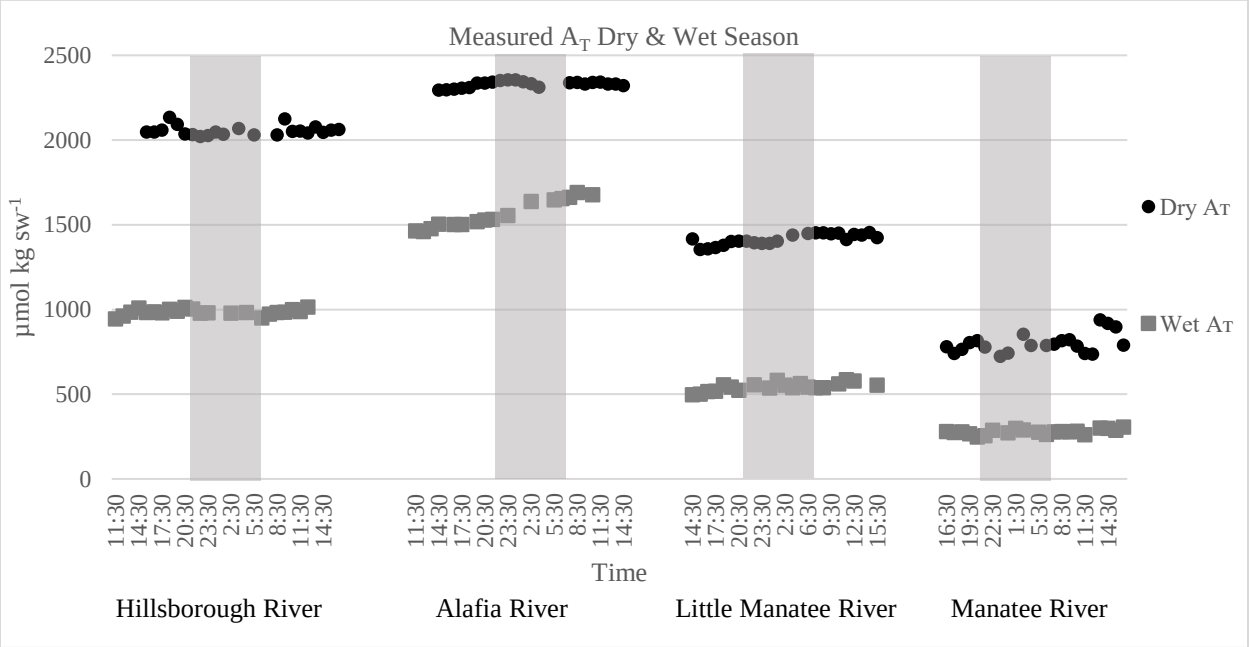

Figure 2.3. Measured total alkalinity (A_T) from each river during the dry and wet season. Shaded areas indicate nighttime on each river.

The ratio of A_T to C_T (A_T/C_T) during the dry season was broadly consistent between rivers. The dry season ratios were: 0.90 (Hillsborough), 0.94 (Alafia), 0.89 (Little Manatee), and 0.85 (Manatee) (Table 2.2). Wet season A_T/C_T ratios showed more variation. Wet season ratios were: 0.74 (Hillsborough), 0.89 (Alafia), 0.64 (Little Manatee) and 0.55 (Manatee) (Table 2.2).

Table 2.2. Mean and standard deviation of measured carbonate system parameter results for each river during the dry and wet season.

	Dry Season (Feb.-Mar.)			Wet Season (Aug.-Sep.)		
River	C_T (µmol kg^{-1})	A_T (µmol kg^{-1})	pH_T	C_T (µmol kg^{-1})	A_T (µmol kg^{-1})	pH_T
Hillsborough	2295 ± 40	2055 ± 29	7.448 ± 0.053	1324 ± 18	985 ± 18	6.971 ± 0.088
Alafia	2475 ± 23	2329 ± 18	7.659 ± 0.024	1767 ± 72	1563 ± 83	7.420 ± 0.040
Little Manatee	1595 ± 35	1414 ± 32	7.476 ± 0.048	865 ± 22	544 ± 25	6.748 ± 0.085
Manatee	937 ± 56	801 ± 59	7.333 ± 0.115	505 ± 10	279 ± 15	6.752 ± 0.146

The average seasonal differences for pH_T for the four rivers (Table 2.2) were 0.477 (Hillsborough), 0.240 (Alafia), 0.723 (Little Manatee), and 0.572 (Manatee). Due to higher dry-season A_T/C_T ratios, pH_T was substantially elevated in the dry season (Figure 2.4). While the dry-season pH_T of the Alafia was somewhat higher than the other rivers, the wet-season pH_T for the Alafia was quite notably elevated compared to the other rivers.

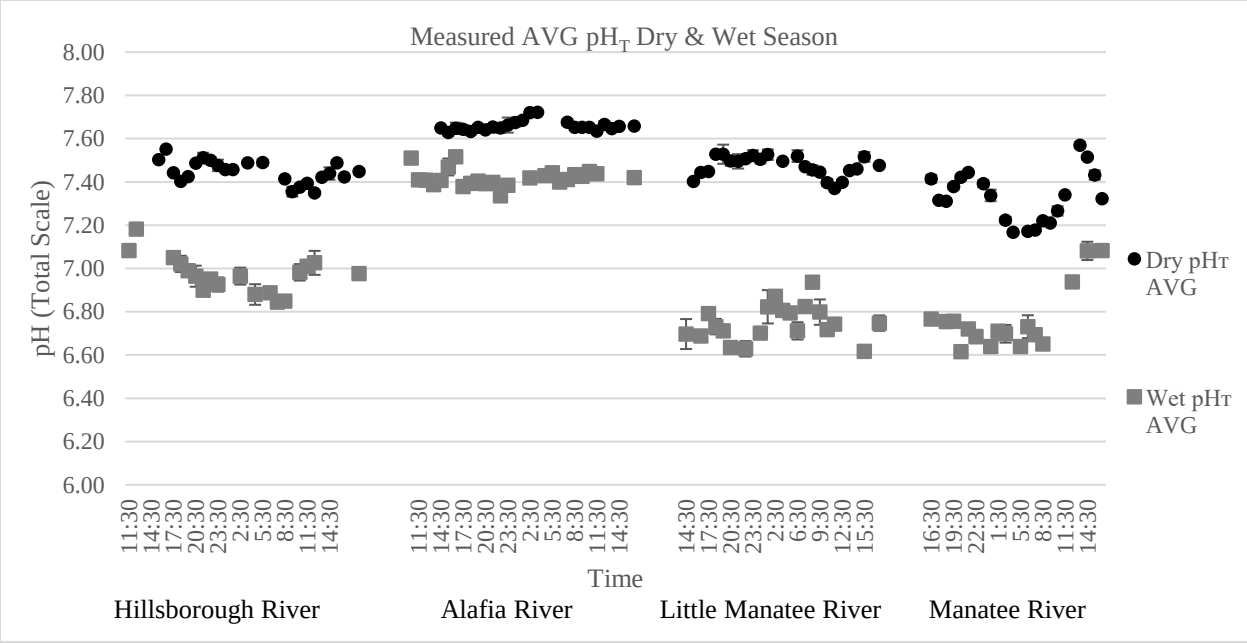

Figure 2.4. Measured average pH_T from each river during the dry and wet season. Shaded areas indicate nighttime on each river. Error bars represent standard deviation. When error bars cannot be seen it is because they are smaller than the symbols (circles and squares) in the figure.

Solution pH_T is strongly controlled by A_T/C_T ratios. Consistent with this expectation, Figure 2.5 shows robust relationships between pH_T and A_T/C_T for both the wet and dry seasons. In addition to the strong correlation between pH_T and A_T/C_T (i.e., $R^2 > 0.8$ in both seasons), Figure 2.5 shows that the pH_T range in the wet season is substantially larger than the pH_T range in the dry season ($\Delta pH \approx 0.9$, wet; $\Delta pH \approx 0.55$, dry). Substantial distinctions are also observed in the rivers' buffering intensity.

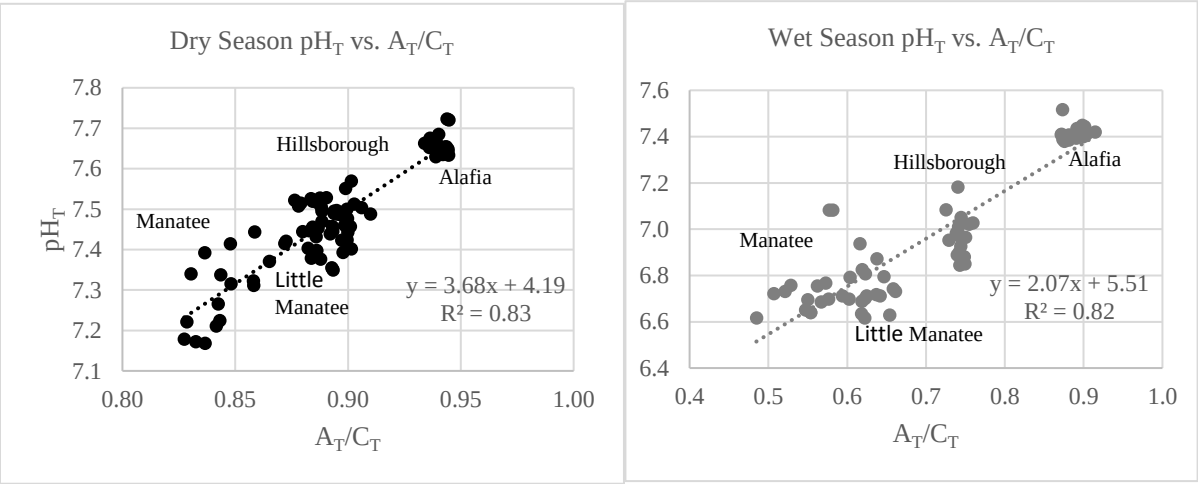

Figure 2.5. Plotted results of the ratio of A_T to C_T versus pH_T for the dry season (left) and wet season (right).

Diel variability in the rivers' pH_T is a reflection of the magnitude of each river's buffer intensity, whereby the combination of lower A_T and lower C_T creates a higher susceptibility to pH_T change. While the standard deviations (SD) of the individual pH_T measurements shown in Figure 2.4 are generally smaller than the size of the symbols in the figure ($SD \approx 0.018$), the standard deviations for the 24-hour average pH_T values shown in Table 2.2 are much larger ($0.024 \leq SD \leq 0.146$). The relationship between the rivers' buffer intensities and river pH_T is highlighted in Figure 2.6, where the SD of 24-hour average pH_T for each river is shown as a function of each river's 24-hour average A_T. For each season, the SD of river diel average pH_T decreased as A_T increased. Regressions of pH_T standard deviations against both A_T and C_T (not shown here) were very similar ($R^2 = 0.8$). The larger diel pH_T variations of the poorly buffered Manatee River are particularly notable.

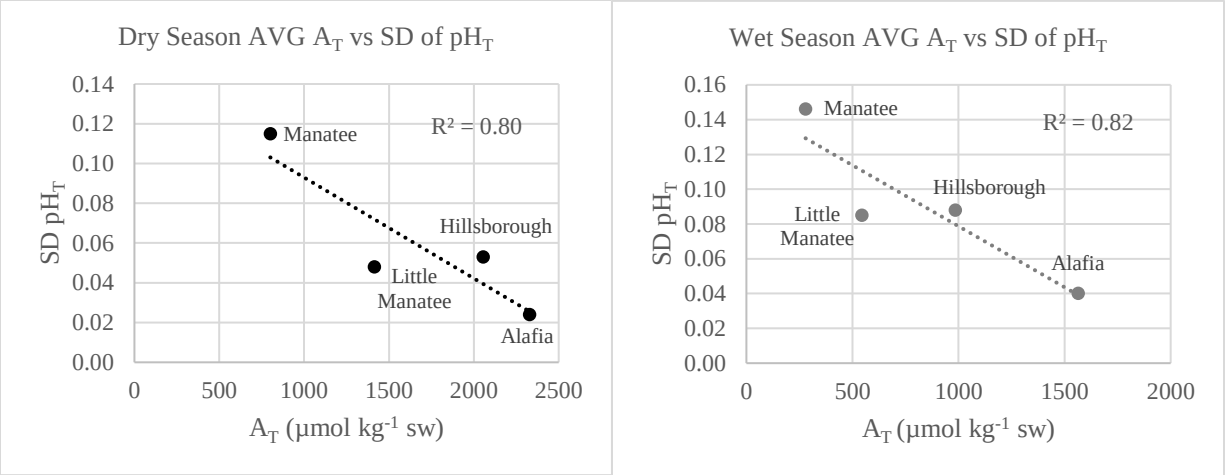

Figure 2.6. Plotted results of the standard deviation (SD) of 24-hours of pH_T data from each river versus the average A_T from each river. Dry season results are on the left and wet season results are on the right.

2.4.2 A_T and C_T Dependencies on Wet-Season River Discharge Rates

Although the observations presented in this work represent only snapshots (diel variations) for the four rivers during each season, the existence of significant short-term relationships between carbonate system concentrations and river discharge rates were notable. Substantial correlations were observed (Figure 2.7) between A_T and C_T concentrations and wet-season discharge rates (obtained during each 24-hour collection period from nearby U.S. Geological Survey (USGS) National Water Information System (NWIS) stream gauge stations) for the free-flowing Alafia and Little Manatee rivers. Correlations over the 24-hour collection periods in the dry season were much weaker and are not shown here (Appendix A5). These diel relationships between river flow and concentrations of A_T and C_T are consistent with the seasonal decrease in C_T and A_T concentrations with increased river flow in the wet season (Table 2.2).

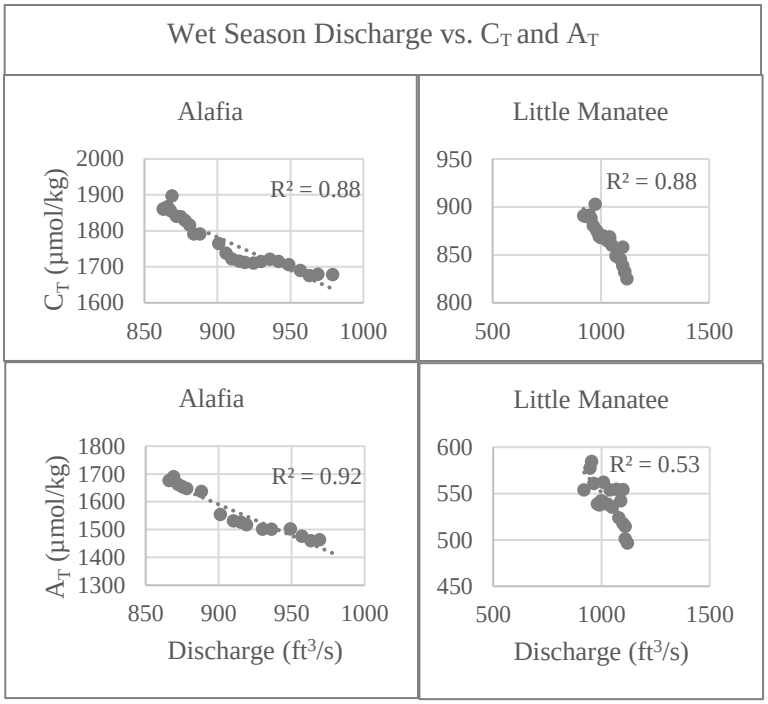

Figure 2.7. Riverine discharge rates versus A_T and C_T for free-flowing rivers during the wet season 2019.

The magnitude of the seasonal relationship between river discharge and carbonate parameters is highlighted in Figure 2.8 where seasonal average discharge rates are compared to average C_T and A_T for each river. This comparison shows the substantial decreases in C_T and A_T concentrations with increasing river discharge. In addition to the influence of discharge rates on the absolute concentrations C_T and A_T, the figure also shows that the differences between C_T and A_T are smaller in the dry season (A_T/C_T ratios are larger). This is consistent with the observed elevation of pH_T in the dry season (Table 2.2 and Figure 2.5).

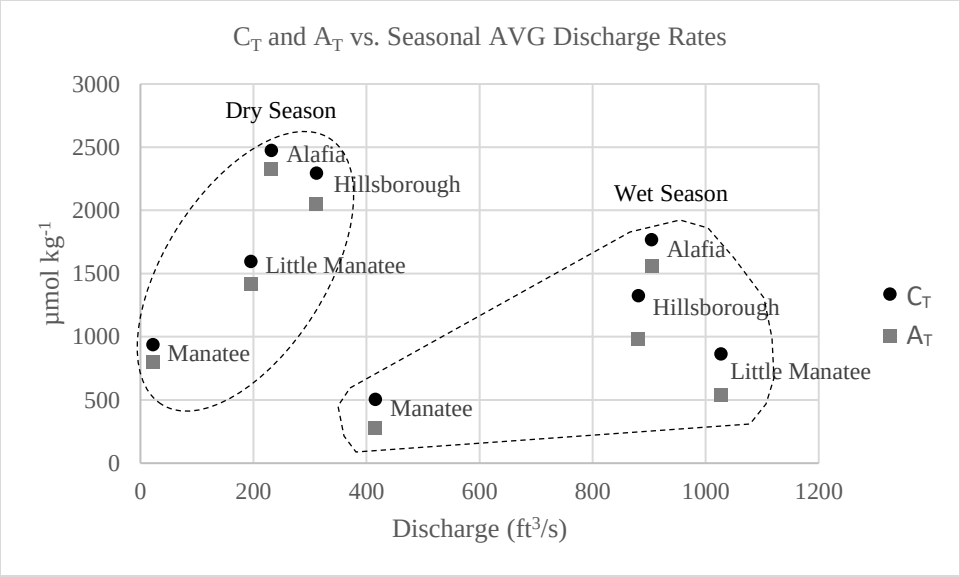

Figure 2.8. Seasonal comparison between each rivers' average C_T and A_T concentrations and average discharge rate. Clear seasonal distinctions can be seen for all rivers.

2.4.3 Seasonal Changes in Calcium Carbonate Saturation States

The four rivers exhibited a wide range of saturation states (**Ω**) in both the dry and wet seasons. In the dry season the average **Ω** values for each river were 0.580 (Hillsborough), 0.995 (Alafia), 0.299 (Little Manatee), and 0.159 (Manatee) (Appendix A6). During the wet season, the **Ω** for each river were considerably reduced. The average wet season **Ω** for the Alafia was 0.313 and **Ω** was <0.1 for the other three rivers. The spring-fed Hillsborough and Alafia rivers had much higher **Ω** than the Little Manatee and Manatee, presumably due to higher in A_T and Ca^{2+} concentrations from dissolution of limestone within the aquifer. Seasonally averaged **Ω** ratios (dry/wet) were 7.53 (Hillsborough), 3.08 (Alafia), 17.6 (Little Manatee), and 14.9 (Manatee). The dry/wet variations in **Ω** are larger than the dry season/wet season variations in other parameters because they are due to multiplicative effects of (a) wet season decreases in Ca^{2+} (Appendix A6), (b) wet season decreases in C_T (Figure 2.8) and (c) wet season decreases in pH (Figures 2.4 and 2.5).

2.4.4 Spatial and Temporal Distribution of Macro-Nutrient Concentrations

Table 2.3 shows the average and SD of 24-hour collection results for measured nutrients: P_T, Si_T, and N_T, for each river during the dry season (Feb. - Mar.) and wet season (Aug. - Sep.). The Alafia River had the highest concentrations of all nutrients in both the wet and dry seasons. P_T concentrations were highest for all rivers in the wet season and, in contrast, Si_T was highest for all rivers in the dry season. N_T showed a complex pattern of seasonality. N_T concentrations in the Alafia were highest in the dry season and highest for the Manatee in the wet season, while N_T in the Hillsborough and Little Manatee showed only weak seasonality. Pillsbury and Byrne (2007) reported similar findings on the Hillsborough River where major ion concentrations showed strong seasonal variability and were lowest at times of highest precipitation except for P_T, which exhibited contrasting behavior.

Ammonia (NH_3+NH_4^+) concentrations (not shown here, Appendix A13) were below detection limits for the dry season and quite low in the wet season. In addition, N_T results for the Manatee River in the dry season were generally below the limits of detection.

Table 2.3. Mean and standard deviation and of measured macro-nutrient results for each river during the dry and wet season.

	Dry Season (Feb.-Mar.)			Wet Season (Aug.-Sep.)		
River	P_T (µmol kg^{-1})	Si_T (µmol kg^{-1})	N_T (µmol kg^{-1})	P_T(µmol kg^{-1})	Si_T (µmol kg^{-1})	N_T (µmol kg^{-1})
Hillsborough	4.93 ± 0.27	85.76 ± 5.90	6.10 ± 1.64	7.20 ± 0.36	65.53 ± 9.77	7.36 ± 1.16
Alafia	22.14 ± 1.00	131.84 ± 2.96	47.57 ± 6.51	30.33 ± 2.68	101.53 ± 9.28	19.39 ± 2.83
Little Manatee	6.38 ± 0.27	39.61 ± 5.65	12.0 ± 0.70	12.67 ± 0.42	22.04 ± 5.41	10.12 ± 0.92
Manatee	8.19 ± 0.76	23.44 ± 3.91	0.21 ± 0.15	11.96 ± 0.21	15.18 ± 5.73	12.91 ± 1.09

Unlike C_T and A_T dependencies on river discharge rates, nutrients did not strongly correlate with river discharge. Instead, strong seasonal correlations were observed between carbonate system parameters (A_T and C_T) and average nutrient concentrations, with particularly notable correlations for Si_T. Figure 2.9

shows the strong seasonal relationship between A_T/C_T ratios and Si_T. These strong correlations between Si_T concentrations and A_T/C_T ratios suggest that the remineralization of Si_T from solid and organic substrates is similar to the relative transfer rates of A_T and C_T from solid substrates to dissolved forms in river waters.

Correlations between P_T concentrations and the A_T/C_T ratios were also relatively high. $R^2 = 0.60$ in the dry season and $R^2 = 0.49$ in the wet season. Coefficients of correlation between N_T and A_T/C_T ratios were $R^2 = 0.86$ in the dry season and $R^2 = 0.27$ in the wet season. As such, dry season correlations for all three nutrients and A_T/C_T ratios were relatively high in the dry season.

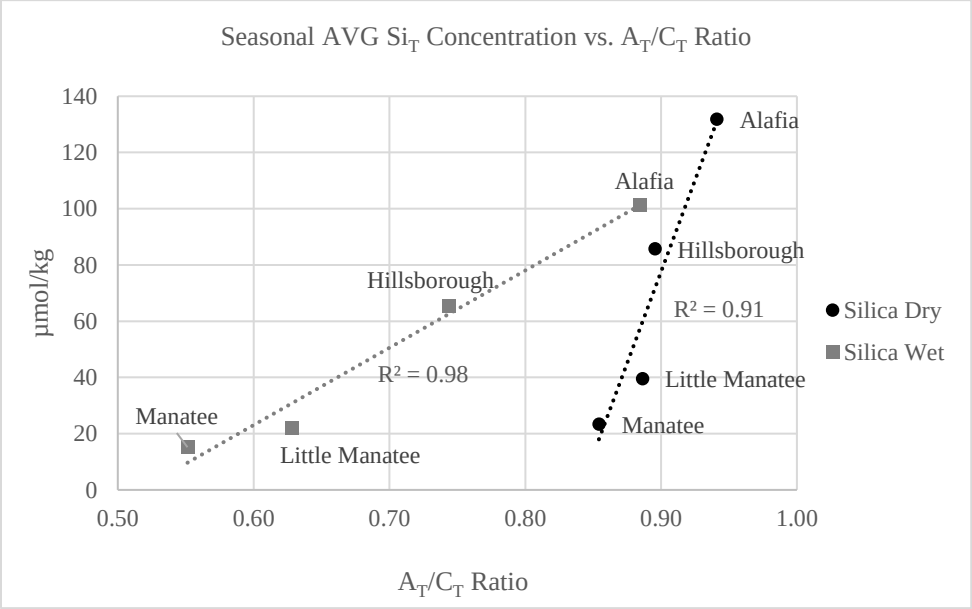

Figure 2.9. Comparison of A_T/C_T ratios to 24-hour average silica (Si_T) concentrations for each river during the dry season (left) and wet season (right).

2.5 Impacts on Tampa Bay

2.5.1 Comparison of Riverine Carbon System Parameters to Middle Tampa Bay

Toward a broad general perspective of the significance of riverine carbon system inputs to Tampa Bay, it is useful to compare the average C_T and A_T input from the four rivers (mixed) during each season to C_T and A_T measurements made at the U.S. Geological Survey's Middle Bay study site (Figure 2.1) in 2019 (Yates et al., 2019). The Middle Bay study site is located in a narrow section of the Bay where tidal flow is strong and the area is considered to be well-mixed (Yates, et al., 2019). Table 2.4 compares combined inputs of river C_T and A_T (flow-weighted averages) to seasonal averages for Middle Tampa Bay in 2019 (Appendix A7). Weighted average river concentrations in the dry season are very similar to the Middle Bay concentrations. Therefore, mixing of Bay water with river waters results in a zone of changing salinity but roughly constant C_T and A_T. During the wet season, concentration averages are about half of dry season concentrations. Therefore, C_T and A_T input from the rivers in the wet season contribute to lowering the Bay's average C_T and A_T concentrations. During the wet seasons in 2018-2020, Yates et al., (In Review) found that freshwater inflow contributed to lower pH_T and higher pCO_2 values measured by the OCS system at the Middle Bay site. This is consistent with the lower wet-season pH_T conditions for rivers as shown in Figure 2.4 and Table 2.2.

Table 2.4. Weighted seasonal average C_T and A_T concentrations (i.e., weighted by relative discharge rates) from all four rivers compared to Middle Tampa Bay seasonal average concentrations for the dry and wet seasons.

	Rivers (Dry (Feb.-Mar.) and Wet (Aug.-Sep.))			Middle Bay (Dry (Apr.-May) and Wet (Jun.-Oct.))	
	Discharge AVG (ft^3/s)	C_T Weighted AVG ($\mu mol\ kg^{-1}$)	A_T Weighted AVG ($\mu mol\ kg^{-1}$)	C_T AVG ($\mu mol\ kg^{-1}$)	A_T AVG ($\mu mol\ kg^{-1}$)
Dry Season	761	2131	1938	2143 ± 10	2361 ± 12
Wet Season	3228	1196	915	2039 ± 34	2269 ± 41

As a means of conceptualizing river carbon system inputs to Tampa Bay, it's useful to consider C_T and A_T replacement times for Tampa Bay: replacement time = (amount in Tampa Bay)/(riverine discharge rate). Using the weighted average C_T and A_T discharge rates of the four rivers in the wet season, along with the Middle Bay C_T and A_T concentrations (Table 2.2) and the total water volume of the Bay, the replacement times for C_T and A_T are 5.9 and 7.2 years (Appendix A8). In contrast, a similar calculation for the C_T and A_T replacement times of Hillsborough Bay in the wet season, using inputs from the Hillsborough and Alafia Rivers, results in replacement times of 2.5 and 2.9 months respectively (a twenty-fold decrease in the replacement time) (Appendix A9). As such, rivers appear to exert a modest impact on C_T and A_T in Tampa Bay as a whole but have a substantial impact on Hillsborough Bay in the wet season.

2.5.2 Comparison of Riverine Nutrients to Tampa Bay

Flow-weighted averages of riverine nutrient concentrations from all four rivers were compared to monthly P_T and N_T concentrations reported for Hillsborough Bay, Middle Bay, and Lower Bay by the EPC-HC (Figure 2.10). EPC-HC does not measure Si_T.

During each season, P_T comparisons showed similar concentrations between the weighted river average and the Bay segments with the exception of Hillsborough Bay, which displayed concentrations nearly twice that of the river weighted average and Bay segments. The elevated P_T concentration of Hillsborough Bay is a long-standing phenomenon and is explained by its small volume, high nutrient loading from three river point sources, and limited water mass exchange with Middle Bay (Stoker et al., 1996). Nevertheless, the constancy in average seasonal concentrations between the rivers and Bay segments shows that mixing of Bay water with river waters in both seasons results in zones of changing salinity but roughly constant P_T.

N_T concentration comparisons displayed contrasting patterns of seasonality between the flow-weighted river average and the Bay segments. The averaged river concentrations (dry and wet) were substantially higher than the concentrations in all segments of the Bay. Therefore, in contrast to P_T, mixing of Bay water with river waters results in estuarine zones where N_T sharply increases with decreasing salinity. Given the low N_T concentrations in the Bay, the delivery of riverine N_T to the Bay presumably fuels rapid biological uptake. As nitrogen is the limiting nutrient in the Bay (Vargo et al., 1994; Johansson, 2009; Greening et al, 2014), this zone likely exerts a strong influence on primary production in Tampa Bay.

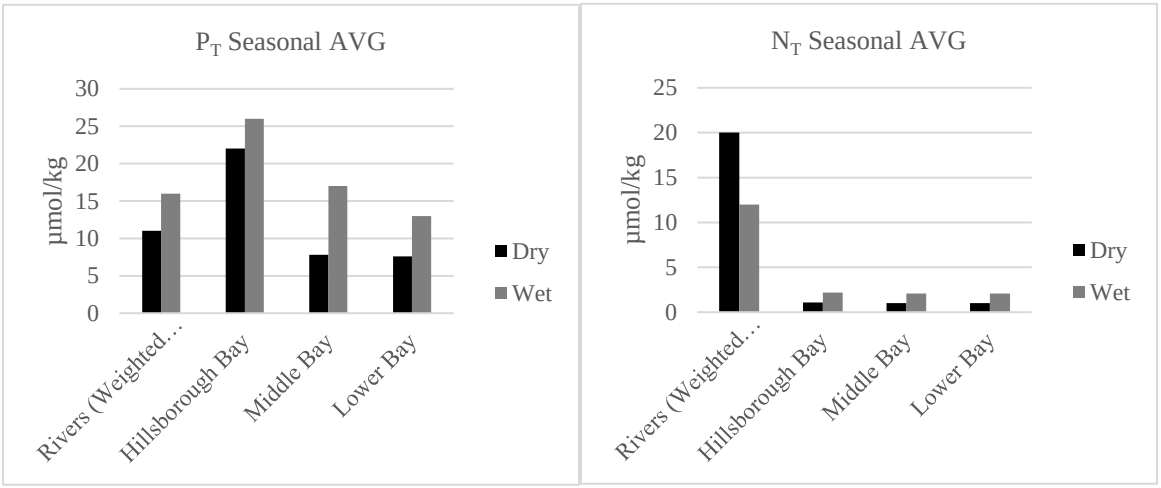

Figure 2.10. Seasonal comparison of nutrients P_T and N_T to the weighted average from all four rivers and three Bay segments.

Because EPC-HC does not measure Si_T, seasonal river weighted averages of all four rivers were compared to similar monthly nutrient measurements made at the USGS Middle Bay site (Yates et al., 2019). Weighted-average river concentrations (dry and wet) were substantially higher than Bay concentrations at this location. River/Bay ratios for Si_T were 19 in the dry season and 3.3 in the wet season (Appendix A10). Consequently, the combined inputs from the four rivers studied in this work constitute a substantial Si_T source for diatomaceous primary production (Badylak and Phlips, 2008).

2.6 Parameter Variations with Changes in Discharge Rates

This study serves as a substantial extension of previous carbonate system investigations in and around Tampa Bay. A variety of distinctive characteristics regarding riverine carbonate parameters and nutrient parameters and their impacts on Tampa Bay were identified. Each of the four rivers studied in this work exhibited carbon parameter concentration variations that were related to riverine discharge, and these variations were observed on both short (diurnal) and long (seasonal) time scales.

During low flow conditions in the dry season (Table 2.1), A_T and C_T were elevated (Figures 2.2 and 2.3) and A_T/C_T ratios were broadly consistent between rivers (0.85-0.94). During high flow conditions in the wet season, A_T and C_T decreased and A_T/C_T ratios were reduced and much more variable between rivers (0.55-0.89). Solution pH_T, which is strongly controlled by A_T/C_T ratios (Figure 2.5), followed the same seasonal pattern as flow conditions where pH_T values were elevated in the dry season and lower in the wet season (Figure 2.4). $CaCO_3$ saturation states (Ω) responded to seasonal flow conditions where the dilution of Ca^{2+} and C_T, and decreased pH_T during high flow conditions decreased Ω. These findings are consistent with Pillsbury and Byrne (2007) where the Hillsborough River's pH and $CaCO_3$ saturation state decreased dramatically during periods of high river flow.

Riverine discharge is ultimately controlled by precipitation, watershed size and groundwater discharge. Figure 2.11 shows that the average annual discharge of each river is strongly related to watershed area ($R^2 = 0.93$). Notably, larger watershed areas are likely to encompass a larger number of identified springs that also contribute strongly to overall discharge.

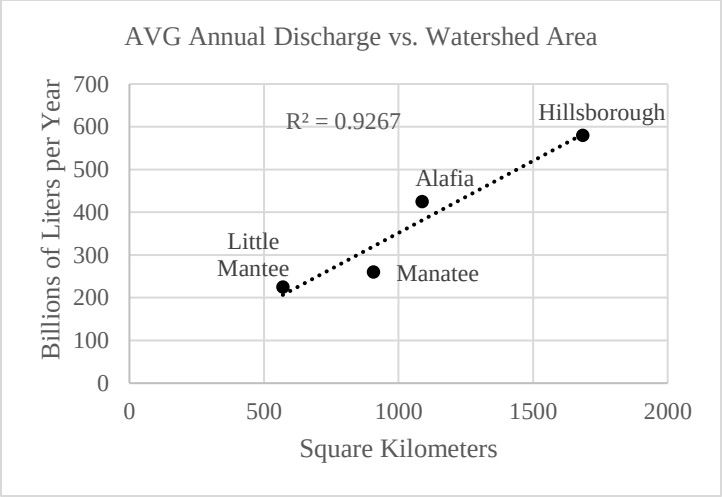

Figure 2.11. Comparison of average annual discharge (Table 2.1) and the watershed areas of the four major rivers (Lewis and Estevez, 1988).

Freshwater springs account for 90% of the *leakage* from the Florida Aquifer (Ryder, 1982; Lewis and Estevez, 1988). Due to increased thickness of confining layers overtop the Florida aquifer, the Little Manatee and Manatee Rivers have no known springs, while the Alafia and Hillsborough River basins both contain several (Lewis and Estevez, 1988). This distinction with respect to spring discharge suggests that groundwater leakage from springs significantly contributes to the observed discharge differences between the four rivers. It is reasonable to presume that the elevated C_T and A_T concentrations of the Hillsborough and Alafia Rivers are due in part to prolonged contact time of spring water and limestone within the aquifer. The Hillsborough River study of Pillsbury and Byrne (2007) indicated that limestone dissolution is the major controlling factor for Ca^{2+} and CO_3^{2-} concentrations observed in the river's major freshwater source, Crystal Springs.

Macro-Nutrient concentrations did not exhibit a strong co-variation with discharge rates but, like carbonate parameter results, nutrients did show distinct seasonal differences which are likely attributable to flow conditions. Seasonal P_T concentration characteristics of the Hillsborough River were consistent with Pillsbury and Byrne (2007) where P_T significantly increased during the rainy season (Table 2.3).

Ultimately, nutrient concentrations strongly correlated with A_T/C_T ratios. For P_T and N_T, correlations were notably stronger during the dry season, while correlations between Si_T and A_T/C_T ratios were strong during both seasons ($R^2 \geq 0.91$). The mechanisms underlying the covariation between nutrient concentrations and A_T/C_T ratios merits further attention.

2.6.1 Future Work

Additional research on relationships between CO_2-system parameters and river discharge could substantially improve interpretations of the effects of land use on water quality. One means of exploring this is through comparative studies that would be similar to those described in our river investigations but, in contrast, would be made on river tributaries that drain well-defined and contrasting watershed-types. Such studies should be performed over a broad range of precipitation conditions. In addition, future investigations should assess the extent to which temporal variations in spring discharge influence carbonate system characteristics and nutrient concentrations, including Si_T, in major springs.

Because acidification of natural waters is a ubiquitous problem, with substantial and diverse environmental impacts, investigation of potential refugia (e.g., Beckwith et al., 2019) in the transition zones between river mouths and the Bay should be considered. Although rising levels of atmospheric CO_2, and therefore acidification, appear to be inexorable, the extensive contact times between groundwater and karst in Floridian systems, via springs that feed the Hillsborough and Alafia rivers, may significantly ameliorate acidification in at least some portions of Tampa Bay. As an important extension of ad hoc investigations of the Tampa Bay watershed, it would be beneficial for the EPC-HC's long-term monthly water quality program in and around the Bay to include C_T and A_T, as well as the impact of these variables (via A_T/C_T ratios) on dissolved Si_T.

2.7 Acknowledgements

I would like to thank Dr. Sherwood Liu and several volunteers for their extensive assistance with the 24-hour data collection portion of the project.

Chapter Three:

Measurements of pH, Dissolved Inorganic Carbon and Total Alkalinity in an Organic-Rich Estuary: The Beneficial and Detrimental Effects of Hg^{II} Added as a Preservative

3.1 Abstract

This work assesses the effectiveness of sample preservation procedures for measurements of pH_T (total scale), total dissolved inorganic carbon (C_T), and total alkalinity (A_T) in organic-rich estuarine waters. Using Hg^{II}-poisoned and unpoisoned water samples, measurements of these CO_2-system parameters were examined over a period of three months. Respiration of dissolved organic matter (DOM) in unpoisoned samples created large changes in C_T. In contrast, C_T was effectively constant in poisoned samples. Changes in A_T were observed for both poisoned and unpoisoned samples, with poisoned samples showing the greatest variation. In response to changing A_T/C_T ratios, pH_T changes were observed in both poisoned and unpoisoned samples but were relatively small in poisoned samples. In order to obtain results in organic-rich estuarine waters that reflect the in-situ CO_2-system characteristics of the samples at the time of collection, we recommend that samples obtained for C_T and A_T analysis be collected and stored separately. Samples obtained for C_T analyses should be preserved with $HgCl_2$. Samples obtained for A_T analysis should be preserved by filtration and storage in polypropylene bottles at 4°C rather than addition of $HgCl_2$. Samples obtained for pH_T analysis should be measured promptly in the field or, alternatively, preserved with $HgCl_2$ and measured in the laboratory within one week.

3.2 Introduction and Background

Field samples obtained for carbonate system analysis commonly cannot be measured promptly and are, instead, saved for subsequent analysis in a laboratory. During an investigation of the comparative geochemistries of rivers that discharge into Tampa Bay, we became interested in examining the extent to which our sample preservation procedures were effective. Consequently, we undertook time series measurements in which comparative CO_2-system changes in Hg^{II}-poisoned and unpoisoned water samples were examined over a period of three months. After our experiments had concluded, a relevant publication appeared (Mos et al., 2021), describing the effectiveness of diverse preservation and storage methods on the total alkalinity (A_T) of aqueous environmental samples (seawater, estuarine water, freshwater, and groundwater) over a period of six months. Our investigation adds to the perspectives of Mos et al. (2021) by documenting daily to weekly changes in three CO_2-system parameters (pH_T (i.e., $-\log[H^+]_T$), total dissolved inorganic carbon (C_T), and A_T) for estuarine samples stored with and without added $HgCl_2$ as a preservative.

In addition to addressing sample stability issues, and thereby the extent to which stored samples can be used to infer water sample characteristics at the time of collection, our measurements of three CO_2-system variables allows assessment of how sample-storage/preservation influences relationships between directly measured parameters (e.g., A_T) and parameters such as A_T that are calculated from C_T and pH_T. Investigations of the internal consistency of carbonate system measurements in oceanic waters (direct measurements vs. calculations) have been conducted over several decades. The internal consistency between measured and calculated CO_2-system parameters has improved over time due to improvements in both measurement procedures and refinements of the models that are used in carbonate system calculations. For oceanic data sets, a variety of investigations have shown the differences between measured total alkalinity and A_T that is calculated from pH_T and C_T are currently on the order of 3 to 4 $\mu mol\ kg^{-1}$. This difference between measured and calculated alkalinities is similar to typically observed uncertainties for A_T measurements (Millero et al., 1993; Patsavas et al., 2015; Fong and Dickson, 2019).

Prior assessments of CO_2-system internal consistency (i.e., measurements and calculations of A_T) have been limited to the range of salinity (S) within which sulfonephthalein pH indicators, such as meta–Cresol Purple (mCP) have been carefully calibrated ($20 \leq S \leq 40$). Until the recent publications of Douglas and Byrne (2017) and Müller and Rehder (2018), carbonate system internal consistency evaluations using modern pH measurement techniques in estuarine and fresh waters have not been possible. In addition to providing a general assessment on the use of Hg^{II} as a preservative for measurements of CO_2-system parameters, our investigation provides perspectives on the influence of Hg^{II} on CO_2 internal consistency calculations under estuarine conditions.

3.3 Methods and Materials

3.3.1 Sample Collection

Hillsborough River water samples were collected within 30 meters of the 2019 Hillsborough River 24-hour collection site from the boardwalk of the Lowry Park Riverside Trail (1204 W Flora St. Tampa, FL 33604) on January 26, 2021 (Figure 2.1). Water temperature and salinity were measured and recorded (Seabird Scientific Micro Thermosalinograph), and then two 30 L Niskin bottles were used to collect surficial river water. After the Niskin bottles were secured on deck, the water from each Niskin was filtered and promptly analyzed spectrophotometrically to establish the samples' initial pH_T. The filtration was performed under positive pressure using a 12V peristaltic pump (GeoTech™) and Peristaltic tubing (Masterflex®). The tubing was connected to a 142 mm diameter acrylic filter housing (GeoTech™) that contained a 0.45 µm cellulose nitrate filter (GeoTech™). Using this procedure, water samples from each Niskin were consecutively filtered into a total of 70 borosilicate glass bottles (300 mL total volume) using the methods described by Dickson et al. (2007). Half of the samples (i.e., 35 samples from one Niskin bottle) were poisoned with 100 µL of 6.5% $HgCl_2$ (LabChem™). The 35 filtered water samples from the other Niskin were not poisoned. Both sets of bottles were promptly sealed with

Apiezon™ M grease for transport. After these samples were collected and processed, additional water from each Niskin was filtered and analyzed spectrophotometrically to determine the final pH_T at the time of sampling. All water samples were then transported to the Carbon Laboratory at the U.S. Geological Survey (600 4th St. S St. Petersburg, FL 33701) where they were stored in the dark at room temperature (25°C) and sequentially analyzed, beginning hours after collection, over a period of three months for pH_T (total scale), total inorganic carbon (C_T) and total alkalinity (A_T).

3.3.2 Sample Analysis

3.3.2.1 Field Analysis (pH_T)

Recent advancements in the characterization of spectrophotometric indicator dyes and pK2e2 models for spectrophotometric pH_T and A_T analysis have enabled analysis in waters over a full river-to-sea range of salinity ($0 \leq S \geq 40$) and temperature ($0 \leq T \geq 40$) (pH: Douglas and Byrne, 2017, Rehder and Müller, 2018; A_T: Hudson-Heck et al., 2021). Spectrophotometric pH_T analyses were performed using the methods of Clayton and Byrne (1993). Each filtered pH_T sample was collected in a 10 cm pathlength cylindrical glass cell and placed within an aluminum housing (Ocean Optics) connected to an Ocean Optics LS-1 Tungsten light source and an Ocean Optics USB2000 spectrometer. Two 10 µL additions of purified M-cresol purple (mCP) indicator dye were administered with a Gilmont GS-1100 Micrometer Syringe, where pH_T was corrected for any indicator dye perturbation by back correction from the second dye addition (Clayton and Byrne, 1993). Absorbance measurements were made using the Ocean Optics software package OOIBase 32. The measurement temperature for these analyses (approximately 26.5° Celsius) was determined using a Fluke 51 II Handheld Digital Probe Thermometer. Sample pH_T was calculated on the total scale using the algorithm of Müller and Rehder (2018). Each pH_T was temperature-corrected to 20° Celsius in CO2sys.m (Van Heuven et al., 2011) using the K1K2

constants of Waters, Millero, & Woosley (2014), the KSO_4 constants of Dickson (1990), and the total boron to salinity ratio (B_T/S) of Lee et al. (2010).

3.3.2.2 Laboratory Analysis (pH_T, C_T, and A_T)

Poisoned and unpoisoned water samples bottles were analyzed over a period of three months where samples were first analyzed within hours of collection and subsequently analyzed every other day for one week. After the first week, samples were analyzed weekly for the duration of the experiment. The measurement methods used over this three-month period were identical for each type of analysis. Sample bottles were analyzed in the order they had been filled. On each day of analysis four sample bottles, two poisoned samples and two unpoisoned samples (four total) were analyzed in the following order: pH_T, C_T and A_T.

Spectrophotometric pH_T analysis in the laboratory were performed using the methods of Clayton and Byrne (1993). Sample water was poured from the borosilicate bottle into two 10 cm pathlength cylindrical glass cells. Each cylindrical cell was placed in a temperature-controlled aluminum housing (Ocean Optics) connected to an Ocean Optics LS-1 Tungsten light source and Ocean Optics USB2000 spectrometer. 10 µL of purified M-cresol purple indicator was administered with a Gilmont GS-1100 Micrometer Syringe. Absorbance measurements were made using the Ocean Optics software package OOIBase 32. The temperature of pH_T analysis (approximately 20.5° C) was measured using a Fluke 51 II Handheld Digital Probe Thermometer. Sample pH_T was calculated on the total scale from absorbance ratio measurements using the algorithm of Müller and Rehder (2018). Next, as was the case for measurements in the field, the pH_T measured after a second dye addition was used to extrapolate the two pH_T measurements to the original pH_T of the sample prior to the addition of mCP (Clayton and Byrne, 1993). The pH_T of each sample was temperature corrected to 20.0° Celsius with CO2sys.m using the

K1K2 constants of Waters, Millero, & Woosley (2014), the KSO_4 constants of Dickson (1990), and the B_T/S constant of Lee (2010).

Immediately after the pH_T measurements, water samples for duplicate total inorganic carbon (C_T) analyses were withdrawn from the same sample bottle. Using a 60 mL syringe connected to a 3-way Luer lock valve and stopper to minimize gas exchange, two 20 mL samples were drawn from each bottle. Analyses were performed with a CM5017 CO_2 carbon coulometer coupled to a CM5330 Acidification Module acidification module (UIC, Inc.) following the methods described by Dickson and Goyet (1994). Sample weights were determined using a Denver Instruments PI-214 analytical balance (± 0.1 mg). Injected sample mass was determined as the difference in syringe weights before and after each sample was injected through a septum into the stripping chamber of the acidification module. Samples were acidified with ~10 mL of 8.5% $H_3PO_4^-$ Analytical grade N_2 gas was used as the carrier gas for CO_2 from acidified samples to the coulometer. The titration endpoint was determined by the coulometer, and C_T was calculated using software from UIC, Inc. Accuracy and precision was determined from analysis of certified reference materials (CRM) from Scripps Institution of Oceanography (Dr. Andrew Dickson, Dickson, 2010) Repeated measurements (N = 51) of CRM Batch 189 and CRM Batch 183 yielded precisions of ± 1.09 and ± 0.71μmol kg^{-1} respectively (standard deviation of each average daily CRM analysis) and an accuracy of 1.43 ± 1.04 μmol kg^{-1} (average of the absolute value of the difference between each measured CRM and the reported batch concentration).

After completion of the C_T analyses, measurements of total alkalinity (A_T) were performed using the spectrophotometric methods of Yao and Byrne (1998) and Liu et al. (2015). Water sample mass (~100 g) and masses of added acid were determined gravimetrically using a Denver Instruments PI-214 analytical balance (± 0.1 mg). Water samples were analyzed in an open square glass cell (Hellma Cells, Inc.) placed within a custom plastic frame connected to an Ocean Optics LS-1 Tungsten light source and Ocean Optics USB2000 spectrometer. 100 µL of bromocresol purple (BCP) indicator dye (4 mM stock solution) was administered by pipette and the sample was titrated using 0.100 ± 0.0001 N standardized

HCl (Lab Chem) added with a plastic 10 mL syringe fitted with a Teflon syringe needle. Absorbance measurements were made using the Ocean Optics software package OOIBase 32. The pH_T of each solution was measured throughout the titration to an endpoint near pH_T 4.3. The total weight of added acid was determined from the difference in the syringe weight before and after acid addition. At the end of each titration, the solution was purged of CO_2 with a stream of N_2 gas that had been pre-saturated with H_2O. After purging, final absorbance measurements were made, and solution temperature was determined using a Fluke 51 II Handheld Digital Probe Thermometer. A_T was calculated using the BCP equations of Hudson-Heck et al. (2021). Accuracy and precision were determined from analysis of Andrew Dickson's certified reference materials (CRM). Repeated measurements (N = 33) of CRM Batch's 183, 186, and 189 yielded precisions of ± 0.93 μmol kg^{-1}, ± 0.76 μmol kg^{-1}, ± and 1.39 μmol kg^{-1} respectively and an accuracy of 0.77 ± 0.93 μmol kg^{-1}.

Internal consistency calculations of A_T, from measured pH_T and C_T were performed in CO2sys.m (Van Heuven et al., 2011) using the K1K2 constants of Waters, Millero, & Woosley (2014), the KSO_4 constants of Dickson (1990), and the B_T/S constant of Lee (2010).

3.4 Results

Clear distinctions were observed over three months between unpoisoned (pure) and poisoned ($HgCl_2$) samples for all three measured carbonate system parameters: pH_T, C_T, and A_T. Figure 1 shows measurement results for C_T analyses. From the inception of the analyses, C_T(unpoisoned) > C_T(poisoned) and the difference between C_T(unpoisoned) and C_T(poisoned) increased throughout the 91 days of analysis. The C_T of Hg^{II}-poisoned samples was essentially constant throughout the duration of the experiment (3095.5±3.2) while the C_T of unpoisoned samples increased by approximately 37 μmol kg^{-1} over 91 days. The Figure 3.1 regression of C_T vs time for the unpoisoned samples (C_T = 3100.2 + 0.4088x) indicated that C_T increased by approximately 0.41 μmol kg^{-1} per day over the course of the

experiment (Note that anomalous results obtained on day 2 for both pure and Hg^{II}-poisoned samples are not included in the figure but are shown in Appendix B Table B2.1 and B2.2).

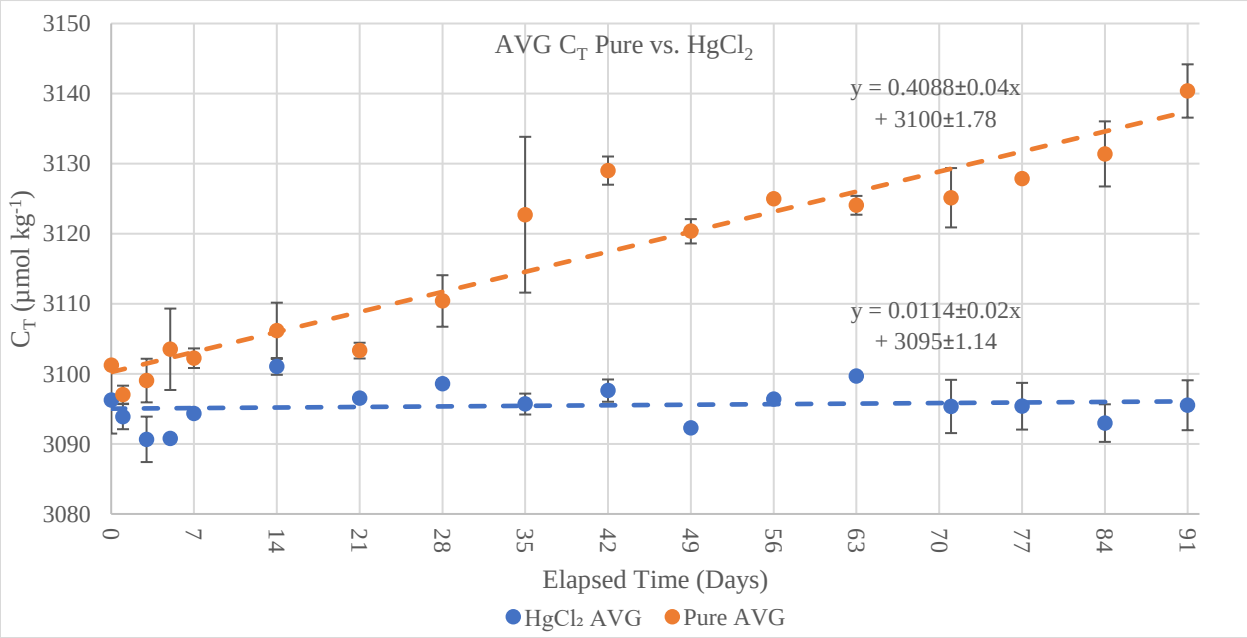

Figure 3.1. Measured C_T over time where error bars are the standard deviation of the average from each day of analysis.

A_T results also show a large difference between poisoned unpoisoned samples (Figure 3.2). Unlike C_T observations, however, a large difference between the Hg-treated and untreated samples is observed at the inception of the measurement period. Furthermore, in contrast to the near constancy of C_T for the Hg^{II}-treated samples, the A_T of the unpoisoned samples is approximately constant, while the A_T of poisoned samples decreased by approximately 26 µmol kg^{-1} over the course of the experiment. Overall, at the beginning of the measurement period the A_T of the Hg^{II}-treated samples is lower than the A_T of the untreated samples by more than 26 µmol kg^{-1}, and this difference grew to more than 45 µmol kg^{-1} at the end of the three-month period of measurements.

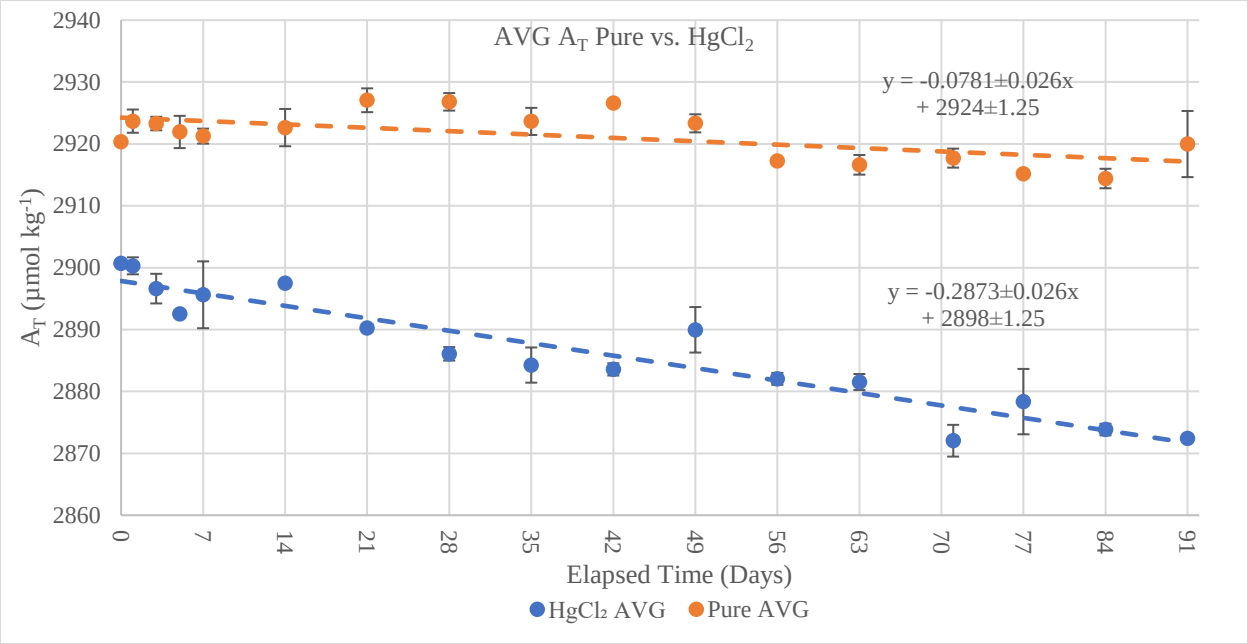

Figure 3.2. Measured A_T over time where error bars are the standard deviation of the average from each day of analysis.

Figure 3.3 shows measurement results for pH_T. Prompt pH_T measurements made in the field (shown in green) are separated from subsequent laboratory measurements by a vertical line at time zero. As was observed for C_T and A_T, a clear difference is observed between poisoned and unpoisoned samples. Consistent with the decreasing A_T and the substantially increasing C_T for the unpoisoned samples, pH_T (unpoisoned) decreased from an average of 7.377±0.022 for days 1 through 21 to 7.317±0.024 for days 28 through 91. The pH_T changes of the poisoned samples are smaller than those of the unpoisoned samples, averaging 7.302±0.018 for days 1 through 21 and 7.275±0.020 for days 28 through 91.

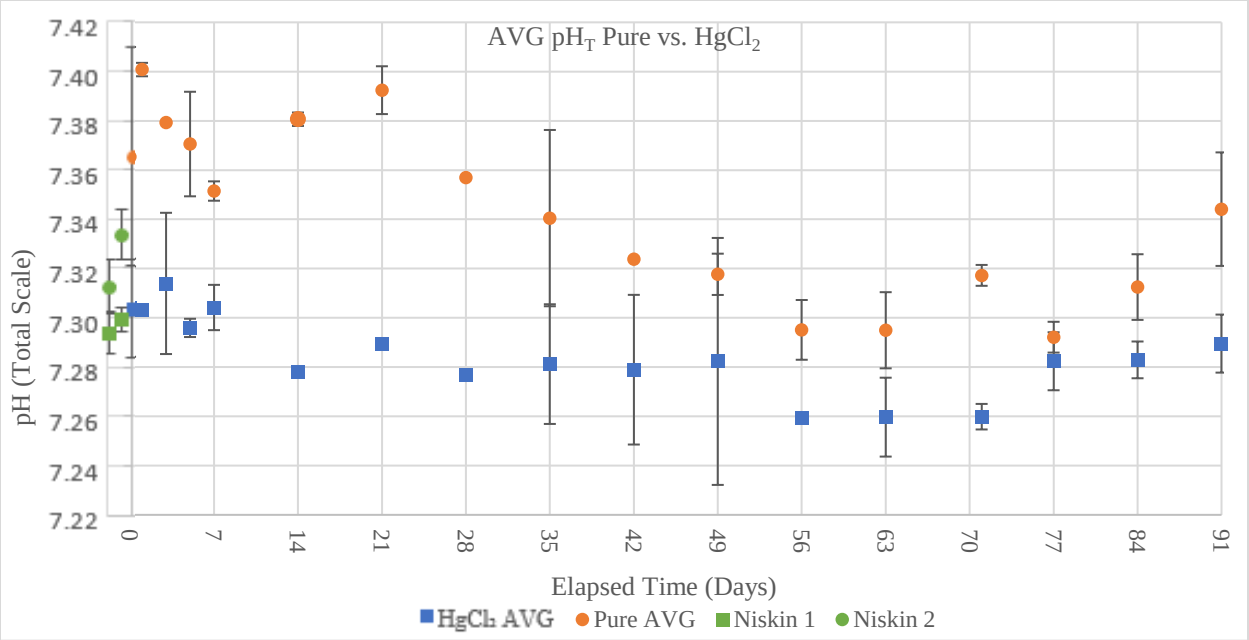

Figure 3.3. Average measured pH_T from the field, notated as Niskin, and from the laboratory, notated as $HgCl_2$ and Pure, over time where error bars are the standard deviation of the average from each day of analysis.

Figure 3.4 compares calculated and measured A_T values for unpoisoned and poisoned samples. Calculated values were larger than measured values for both the unpoisoned and poisoned samples. For unpoisoned samples the average difference between measured and calculated A_T (A_T(measured) - A_T(calculated) was -19.5±9.2 µmol kg^{-1} and the average difference for the poisoned samples was -7.52±6.8 µmol kg^{-1}.

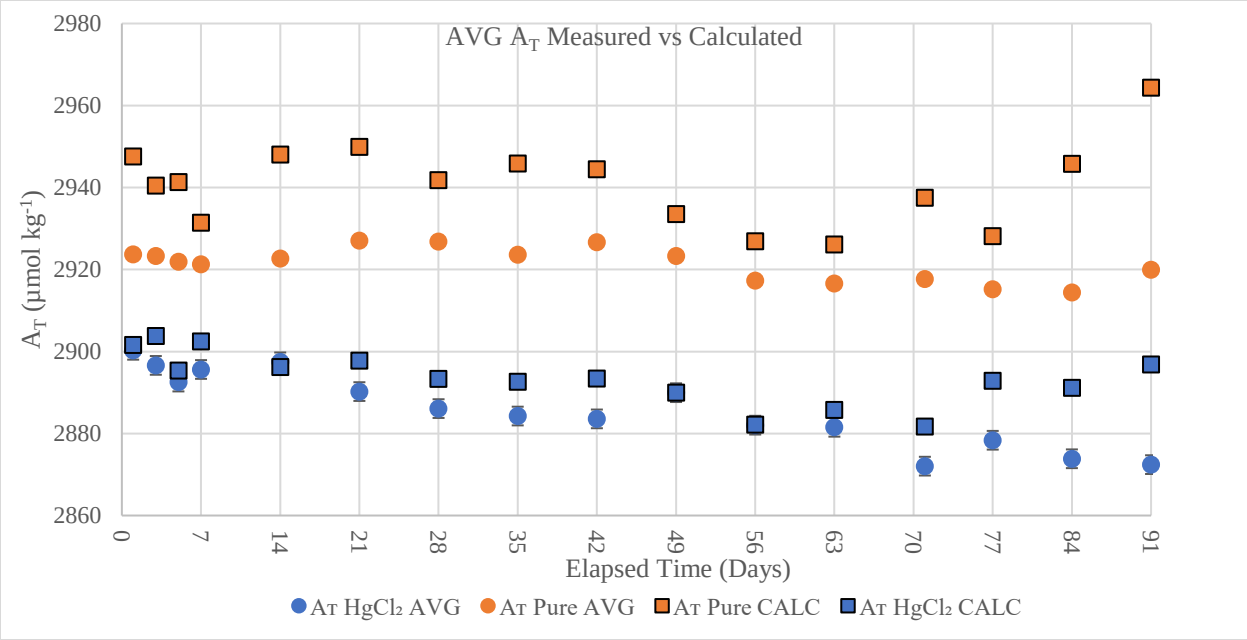

Figure 3.4. Measured versus calculated A_T for unpoisoned (pure) and poisoned ($HgCl_2$) samples over elapsed time. Calculated A_T measurements were performed using CO2sys.m using measured pH_T and C_T for the respective sample type.

3.5 Discussion

Figure 3.1 shows that respiration of dissolved organic matter (DOM) dramatically increased C_T in the unpoisoned samples. Results for the poisoned C_T samples show that the addition of $HgCl_2$ was effective at curtailing respiration. C_T results for poisoned samples were invariant over a period of three months. It is noted that, at the inception of the experiment, Figure 3.1 reveals a small C_T difference between the two sample types (poisoned and unpoisoned). The calculated C_T intercepts differ by about 5.2 ± 2.4 µmol kg^{-1}. Although this 5.2 µmol kg^{-1} difference may be a real sampling artifact (i.e., a small difference between samples collected simultaneously at the same location), the difference is quite similar to the 1 σ uncertainty (± 2.4 µmol kg^{-1}) in the calculated difference between the two intercepts. Therefore, it is likely of modest consequence.

Figure 3.2 indicates that respiration of DOM caused A_T to decrease through time in the unpoisoned samples. Consistent with the modern revised Redfield equation (P_T:N_T:C_T = 1:16:124)

(Takahashi et al., 1985, Broecker et al., 1985; Anderson and Sarmiento, 1994; Körtzinger et al., 2001)), respiration of DOM produces an increase in C_T that is about 7.3 times larger than the accompanying decrease in A_T. Based on the 37 μmol kg^{-1} increase in C_T over 91 days, and the expected factor of 7.3 difference between changes in C_T and changes in A_T (i.e., $\Delta C_T/\Delta A_T = 7.3$), the expected decrease in A_T is somewhat smaller than the observed decrease. However, considering the uncertainties in the Figure 3.1 and Figure 3.2 slopes for the unpoisoned samples, the expected change in A_T calculated as $\Delta C_T/7.3$ (i.e., 5.1 ± 0.5 μmol kg^{-1}) is reasonably consistent with the observed change in A_T (7.1 ± 2.4 μmol kg^{-1}).

Contrary to our original expectations, the poisoned A_T samples (Figure 3.2) show a larger decrease in A_T than the unpoisoned samples. Our interpretation that this decrease is due to complexation of DOM by Hg^{II} is in accord with the results and interpretation of Mos et al. (2021). Hg^{II} has a strong affinity for organic ligands such as are found in the DOM of natural waters (Andren and Harriss, 1975; Mierle and Ingram, 1991; Varshal et al., 1996; Ravichandran, 2004). The increasing A_T difference between poisoned and unpoisoned samples over time is plausibly attributable to a slowly increasing extent of DOM complexation by Hg^{II}. After the addition of a comparable concentration (0.03%) of $HgCl_2$ to fresh, estuarine and groundwater water samples stored in borosilicate glass bottles, Mos et al. (2021) observed a rapid decrease in A_T followed by a subsequent decrease over a period of 1 or 6 months. A decrease in the alkalinity of poisoned DOM-rich samples would be expected if organic bases are complexed by Hg^{II} and a portion of these complexes do not dissociate (i.e., remain untitrated) at the lowest pH in an alkalinity titration.

Figure 3.3 shows, for unpoisoned samples, the expected temporal decrease in pH_T that results from increasing C_T and decreasing A_T. For the poisoned samples, the observed decrease in pH is solely attributable to decreasing A_T through time. The initial offset in pH_T, whereby pH_T(unpoisoned) > pH_T(poisoned), is expected based on the substantial initial alkalinity difference between the poisoned and unpoisoned samples. The initial pH_T and A_T differences (poisoned vs unpoisoned) in the first weeks of the measurements were unexpected. The most plausible explanation for the initial A_T, pH_T and C_T differences

in the poisoned and unpoisoned water samples is that the two water samples had real differences in their characteristics even though they were collected in close proximity.

In the context of internal consistency measurements for open ocean conditions, Figure 3.4 observations for poisoned samples (A_T(measured) - A_T(calculated) = -7.52±6.8 µmol kg^{-1}) are quite good compared to internal consistency calculations made in marine waters of relatively similar concentration (Patsavas et al., 2015). In contrast, the corresponding relationship for unpoisoned samples is much worse. The reason for the substantial difference in the magnitudes of A_T(measured) and A_T(calculated) between poisoned and unpoisoned samples is unclear. Furthermore, the results shown in Figure 3.2 imply that the contributions of organic alkalinity to A_T are substantial, the observation that A_T(calculated) > A_T(measured) for both poisoned and unpoisoned samples is inconsistent with the fact that CO2sys.m calculations do not (i.e., cannot) account for organic alkalinity contributions to A_T. Measured A_T should be larger than calculated A_T. The fact that this is not observed points to potential problems with algorithms for CO_2-system calculations at low salinities. Resolution of this issue (i.e., differences in measured and calculated A_T) will require further detailed investigation of CO_2-system characteristics in organic-rich estuarine waters.

3.5.1 Recommendations for Sample Preservation in Organic Rich Waters

The overarching objective of storage and preservation methods is to provide samples that reflect the in-situ CO_2-system characteristics of the samples at the time of collection. The results shown in Figure 3.1 demonstrate that, for C_T measurements, poisoning samples with $HgCl_2$ is effective in achieving this objective. Over a period of three months, C_T measurements for the poisoned samples were essentially invariant while the filtered samples that were not poisoned exhibit very large changes. Although it is possible that sample storage at low temperatures, as advocated by Mos et al. (2021), would reduce or even eliminate the respiration-derived generation of C_T shown in unpoisoned samples, the effectiveness of

$HgCl_2$ additions is unequivocal. A key point here is that, while Mos et al. (2021) demonstrated that their procedures effectively eliminated changes in A_T, it is much easier to detect changes in C_T than for A_T (i.e., $\Delta C_T/\Delta A_T = 7.3$), Unless further work demonstrates that filtration in conjunction with low temperature storage eliminates changes in C_T, it appears prudent to preserve samples intended for analysis of C_T with $HgCl_2$ additions.

With respect to preservation of organic-rich samples for A_T analysis, Figure 3.2 shows that addition of $HgCl_2$ and subsequent long-term storage is inadvisable. Interactions of DOM and Hg^{II} in organic-rich samples appear to increase with time, and this confounds interpretation of A_T results that are obtained using poisoned samples. In contrast, for unpoisoned samples, although decreases in A_T are observed that are broadly consistent with the Figure 1 increases in C_T, the changes are small. As such, as shown in the study of Mos et al. (2021), it is possible that storage at lower temperature would further reduce changes in A_T during storage. As such, consistent with the results of Mos et al. (2021), samples for A_T analysis should be filtered, stored in polypropylene bottles, and refrigerated at 4°C. The results shown in Figure 3.2 suggest, as well, that the time between sample collection and analysis should be minimized. Notably, the recommendation that samples for analysis of C_T, but not A_T, are preserved with $HgCl_2$, requires that the two types of samples are stored separately.

The results shown in Figure 3.3 indicate that long-term storage of samples for pH_T analyses is problematic. Sample pH_T is very sensitive to changes in C_T and A_T. In the absence of Hg^{II} additions, respiration increases C_T (Figure 3.1) thereby decreasing the pH_T. For poisoned samples, small changes in A_T can also create problems with pH_T measurements. The solution to this issue is prompt pH_T measurements at the time of collection. In contrast to measurements of C_T and A_T, spectrophotometric pH_T measurements are uniquely amenable to analysis in the field. As an alternative, if measurements of pH_T in the laboratory are strongly preferred, it should be noted that measurements of pH_T over one week of storage (Figure 3.3) were very similar to field pH_T measurements obtained immediately before the samples were bottled.

Although further investigations of sample preservation and storage are advisable, the results obtained in this study support the following recommendations:

- Samples obtained for C_T analyses should be preserved with $HgCl_2$.
- Samples obtained for A_T analyses should be preserved by filtration and storage in polypropylene bottles at 4°C (Mos et al., 2021). Preservation with $HgCl_2$ is inadvisable.
- Measurements of pH_T should be obtained promptly in the field. If this is infeasible, samples should be preserved with $HgCl_2$ and subsequent measurements in the laboratory should be obtained within approximately one week.

3.6 Acknowledgments

I would like to thank Andrew Warren and Robert Walker at the Florida Institute of Oceanography (FIO) for providing the Niskin bottles used in this work.

Chapter Four:
Recommendations for Future Studies

In view of the CO_2-system observations described in this thesis, follow-up studies of the key variables/processes that control the relationships between CO_2-system parameters, nutrients, and discharge rates would benefit from a revised sample-collection plan. In particular, it is reasonable to recommend a detailed comparative investigation of the characteristics of the Alafia and Little Manatee Rivers. These two rivers encompass a wide range of drainage characteristics and exhibited distinctive discharge characteristics and contrasting CO_2-system profiles. Rather than utilizing a single time-series sampling location on each river, four to six sampling locations should be chosen, each of which responds to drainage from well-defined water sources (springs, wetlands, and urban streams), as well as tributaries that integrate discharge from distinct land-types (urban, agricultural, and pristine). Over a period of six months spanning the dry and wet seasons, water samples should be collected for CO_2-system and nutrient measurements before and immediately after periods of locally high discharge (i.e., as opposed to regionally high discharge). Samples for CO_2-system analysis need to be filtered and collected separately (i.e., C_T vs A_T), with samples collected for pH_T promptly analyzed in the field. The filtered samples for A_T analysis should be promptly analyzed in the laboratory, and samples obtained for C_T should be poisoned with $HgCl_2$ and measured within three months. These revised sample-collection and sample-processing strategies would more insightfully elucidate relationships between terrestrial environments and water chemistry, and more accurately represent in-situ sample conditions at the time of collection. To improve future studies regarding the preservation effects of Hg^{II} on CO_2-stsyem parameters in low salinity organic rich waters, sample types should be extracted from a single container to improve the likelihood of equivalent chemical characteristics at the inception of the experiment.

Chapter Five:

References

Anderson, L. A., & Sarmiento, J. L. (1994). Redfield ratios of remineralization determined by nutrient data analysis. *Global Biogeochemical Cycles*, *8*(1), 65–80. https://doi.org/10.1029/93gb03318

Andren, A. W., & Harriss, R. C. (1975). Observations on the association between Mercury and organic matter dissolved in Natural Waters. *Geochimica Et Cosmochimica Acta*, *39*(9), 1253–1258. https://doi.org/10.1016/0016-7037(75)90132-5

Badylak, S., & Phlips, E. J. (2008). Spatial and temporal distributions of zooplankton in Tampa Bay, Florida, including observations during a HAB event. *Journal of Plankton Research*, *30*(4), 449–465. https://doi.org/10.1093/plankt/fbn010

Beckwith, S. T., Byrne, R. H., & Hallock, P. (2019). Riverine calcium end-members improve coastal saturation state calculations and reveal regionally variable calcification potential. *Frontiers in Marine Science*, *6*. https://doi.org/10.3389/fmars.2019.00169

Boning, C. R. (2016). Alafia River, Hillsborough River, Little Manatee River, Manatee River. In *Florida's Rivers* (pp. 168–202). essay, Pineapple Press, Inc.

Broecker, W. S., Takahashi, T., & Takahashi, T. (1985). Sources and flow patterns of deep-ocean waters as deduced from potential temperature, salinity, and initial phosphate concentration. *Journal of Geophysical Research*, *90*(C4), 6925. https://doi.org/10.1029/jc090ic04p06925

Champion, K.M., & Starks, R., (2001). The Hydrology and Water Quality of Springs in West-Central Florida. Southwest Florida Water Management District, (105-126) Brooksville, FL.

Clayton, T. D., & Byrne, R. H. (1993). Spectrophotometric seawater pH measurements: Total hydrogen ion concentration Scale calibration of m-cresol purple and at-sea results. *Deep Sea Research Part I: Oceanographic Research Papers*, *40*(10), 2115–2129. https://doi.org/10.1016/0967-0637(93)90048-8

Dickson, A. G. (1990). Standard potential of the reaction: $AgCl(s)+12H_2(g)=Ag(s)+HCl(aq)$, and the standard acidity constant of the ion HSO_4^- in synthetic sea water from 273.15 to 318.15 K. *The Journal of Chemical Thermodynamics*, *22*(2), 113–127. https://doi.org/10.1016/0021-9614(90)90074-z

Dickson, A. G., & Goyet, C. (1994). Handbook of methods for the analysis of the various parameters of the carbon Dioxide system in sea Water. version 2. https://doi.org/10.2172/10107773

Dickson, A. G., Sabine, C. L., & Christian, J. R. (2007). *Guide to best practices for ocean CO2 measurements*. OCADS. https://www.ncei.noaa.gov/access/ocean-carbon-data-system/oceans/Handbook_2007.html.

Dickson, A. G. (2010). Standards for ocean measurements. Oceanography, 23(3), 34–47. https://doi.org/10.5670/oceanog.2010.22

Douglas, N. K., & Byrne, R. H. (2017). Spectrophotometric pH measurements from river to sea: Calibration of MCP for $0 \leq S \leq 40$ and $278.15 \leq T \leq 308.15$ K. *Marine Chemistry*, *197*, 64–69. https://doi.org/10.1016/j.marchem.2017.10.001

Duan, S., Banger, K., & Toor, G. (2021). Evidence of phosphate mining and Agriculture influence on Concentrations, forms, and ratios of nitrogen and phosphorus in a Florida River. *Water*, *13*(8), 1064. https://doi.org/10.3390/w13081064

Environmental Protection Commission of Hillsborough County Monthly Water Quality Data. (2020, January). Tampa Bay 2019 - Inorganic Nutrient Data

Florida Department of Environmental Protection, Report to the environmental Regulation Commission on the proposed designation of the little Manatee River as outstanding Florida WATERS (OFW) (1982). Tallahassee, FL.

Galavotti, H., Vasslides, J., Poach, M., Bohlen, C., Hunt, C. W., Liebman, M., Hu, X., McCutcheon, M., O'Donnell, J., Howard-Strobel, K., Vella, P., Lehrter, , J., Nielson, K., Largier, J., Ford, T., Steele, A., Yates, K. K., Johnson, Y., Brown, C., & Pacella, S. R. (2021). Measuring coastal acidification using in situ sensors in the National Estuary Program (2021). USGS Publications Warehouse. http://pubs.er.usgs.gov/publication/70220586.

Gordon, W. S., & Jackson, R. B. (2000). Nutrient concentrations in fine roots. *Ecology*, *81*(1), 275–280. https://doi.org/10.1890/0012-9658(2000)081[0275:ncifr]2.0.co;2

Greening, H. S. (2000, August 22). *Seagrass management: It's not just nutrients!*. Tampa Bay Water Atlas. https://pinellas.wateratlas.usf.edu/upload/documents/TBEP_04_02Notnutrients.pdf. Proceedings of a Symposium St. Petersburg, Florida

Greening, H. S., Cross, L. M., & Sherwood, E. T. (2011). A multiscale approach to Seagrass recovery in Tampa Bay, Florida. *Ecological Restoration*, *29*(1-2), 82–93. https://doi.org/10.3368/er.29.1-2.82

Greening, H., Janicki, A., Sherwood, E. T., Pribble, R., & Johansson, J. O. R. (2014). Ecosystem responses to long-term nutrient management in an urban estuary: Tampa Bay, Florida, USA. *Estuarine, Coastal and Shelf Science*, *151*, A1–A16. https://doi.org/10.1016/j.ecss.2014.10.003

Hudson-Heck, E., Liu, X., & Byrne, R. H. (2021). Purification and physical–chemical characterization of bromocresol purple for Carbon System measurements in Freshwaters, Estuaries, and oceans. *ACS Omega*, *6*(28), 17941–17951. https://doi.org/10.1021/acsomega.1c01579

Janicki, A., Pribble, R., Janicki, S., & Winowitch, M. (2001, March). *An analysis of long-term trends in Tampa Bay water quality*. Tampa Bay Water Atlas. https://www.tampabay.wateratlas.usf.edu/upload/documents/AnalysisLongTermTrendsTampWaterQuality.pdf.

Johansson, J. O. R. (2009, November). *Nutrient enrichment studies of natural phytoplankton populations in Tampa Bay*. University of South Florida Scholar Commons. https://digitalcommons.usf.edu/cgi/viewcontent.cgi?article=1042&context=basgp_report.

Körtzinger, A., Hedges, J. I., & Quay, P. D. (2001). Redfield ratios revisited: Removing the biasing effect of anthropogenic CO2. *Limnology and Oceanography*, *46*(4), 964–970. https://doi.org/10.4319/lo.2001.46.4.0964

Lee, K., Kim, T.-W., Byrne, R. H., Millero, F. J., Feely, R. A., & Liu, Y.-M. (2010). The universal ratio of boron to chlorinity for the North Pacific and North Atlantic Oceans. *Geochimica Et Cosmochimica Acta*, *74*(6), 1801–1811. https://doi.org/10.1016/j.gca.2009.12.027

Lewis, R. R., & Estevez, E. D., The ecology of Tampa Bay, Florida--an estuarine profile (1988). Washington, D.C.; Fish and Wildlife Service, U.S. Dept. of the Interior.

Liu, X., Byrne, R. H., Lindemuth, M., Easley, R., & Mathis, J. T. (2015). An automated procedure for laboratory and shipboard spectrophotometric measurements of seawater alkalinity: Continuously monitored single-step acid additions. *Marine Chemistry*, *174*, 141–146. https://doi.org/10.1016/j.marchem.2015.06.008

Liu, X., Patsavas, M. C., & Byrne, R. H. (2011). Purification and characterization of meta-Cresol purple for spectrophotometric seawater pH measurements. *Environmental Science & Technology*, *45*(11), 4862–4868. https://doi.org/10.1021/es200665d

Liu, X., Wang, Z. A., Byrne, R. H., Kaltenbacher, E. A., & Bernstein, R. E. (2006). Spectrophotometric measurements of pH in-Situ: Laboratory and Field evaluations of Instrumental Performance. *Environmental Science & Technology*, *40*(16), 5036–5044. https://doi.org/10.1021/es0601843

Meyers, S. D., & Luther, M. E. (2008). A numerical simulation of residual circulation in Tampa Bay. Part II: Lagrangian residence time. *Estuaries and Coasts*, *31*(5), 815–827. https://doi.org/10.1007/s12237-008-9085-0

Meyers, S. D., Luther, M. E., Wilson, M., Havens, H., Linville, A., & Sopkin, K. (2007). A numerical simulation of residual circulation in Tampa Bay. Part I: Low-frequency temporal variations. *Estuaries and Coasts*, *30*(4), 679–697. https://doi.org/10.1007/bf02841965

Mierle, G., & Ingram, R. (1991). The role of Humic Substances in the mobilization of Mercury from watersheds. *Water Air & Soil Pollution*, *56*(1), 349–357. https://doi.org/10.1007/bf00342282

Mining and Mitigation Division. (2021, September 15). *Phosphate*. Florida Department of Environmental Protection. Retrieved November 4, 2021, from https://floridadep.gov/water/mining-mitigation/content/phosphate.

Mos, B., Holloway, C., Kelaher, B. P., Santos, I. R., & Dworjanyn, S. A. (2021). Alkalinity of diverse water samples can be altered by mercury preservation and Borosilicate Vial Storage. *Scientific Reports*, *11*(1). https://doi.org/10.1038/s41598-021-89110-w

Mucci, A. (1983). The solubility of calcite and aragonite in seawater at various salinities, temperatures, and one atmosphere total pressure. *American Journal of Science*, *283*(7), 780–799. https://doi.org/10.2475/ajs.283.7.780

Müller, J. D., & Rehder, G. (2018). Metrology of pH measurements in Brackish Waters—part 2: Experimental characterization of Purified meta-Cresol purple For Spectrophotometric pH_T measurements. *Frontiers in Marine Science*, *5*. https://doi.org/10.3389/fmars.2018.00177

Patsavas, M. C., Byrne, R. H., Wanninkhof, R., Feely, R. A., & Cai, W.-J. (2015). Internal consistency of marine carbonate system measurements and assessments of aragonite saturation state: Insights from two U.S. coastal cruises. *Marine Chemistry*, *176*, 9–20. https://doi.org/10.1016/j.marchem.2015.06.022

Pillsbury, L. A., & Byrne, R. H. (2007). Spatial and temporal chemical variability in the Hillsborough river system. *Marine Chemistry*, *104*(1-2), 4–16. https://doi.org/10.1016/j.marchem.2006.12.005

Ravichandran, M. (2004). Interactions between Mercury and dissolved organic matter—a review. *Chemosphere*, *55*(3), 319–331. https://doi.org/10.1016/j.chemosphere.2003.11.011

Russell, M., & Greening, H. (2013). Estimating benefits in a Recovering Estuary: Tampa Bay, Florida. *Estuaries and Coasts*, *38*(S1), 9–18. https://doi.org/10.1007/s12237-013-9662-8

Ryder, P. D. (1982). Digital model of predevelopment flow in the Tertiary limestone (FLORIDAN) aquifer system in West-Central Florida. *U.S. Geological Survey, Water Resources Division*, *61*. https://doi.org/10.3133/wri8154

Sherwood, E. T., Greening, H. S., Janicki, A. J., & Karlen, D. J. (2016). Tampa Bay estuary: MONITORING long-term recovery through Regional partnerships. *Regional Studies in Marine Science*, *4*, 1–11. https://doi.org/10.1016/j.rsma.2015.05.005

Stocker, Y. V., Woodham, W. M., & Levesque, V. A. (1996). (rep.). *The effect of discharge and water quality of the Alafia River, Hillsborough River, and the Tampa Bypass Canal on nutrient loading to Hillsborough Bay, Florida* (Vol. v, 69 p. :ill. (some col.), amps ;28cm.). United States Geological Survey. Retrieved from https://doi.org/10.3133/wri954107

Takahashi, T., Broecker, W. S., & Langer, S. (1985). Redfield ratio based on chemical data from isopycnal surfaces. *Journal of Geophysical Research*, *90*(C4), 6907. https://doi.org/10.1029/jc090ic04p06907

U.S. Geological Survey, 2016, National Water Information System data available on the World Wide Web (USGS 02304510), accessed January 2021, at http://dx.doi.org/10.5066/F7P55KJN

U.S. Geological Survey, 2016, National Water Information System data available on the World Wide Web (USGS 02301500), accessed January 2021, at http://dx.doi.org/10.5066/F7P55KJN

U.S. Geological Survey, 2016, National Water Information System data available on the World Wide Web (USGS 02300500), accessed January 2021, at http://dx.doi.org/10.5066/F7P55KJN

U.S. Geological Survey, 2016, National Water Information System data available on the World Wide Web (USGS 02299950), accessed January 2021, at http://dx.doi.org/10.5066/F7P55KJN

Van Heuven, S., Rae, J. W. B., Wallace, D. W. R., Lewis, E., & Pierrot, D. (2011). MATLAB program developed for CO2 System Calculations. *Carbon Dioxide Information Analysis Center*. https://doi.org/10.3334/cdiac/otg.co2sys_matlab_v1.1 CO2SYS.m v3.1 (Sept 2020:

https://github.com/jonathansharp/CO2-System-Extd) CO2SYS.m v2 (Dec 2016: https://github.com/jamesorr/CO2SYS-MATLAB) CO2SYS.m v1 (Sept 2011: https://cdiac.ess-dive.lbl.gov/ftp/co2sys/CO2SYS_calc_MATLAB_v1.1/)

Vargo, G. Bendis, B., Reineman, V., Neeley, M.B., & Amadi-Davis I. (1994). Nutrient Bioassays in Tampa Bay: June 1993 to June 1994 Report submitted to the City of Tampa Department of Sanitary Sewers.

Varshal, G. M., Buachidze, N. S., Velyukhanova, T. K., & Chkhetia, D. N. (1996). The role of organic matter in Mercury cycle. *Global and Regional Mercury Cycles: Sources, Fluxes and Mass Balances*, 403–414. https://doi.org/10.1007/978-94-009-1780-4_20

Water Quality Standards Program, Scott, R., Lopez-Cantera, C., & Valenstein, N. (2017). Factsheet About Outstanding Florida Waters (OFW)1–4 (2017). Tallahassee, FL; Department of Environmental Protection. Section 403.061(27)

Waters, J., Millero, F. J., & Woosley, R. J. (2014). Corrigendum to "The Free proton concentration scale for seawater pH", [MARCHE: 149 (2013) 8–22]. *Marine Chemistry*, *165*, 66–67. https://doi.org/10.1016/j.marchem.2014.07.004

Weisberg, R. H., & Zheng, L. (2006). Circulation of Tampa Bay driven by buoyancy, tides, and winds, as simulated using a finite Volume Coastal Ocean model. *Journal of Geophysical Research*, *111*(C1). https://doi.org/10.1029/2005jc003067

Yao, W., & Byrne, R. H. (1998). Simplified seawater alkalinity analysis. *Deep Sea Research Part I: Oceanographic Research Papers*, *45*(8), 1383–1392. https://doi.org/10.1016/s0967-0637(98)00018-1

Yates, K. K., Dufore, C., Smiley, N., Jackson, C., & Halley, R. B. (2007). Diurnal variation of oxygen and Carbonate system parameters in Tampa Bay and Florida Bay. *Marine Chemistry*, *104*(1-2), 110–124. https://doi.org/10.1016/j.marchem.2006.12.008

Yates, K. K., Greening, H., & Morrison, G. (2011). Integrating science and resource management in Tampa Bay, Florida. *Circular*, i-280. https://doi.org/10.3133/cir1348

Yates, K. K., Moore, C. S., Goldstein, N. H., & Sherwood, E. T., (2019). Tampa Bay Ocean and Coastal Acidification Monitoring Quality Assurance Project Plan. US Department of the Interior, US Geological Survey. https://pubs.usgs.gov/of/2019/1003/ofr20191003.pdf.

Yates, K.K., Moore, C.S., & Lemon, M.K. (2019). Time series of autonomous carbonate system parameter measurements in Middle Tampa Bay, Florida, USA (ver. 3.0, March 2021): U.S. Geological Survey data release, https://doi.org/10.5066/P9BAFC7L

Yates, K. K., Moyer, R. P., Moore, C., Tomasko, D. A., Smiley, N. A., Torres-Garcia, L., Powell, C. E., Chappel, A. R., & Bociu, I. (2016). *Ocean acidification buffering effects of seagrass in Tampa Bay*. USGS Publications Warehouse RSS. https://pubs.er.usgs.gov/publication/70195217.

Appendix A:

Supplemental Information for Chapter Two

Appendix A1. Supplemental Figure for Chapter Two

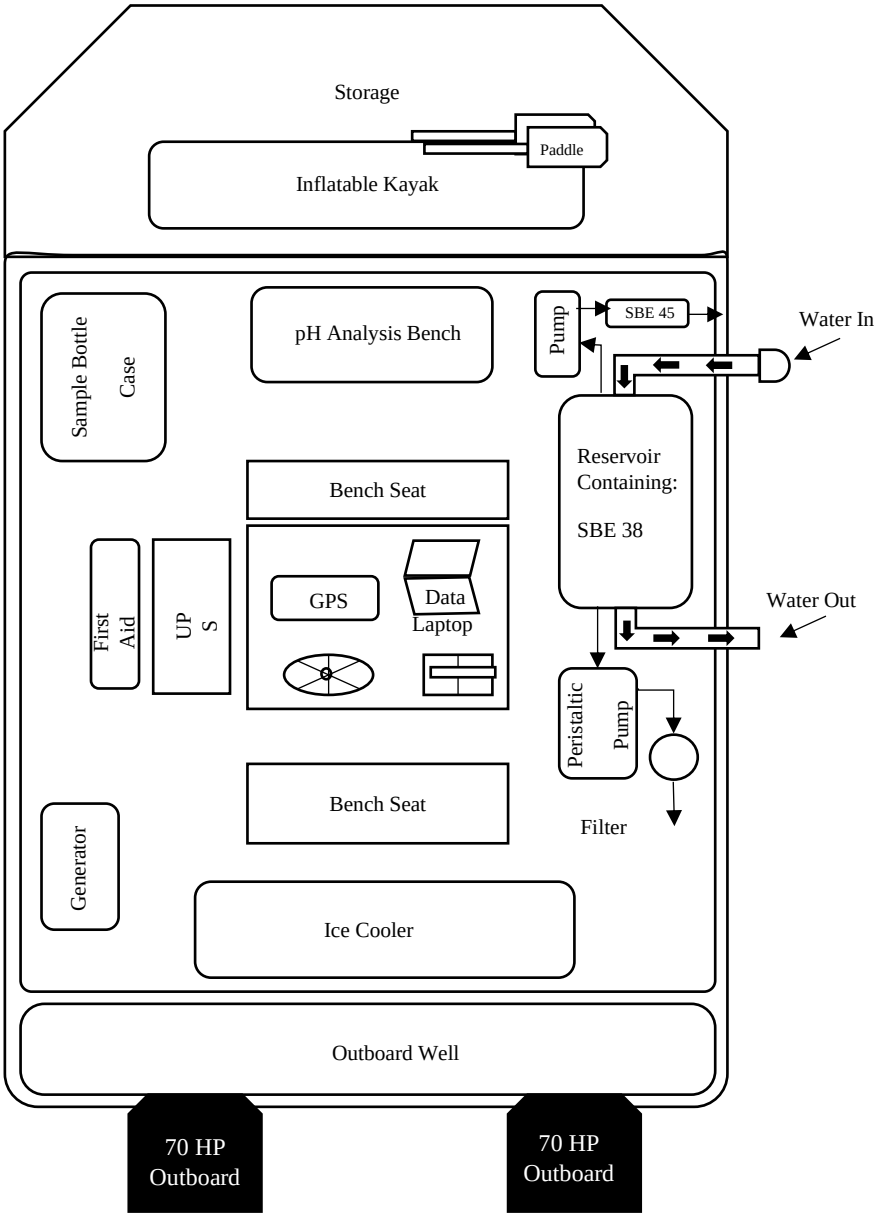

Figure A1.1. Graphic depiction of dry season U.S. Geological Survey research vessel, R/V Twin Vee.

Appendix A2: Supplemental figure for chapter two

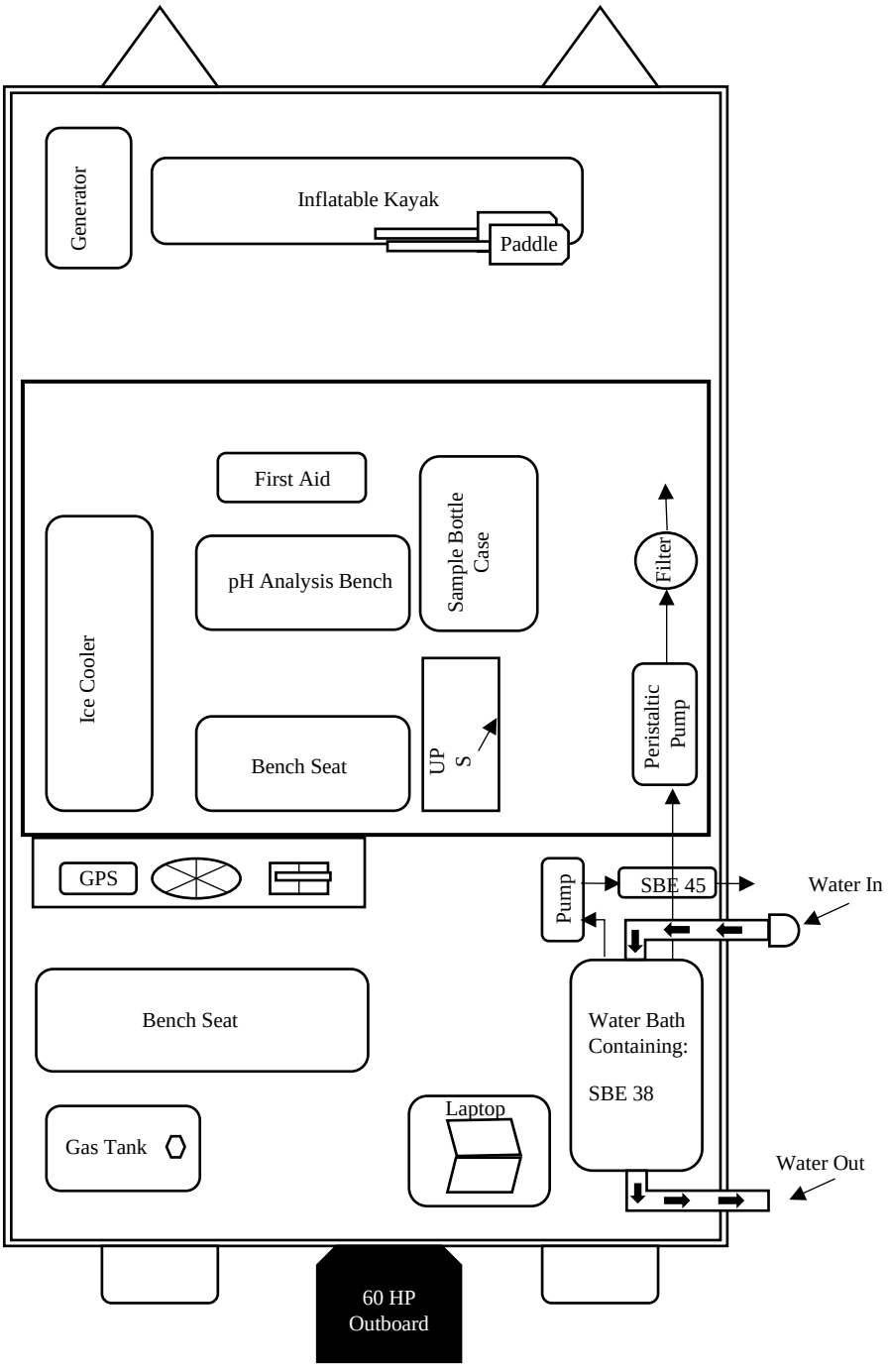

Figure A2.1. Graphic depiction of wet season U.S. Geological Survey vessel R/V Barge.

Appendix A3: Supplemental figure for chapter two

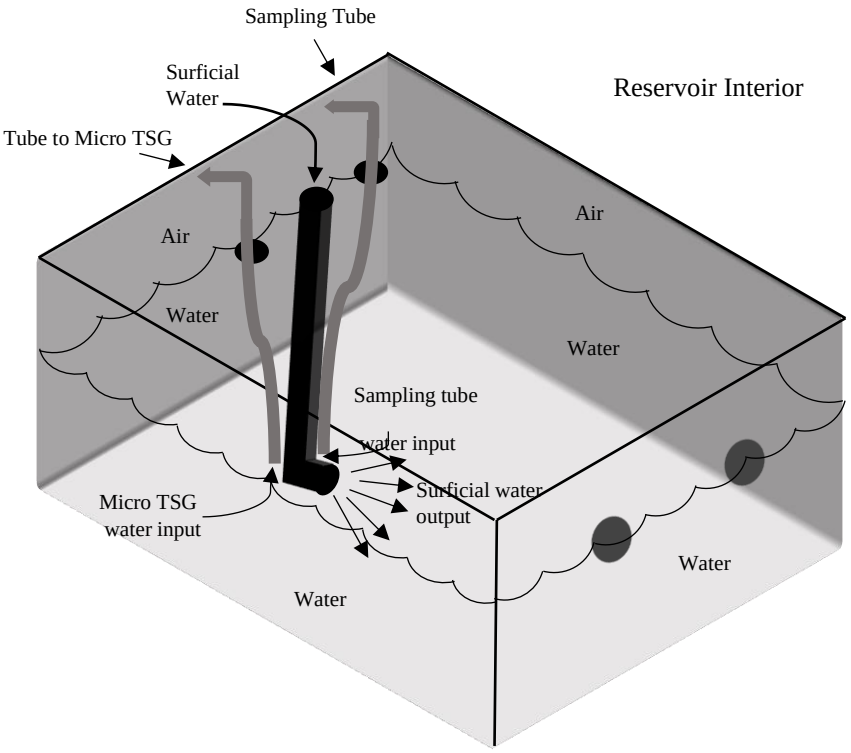

Figure A3.1. Graphic depiction of reservoir interior.

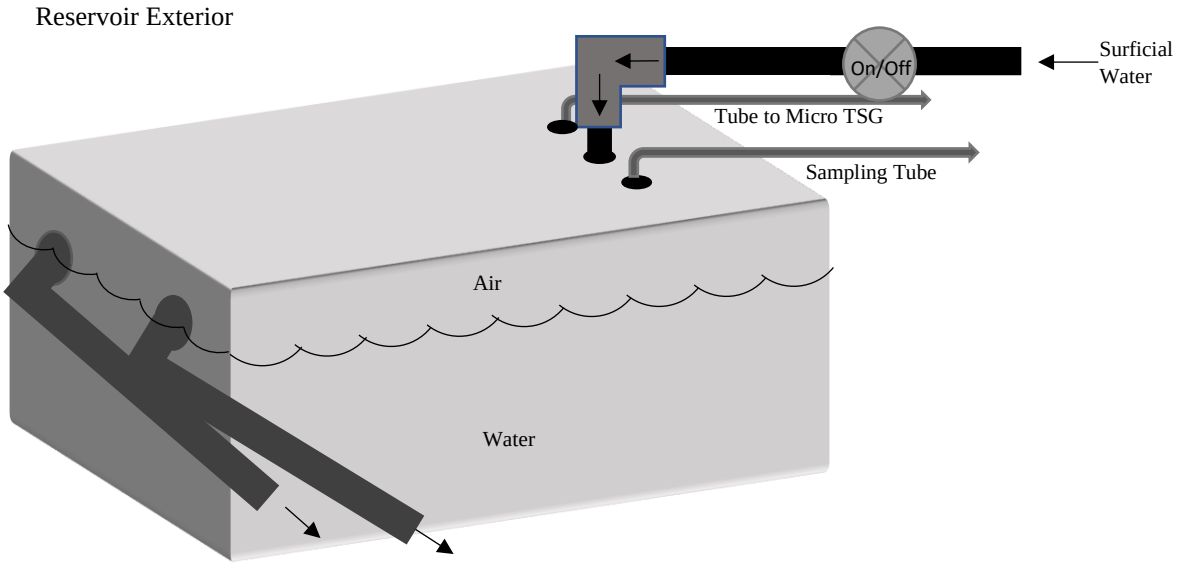

Figure A3.2. Graphical depiction of reservoir exterior.

Appendix A4: Manatee River C_T, A_T, and Ca^{2+} salinity correction

Dry season results for the Manatee River showed an influence from salinity and were corrected for this effect. The C_T, A_T, and Ca^{2+} data were plotted as a function of salinity (SAL) and the observed results were treated as end member water mixed between the River and the Bay. Using equation 1 and the slope of the calculated linear regression from each plotted parameter, (Figure A4.1, A4.2, and A4.3) these parameters were corrected for salinity effects using the average dry season salinity on each river (SAL = 0.25). This correction was necessary only for the Manatee River in the dry season.

Eq. 1. Salinity Corrected Parameter = Measured Parameter – Slope (Measured SAL – 0.25)

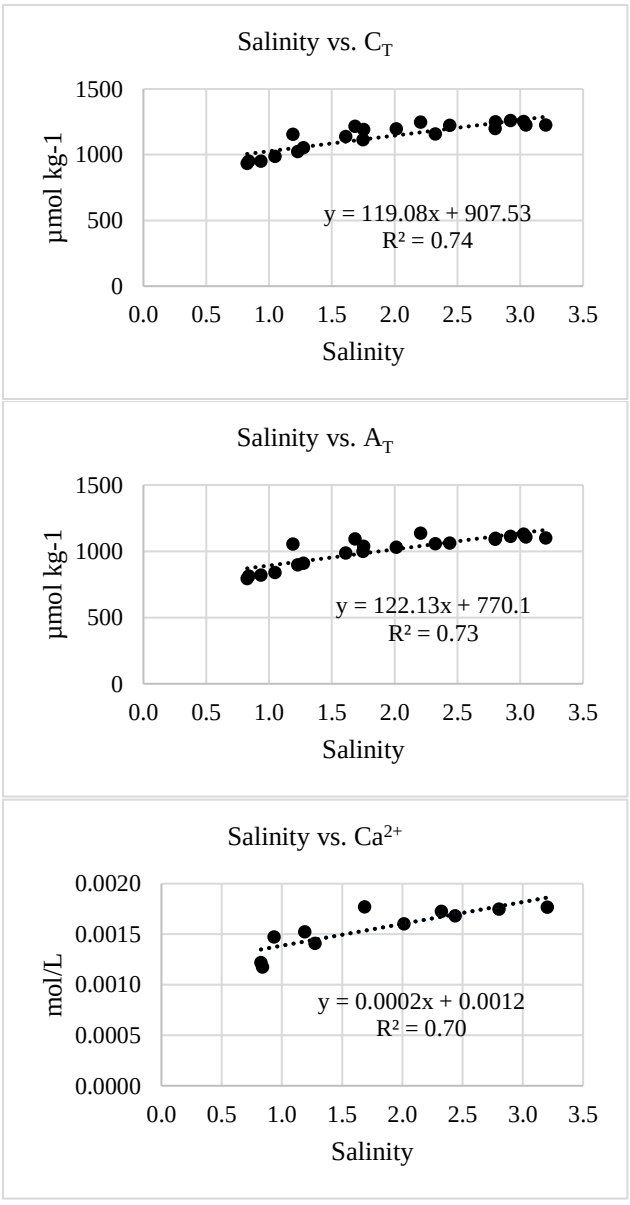

Figure A4.1. Contains the plots of C_T, A_T and Ca^{2+} plotted as a function of salinity on the Manatee River during the dry season. Linear regression from each plot was used in correcting the salinity effect in Equation 1.

Appendix A5: River discharge versus C_T and A_T

24-hour riverine discharge rate versus C_T and A_T for the dry season and the wet season (Figure 7) for each of the four rivers. Discharge data was collected from the nearest U.S. Geological Survey (USGS) National Water Information System (NWIS) stream gauge station on each river.

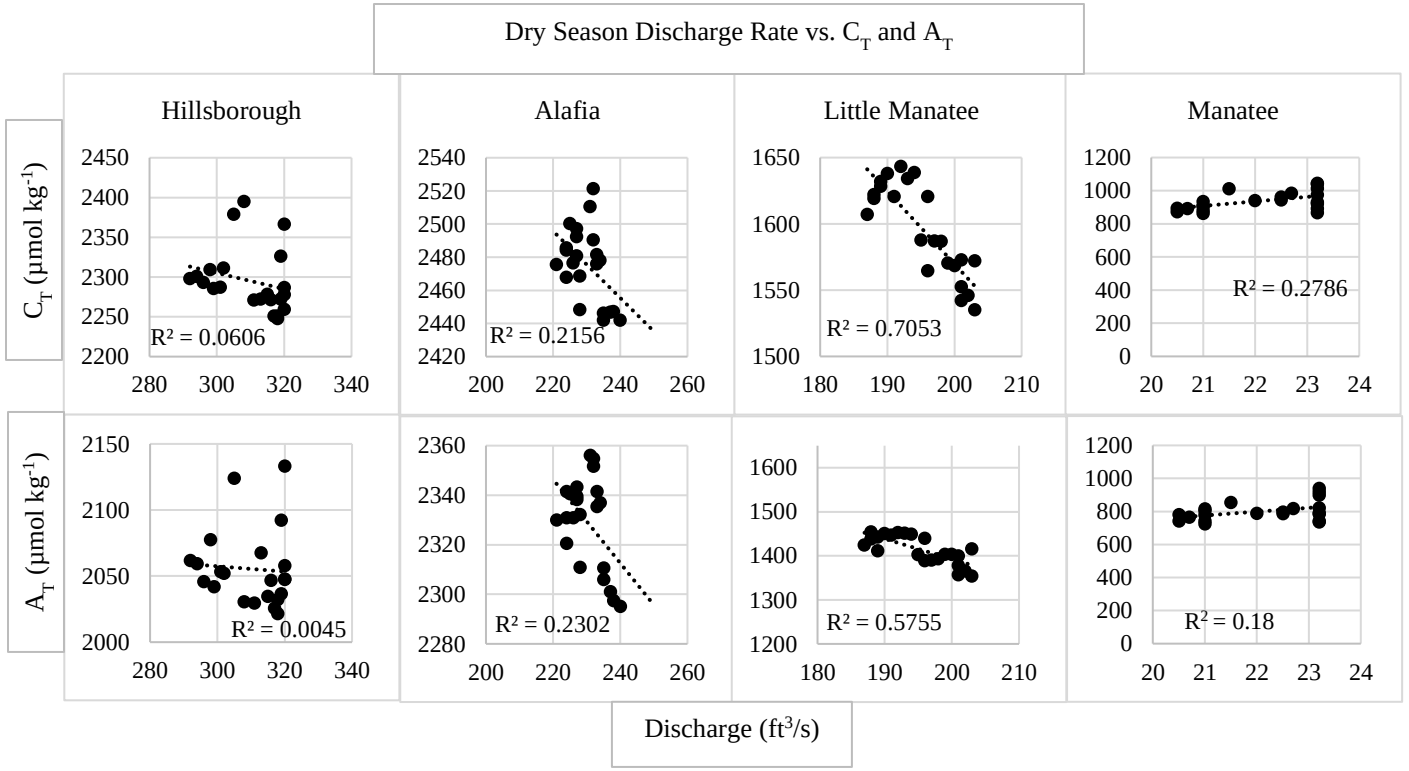

Figure A5.1. 24-hour discharge versus C_T and A_T for the four rivers during the dry season 2019.

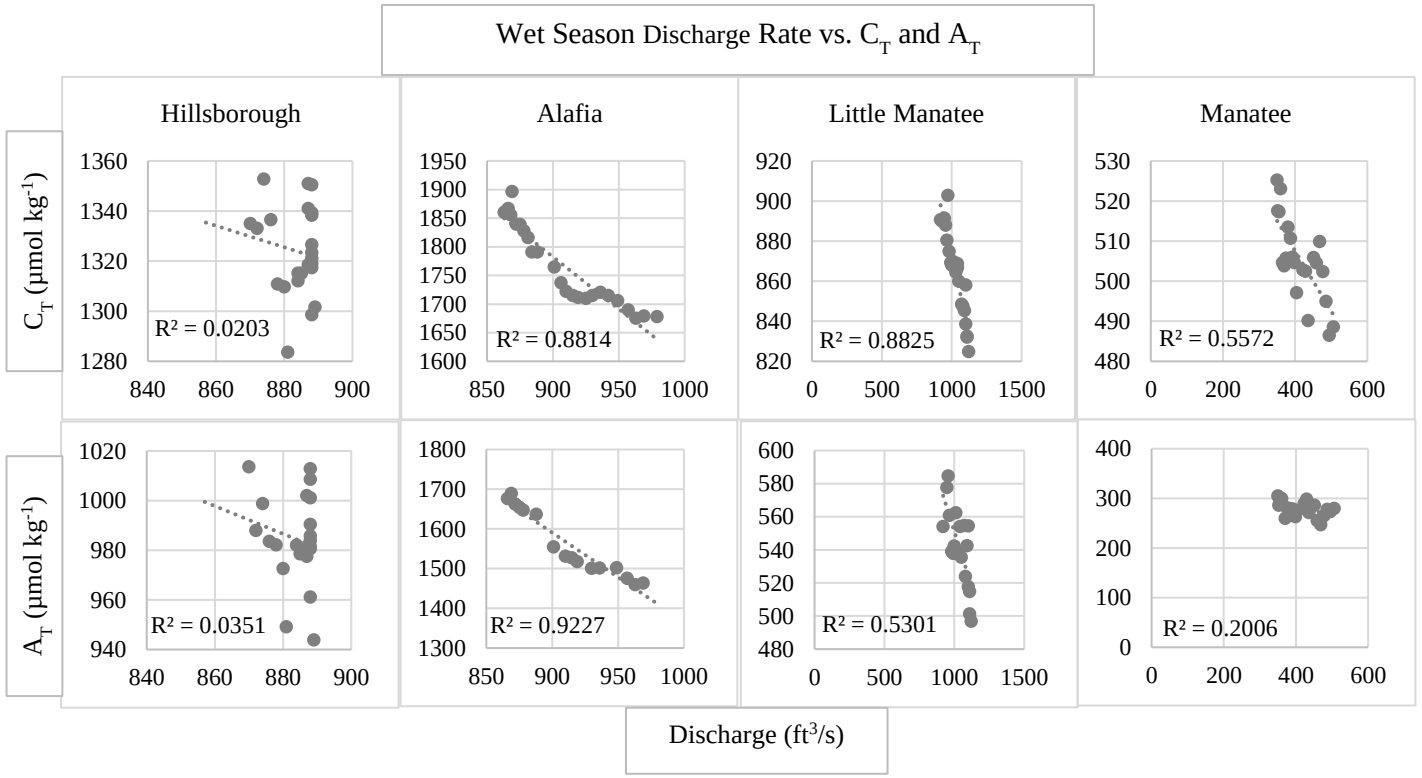

Figure A5.2. 24-hour discharge versus C_T and A_T for the four rivers during the wet season 2019.

Appendix A6: Saturation state (Ω) and associated parameters

Table A6.1. Average seasonal saturation state determined from the ion product of $[Ca^{2+}]$ and $[CO_3^{2-}]$ and the thermodynamic solubility product of Mucci (1983).

	Dry Season				Wet Season			
River	**ΩAr**	**ΩCal**	**$[Ca^{2+}]$ (µmol kg^{-1})**	**$[CO_3^{2-}]$ (µmol kg^{-1})**	**ΩAr**	**ΩCal**	**$[Ca^{2+}]$ (µmol kg^{-1})**	**$[CO_3^{2-}]$ (µmol kg^{-1})**
Hillsborough	0.532	0.580	1482.402	4.971	0.072	0.077	838.19	0.899
Alafia	0.925	0.995	1288.927	8.147	0.306	0.323	835.01	3.204
Little Manatee	0.280	0.299	933.673	3.163	0.016	0.017	544.53	0.247
Manatee	0.139	0.159	1248.899	3.365	0.010	0.011	478.68	0.160

Appendix A7: Seasonal weighted average parameter concentration calculations

Table A7.1. Average 24-hour discharge rate, C_T, and A_T for each river during the wet season.

River	AVG Discharge (ft^3/s)	AVG C_T ($\mu mol\ kg^{-1}$)	AVG A_T ($\mu mol\ kg^{-1}$)
Hillsborough	880.9	1323.9	984.5
Alafia	904.3	1767.2	1563.0
Little Manatee	1027.2	865.4	543.7
Manatee	415.7	505.4	278.6

1. To obtain the seasonal average concentration input for each river, multiply the average 24-hr river concentration ($\mu mol\ kg^{-1}$) by the average 24-hour discharge rate (ft^3/s).

Eq. 2. Average river concentration input = (Average 24-hour concentration ($\mu mol\ kg^{-1}$)) * (Average 24-hour discharge rate (ft^3/s))

2. To determine the seasonal average concentration weighted for the discharge from each of the four rivers, take the sum of each rivers seasonal average concentration input (Eq. 2) and divide it by the sum of the seasonal average 24-hr discharge rate (ft^3/s) from each of the four rivers (Table A7.1).

Eq. 3. Seasonal weighted average concentration = (Sum of average river concentration input) / (Sum of seasonal average river discharge rate (ft^3/s) from each river)

Appendix A8: Tampa Bay replacement times using wet season weighted averages

Table A8.1. Contains the average Middle Bay wet season C_T and A_T (Yates et al., 2019) and average Tampa Bay volume (Clark and MacAuley, 1989; Weisburg and Zang, 2009).

Water Body	AVG C_T ($\mu mol\ kg^{-1}$)	AVG A_T ($\mu mol\ kg^{-1}$)	Volume (ft^3)
Tampa Bay	2039	2269	1.41259E+11

1. To determine the replacement time of a parameter (seconds) in Tampa Bay, use table A8.1 and multiply the Bays volume (ft^3) by the Bays average seasonal concentration ($\mu mol\ kg^{-1}$). Next, use that result and divide it by the seasonal weighted average concentration (Eq. 3) multiplied by the sum of the seasonal average 24-hr discharge rates from each river (Table A7.1).

Eq. 4. Parameter Replacement Time (seconds) = (Bay Volume (ft^3) * Average Bay concentration ($\mu mol\ kg^{-1}$)) / (Seasonal Weighted Average Concentration ($\mu mol\ kg^{-1}$) * Sum of each rivers average 24-hr discharge rate (ft^3/s))

2. To determine the replacement time of a parameter in years, take the replacement time results from Eq 4 (seconds) and divide it by the number of seconds in a year.

Eq. 5. Parameter Replacement Time (years) = Eq. 4 result (seconds) / (number of seconds in a year)

Appendix A9: Hillsborough Bay replacement times using wet season averages

Table A9.1. Contains the average wet season Hillsborough Bay C_T and A_T (average end member Hillsborough and Alafia River concentrations) and average Hillsborough Bay volume (Weisburg and Zang, 2009).

Water Body	AVG C_T (µmol kg^{-1})	AVG A_T (µmol kg^{-1})	Volume (ft^3)
Hillsborough Bay	1801	1776	9888106682

a. Calculate the average seasonal river concentration input from the average 24-hr parameter concentrations and the average 24-hr discharge rates (Table A7.1) using (Eq. 2) of the Hillsborough and Alafia Rivers.
b. Calculate the seasonal weighted average concentration using (Eq. 3) from the sum of the average river concentration inputs determined in (a) and sum of the 24-hr average discharge rates from the Hillsborough and Alafia Rivers (Table A7.1).
c. Calculate the replacement time (seconds) of parameters in Hillsborough Bay from riverine inputs from (b) results using (Eq. 4), the volume of Hillsborough Bay (ft^3), and Hillsborough Bay concentration averages (µmol kg^{-1}) (Table A9.1).
d. Lastly, determine the Hillsborough Bay parameter replacement time in months from (c) results using (Eq. 5) and the number of seconds in a month.

Appendix A10: River versus Middle Bay Si_T results

Table A10.1. Comparison between weighted average Si_T to average Middle Bay Si_T concentrations during the dry and wet season.

	Rivers - Dry (Feb.-Mar.) and Wet (Aug.-Sep.)		Middle Bay - Dry (Nov.-May 2018-2019) and Wet (Jul.-Aug. 2019)
	Discharge AVG (ft^3/s)	**Si_T Weighted AVG (µmol kg^{-1})**	**Si_T AVG (µmol kg^{-1})**
Dry Season	761	86	4.6 ± 3.1
Wet Season	3228	55	16.9 ± 6.6

Appendix A11: Measured dry season CO_2-system parameters (C_T, A_T and pH_T)

Table A11.1. Measured dry season CO_2-system parameters with associated temperature and salinity data and time and location information.

River	Latitude	Longitude	Date	Time	Salinity	Temp	C_T 1	C_T 2	A_T 1	A_T 2	pH_T 1	pH_T 2
Hillsborough	27.88373	-82.45227	3/9/19	11:20	21.4491	21.8500	2048.0		2213.8		7.978	7.968
Hillsborough	27.92525	-82.46304	3/9/19	12:01	20.5467	21.5902	2078.0		2216.1		7.820	
Hillsborough	27.93692	-82.46198	3/9/19	12:35	16.6305	23.2259	2146.7		2195.9		7.749	
Hillsborough	27.96023	-82.46730	3/9/19	14:00	8.6752	22.8080	2275.1		2160.1		7.448	
Hillsborough	27.96966	-82.47891	3/9/19	14:30	2.4610	22.6857	2280.1		2092.0		7.406	7.397
Hillsborough	27.99008	-82.46751	3/9/19	15:00	0.6519	22.7403	2221.2		2024.7		7.425	7.417
Hillsborough	28.01319	-82.46454	3/9/19	15:30	0.3771	22.1616	2259.6		2047.3			7.503
Hillsborough	28.01319	-82.46454	3/9/19	16:30	0.3804	22.3294	2278.1		2047.8		7.552	7.551
Hillsborough	28.01319	-82.46454	3/9/19	17:30	0.3892	21.9238	2286.7		2058.0		7.444	7.441
Hillsborough	28.01319	-82.46454	3/9/19	18:30	0.5448	21.9598	2366.3		2133.3		7.403	7.400
Hillsborough	28.01319	-82.46454	3/9/19	19:30	0.4642	21.7867	2326.2	2324.4	2096.2	2088.4		7.425
Hillsborough	28.01319	-82.46454	3/9/19	20:30	0.3828	21.8528	2272.2		2036.4		7.486	7.488
Hillsborough	28.01319	-82.46454	3/9/19	21:30	0.3500	21.9438	2250.9		2032.1		7.496	7.529
Hillsborough	28.01319	-82.46454	3/9/19	22:35	0.3484	21.9373	2247.6		2021.6		7.511	7.489
Hillsborough	28.01319	-82.46454	3/9/19	23:30	0.3517	21.9106	2251.1		2025.6		7.495	7.458
Hillsborough	28.01319	-82.46454	3/10/19	0:30	0.3474	21.8455	2271.5		2046.6			7.457
Hillsborough	28.01319	-82.46454	3/10/19	1:30	0.3445	21.8181	2278.1		2034.7		7.455	7.459
Hillsborough	28.01319	-82.46454	3/10/19	3:30	0.3426	21.8500	2272.1		2067.5		7.490	7.486
Hillsborough	28.01319	-82.46454	3/10/19	5:30	0.3475	21.7942	2270.9		2029.6		7.500	7.479
Hillsborough	28.01319	-82.46454	3/10/19	8:30	0.5133	21.7716	2395.0		2030.6			7.414
Hillsborough	28.01319	-82.46454	3/10/19	9:30	0.5093	21.6653	2378.9	2380.5	2120.4	2127.8	7.371	7.339
Hillsborough	28.01319	-82.46454	3/10/19	10:30	0.3801	21.4900	2311.3		2052.0		7.372	7.380

Table A11.1. Continued

Hillsborough	28.01319	-82.46454	3/10/19	11:30	0.3477	21.5634	2287.0		2053.4		7.403	7.383
Hillsborough	28.01319	-82.46454	3/10/19	12:30	0.3443	21.7777	2285.6		2041.8		7.342	7.357
Hillsborough	28.01319	-82.46454	3/10/19	13:30	0.3563	21.9707	2309.4		2077.4		7.427	7.417
Hillsborough	28.01319	-82.46454	3/10/19	14:30	0.3588	22.3103	2293.1		2045.7		7.419	7.459
Hillsborough	28.01297	-82.46462	3/10/19	15:30	0.3595	22.6790	2300.7		2059.4		7.497	7.479
Hillsborough	27.95804	-82.46435	3/10/19	16:30	0.3681	22.8986	2297.9		2061.6			7.423
Hillsborough	27.92776	-82.46279	3/10/19	17:30	6.5447	24.1285	2285.9		2135.6		7.321	
Hillsborough	27.90787	-82.46072	3/10/19	17:45	11.1439	23.9975	2272.4		2171.8		7.317	
Hillsborough	27.93866	-82.46068	3/10/19	18:10	16.5406	24.9732	2164.5		2185.7		7.771	7.763
Hillsborough	27.90319	-82.47176	3/10/19	18:55	20.6341	24.1423	2055.2		2222.1		8.025	8.025
Alafia	27.85055	-82.41062	3/16/19	10:49	22.3347	23.5009	2097.9		2249.0		7.584	
Alafia	27.85735	-82.36939	3/16/19	11:30	17.6819	23.9667	2157.6	2152.5	2257.5	2259.2	7.477	7.458
Alafia	27.86728	-82.31995	3/16/19	12:27	12.3745	24.1679	2230.8		2268.8		7.645	
Alafia	27.88565	-82.30304	3/16/19	13:11	4.4197	23.4752	2389.5		2294.0		7.666	
Alafia	27.88546	-82.30204	3/16/19	14:30	0.2493	23.5231	2442.0		2295.2		7.654	7.646
Alafia	27.88548	-82.30208	3/16/19	15:30	0.2485	23.4499	2447.1		2297.5		7.618	7.640
Alafia	27.88548	-82.30208	3/16/19	16:30	0.248	23.4797	2446.8		2301.1		7.667	7.630
Alafia	27.88548	-82.30208	3/16/19	17:30	0.2486	23.1964	2442.0		2306.1		7.631	7.657
Alafia	27.88548	-82.30208	3/16/19	18:30	0.2487	23.095	2446.2		2310.6		7.623	7.643
Alafia	27.88548	-82.30208	3/16/19	19:30	0.2498	22.9329	2476.0		2335.5		7.659	7.646
Alafia	27.88548	-82.30208	3/16/19	20:30	0.2508	22.8586	2478.1		2337.0		7.641	
Alafia	27.88548	-82.30208	3/16/19	21:30	0.2516	22.8008	2481.6		2341.5		7.657	7.652
Alafia	27.88548	-82.30208	3/16/19	22:30	0.2518	22.7384	2490.5		2351.8		7.664	7.634
Alafia	27.88548	-82.30208	3/16/19	23:30	0.2532	22.7171	2521.3		2354.8		7.688	7.638
Alafia	27.88548	-82.30208	3/17/19	0:30	0.2533	22.7231	2510.4		2356.1		7.687	7.661
Alafia	27.88548	-82.30208	3/17/19	1:30	0.2521	22.7541	2492.4		2343.3		7.686	7.684
Alafia	27.88548	-82.30208	3/17/19	2:30	0.2501	22.8719	2468.6		2332.2			7.720

Table A11.1. Continued

Alafia	27.88548	-82.30208	3/17/19	3:30	0.2491	23.0019	2448.3		2310.9		7.717	7.728
Alafia	27.88548	-82.30208	3/17/19	7:30	0.2558	22.785	2497.2		2338.3		7.667	7.685
Alafia	27.88548	-82.30208	3/17/19	8:30	0.2555	22.7308	2480.9		2339.6		7.652	7.654
Alafia	27.88548	-82.30208	3/17/19	9:30	0.2555	22.7056	2476.6		2330.9		7.655	7.651
Alafia	27.88548	-82.30208	3/17/19	10:30	0.2607	22.7635	2500.4		2340.6		7.655	7.650
Alafia	27.88548	-82.30208	3/17/19	11:30	0.2555	22.9089	2485.6		2341.5			7.635
Alafia	27.88548	-82.30208	3/17/19	12:30	0.256	22.9845	2484.3		2330.9		7.653	7.676
Alafia	27.88548	-82.30208	3/17/19	13:30	0.256	23.1294	2475.6		2330.0		7.653	7.640
Alafia	27.86943	-82.32525	3/17/19	14:30	0.2565	23.2585	2467.8		2320.6		7.656	7.657
Alafia	27.85616	-82.39030	3/17/19	15:30	2.3726	2.3726	2339.1		2348.3			
Alafia	27.85267	-82.40451	3/17/19	16:00	9.0779	23.7413	2313.5		2304.2		7.713	
Alafia	27.85736	-82.36226	3/17/19	16:30	17.7675	24.024	2207.2		2270.6		7.751	7.756
Alafia	27.86575	-82.31980	3/17/19	16:50	21.0663	24.2715	2116.8		2253.6		7.951	7.944
Li'l Manatee	27.72762	-82.51127	3/2/19	11:10	25.4920	22.9972	2105.4		2250.4		7.853	7.872
Li'l Manatee	27.73072	-82.48123	3/2/19	11:47	25.1973	23.3693	2089.4		2215.5		7.851	7.852
Li'l Manatee	27.71463	-82.46835	3/2/19	12:32	20.4888	24.5304	2022.0		2118.4		7.842	7.840
Li'l Manatee	27.70172	-82.45079	3/2/19	13:28	11.8399	24.9079	1865.9		1838.0		7.600	7.621
Li'l Manatee	27.68389	-82.43142	3/2/19	14:04	4.3724	24.8740	1617.9		1567.4		7.761	
Li'l Manatee	27.67125	-82.41526	3/2/19	14:44	0.2521	23.8282	1572.2		1416.0			
Li'l Manatee	27.66341	-82.40749	3/2/19	15:45	0.2059	23.5255	1535.2		1354.5		7.408	7.398
Li'l Manatee	27.66340	-82.40750	3/2/19	16:30	0.2053	23.8497	1542.3		1357.1		7.447	7.441
Li'l Manatee	27.66340	-82.40750	3/2/19	17:30	0.2020	23.7347	1546.2		1366.2		7.452	7.444
Li'l Manatee	27.66340	-82.40750	3/2/19	18:30	0.2011	24.0113	1552.7	1490.8	1378.1	1374.5	7.529	7.526
Li'l Manatee	27.66340	-82.40750	3/2/19	19:30	0.2024	22.9192	1572.9		1400.5		7.547	7.560
Li'l Manatee	27.66340	-82.40750	3/2/19	20:26	0.2034	22.7081	1568.5		1403.6		7.511	7.481
Li'l Manatee	27.66340	-82.40750	3/2/19	21:30	0.2026	22.7283	1570.4		1403.6		7.472	7.519
Li'l Manatee	27.66340	-82.40750	3/2/19	22:30	0.2027	22.6344	1586.8		1393.3		7.519	7.496

Table A11.1. Continued

Li'l Manatee	27.66340	-82.40750	3/2/19	23:30	0.2027	22.6019	1587.1		1390.8		7.505	7.539
Li'l Manatee	27.66340	-82.40750	3/3/19	0:30	0.2028	22.4751	1564.6		1389.5		7.518	7.491
Li'l Manatee	27.66340	-82.40750	3/3/19	1:30	0.2037	22.2102	1587.9		1403.0		7.509	7.543
Li'l Manatee	27.66340	-82.40750	3/3/19	3:30	0.2064	21.4959	1620.8		1440.1			7.495
Li'l Manatee	27.66340	-82.40750	3/3/19	6:30	0.2087	21.3069	1638.8		1449.3		7.501	7.539
Li'l Manatee	27.66340	-82.40750	3/3/19	7:30	0.2087	21.2276	1634.2		1451.9		7.470	
Li'l Manatee	27.66340	-82.40750	3/3/19	8:30	0.2086	21.2158	1643.3		1453.1		7.471	7.440
Li'l Manatee	27.66340	-82.40750	3/3/19	9:30	0.2085	21.3798	1620.6		1447.6			7.445
Li'l Manatee	27.66340	-82.40750	3/3/19	10:30	0.2082	21.6363	1638.2		1451.4		7.409	7.385
Li'l Manatee	27.66340	-82.40750	3/3/19	11:30	0.2080	21.7902	1632.1		1412.0		7.370	
Li'l Manatee	27.66340	-82.40750	3/3/19	12:30	0.2095	22.3508	1628.4		1442.9		7.406	7.389
Li'l Manatee	27.66340	-82.40750	3/3/19	13:30	0.2137	23.1006	1622.2		1438.3		7.449	7.457
Li'l Manatee	27.66340	-82.40750	3/3/19	14:30	0.2158	23.6859	1619.2		1454.8		7.460	
Li'l Manatee	27.66340	-82.40750	3/3/19	15:50	0.2190	23.8799	1607.1		1424.6		7.500	7.532
Li'l Manatee	27.68657	-82.43480	3/3/19	16:47	3.2397	25.6221	1615.4		1538.0		7.765	7.760
Li'l Manatee	27.70199	-82.45015	3/3/19	17:12	10.4006	25.8746	1839.0		1795.8		7.521	7.508
Li'l Manatee	27.71486	-82.46831	3/3/19	17:34	16.9427	26.0326	1944.4		2004.3		7.748	7.742
Li'l Manatee	27.71769	-82.48064	3/3/19	17:48	22.8445	25.5479	2024.5		2152.8		7.899	7.897
Li'l Manatee	27.73262	-82.48608	3/3/19	18:15	24.8381	24.3831	2070.4		2241.0		7.919	7.917
Manatee	27.55127	-82.67073	2/22/19	11:30	28.8934	23.7279	2118.7	2129.3	2295.8	2294.6	7.872	7.859
Manatee	27.53934	-82.67202	2/22/19	12:30	29.8738	23.7024	2125.3		2307.6		7.866	
Manatee	27.52409	-82.62958	2/22/19	13:30	28.6890	23.9966	2120.8		2281.2		7.844	
Manatee	27.50675	-82.54318	2/22/19	14:30	22.2985	25.1892	2006.8		2067.9		7.689	
Manatee	27.52177	-82.44903	2/22/19	15:30	10.9327	26.9443	1596.9		1541.7		7.495	
Manatee	27.52281	-82.41085	2/22/19	16:30	2.8013	26.5277	1197.8		1091.1		7.428	7.402
Manatee	27.52279	-82.41082	2/22/19	17:30	3.2034	26.4620	1225.1		1101.5		7.318	7.313
Manatee	27.52277	-82.41087	2/22/19	18:30	3.0444	26.3897	1224.5		1106.5		7.315	7.307

Table A11.1. Continued

Manatee	27.52277	-82.41087	2/22/19	19:30	2.3244	26.3840	1156.6		1057.2		7.369	7.388
Manatee	27.52277	-82.41087	2/22/19	20:30	1.7492	26.4124	1112.9		998.4		7.412	7.429
Manatee	27.52277	-82.41087	2/22/19	22:00	1.2292	26.2376	1022.5		897.4			7.444
Manatee	27.52277	-82.41087	2/22/19	23:40	0.8256	25.9724	932.7		793.2		7.403	7.381
Manatee	27.52277	-82.41087	2/23/19	0:30	0.8397	25.8916	949.9		814.0		7.319	7.357
Manatee	27.52277	-82.41087	2/23/19	2:35	1.7549	25.8181	1191.1		1037.0		7.234	7.214
Manatee	27.52277	-82.41087	2/23/19	4:30	2.9233	25.6983	1259.2		1113.6		7.171	7.164
Manatee	27.52277	-82.41087	2/23/19	6:30	2.8033	25.4676	1249.0		1098.6			7.172
Manatee	27.52277	-82.41087	2/23/19	7:43	2.4382	25.4068	1222.2		1062.9		7.184	7.172
Manatee	27.52277	-82.41087	2/23/19	8:30	2.0137	25.4062	1194.8		1031.3		7.214	7.227
Manatee	27.52277	-82.41087	2/23/19	9:30	1.6110	25.4463	1137.8		987.5		7.207	7.215
Manatee	27.52277	-82.41087	2/23/19	10:30	1.2757	25.5752	1053.1		909.5		7.281	7.251
Manatee	27.52277	-82.41087	2/23/19	11:30	1.0487	25.9352	987.3		838.5			7.340
Manatee	27.52277	-82.41087	2/23/19	12:30	0.9364	25.5262	949.2	994.4	819.9	891.8		
Manatee	27.52277	-82.41087	2/23/19	13:32	1.1900	26.7531	1153.7		1053.9		7.560	7.579
Manatee	27.52277	-82.41087	2/23/19	14:30	1.6862	26.9830	1215.1		1093.2		7.519	7.509
Manatee	27.52277	-82.41087	2/23/19	15:30	2.2082	26.9815	1246.4		1136.8		7.447	7.416
Manatee	27.52277	-82.41087	2/23/19	16:30	3.0266	26.9233	1251.7		1129.5		7.328	7.317
Manatee	27.51951	-82.44710	2/23/19	17:30	8.6933	27.4274	1557.8		1503.5		7.408	7.422
Manatee	West of US-41		2/23/19	18:20	18.3775	26.1061	1818.3		1851.7			
Manatee	River Mouth		2/23/19	18:49	22.0710	25.2762	1994.1		2078.0			

Appendix A12: Measured wet season CO_2-system parameters (C_T, A_T and pH_T)

Table A12.1. Measured wet season CO_2-system parameters with associated temperature and salinity data and time and location information.

River	Latitude	Longitude	Date	Time	Salinity	Temp.	C_T 1	C_T 2	A_T 1	A_T 2	pH_T 1	pH_T 2	pH_T 3
Hillsborough	27.90807	-82.45410	8/24/19	9:00	11.8170	30.1500	1762.4	1761.3	1691.2	1688.6	7.385		
Hillsborough	27.93988	-82.45991	8/24/19	9:49	3.7800	29.0680	1541.1		1319.8		7.103		
Hillsborough	27.95732	-82.46418	8/24/19	10:19	0.8467	28.7400	1378.3		1061.1		7.087	7.100	
Hillsborough	28.01933	-82.46378	8/24/19	11:48	0.1972	28.2773	1301.6		943.9		7.077	7.090	
Hillsborough	28.01933	-82.46378	8/24/19	12:31	0.1968	28.4950	1298.6		961.2		7.182	7.182	
Hillsborough	28.01933	-82.46378	8/24/19	13:29	0.1964	28.6003	1319.1		984.0				
Hillsborough	28.01933	-82.46378	8/24/19	14:28	0.1971	28.7338	1339.4		1008.6				
Hillsborough	28.01933	-82.46378	8/24/19	15:30	0.2009	28.8957	1323.4		981.5				
Hillsborough	28.01933	-82.46378	8/24/19	16:30	0.2026	28.9389	1321.1		985.8				
Hillsborough	28.01933	-82.46378	8/24/19	17:30	0.2054	28.8164	1317.4		980.6		7.046	7.054	
Hillsborough	28.01933	-82.46378	8/24/19	18:30	0.2115	28.7422	1326.6		1001.2		7.056	7.026	6.981
Hillsborough	28.01933	-82.46378	8/24/19	19:30	0.2251	28.5993	1338.4		990.4		7.009	6.987	6.973
Hillsborough	28.01933	-82.46378	8/24/19	20:30	0.2257	28.4880	1350.4		1012.9		6.994	6.991	6.908
Hillsborough	28.01933	-82.46378	8/24/19	21:30	0.2242	28.3895	1351.0		1002.1				6.899
Hillsborough	28.01933	-82.46378	8/24/19	22:30	0.2271	28.3718	1341.0		977.6		6.959	6.953	6.942
Hillsborough	28.01933	-82.46378	8/24/19	23:30	0.2218	28.4055	1318.5		980.6		6.934	6.890	6.954
Hillsborough	27.94583	-82.46378	8/25/19	2:30	0.2123	28.4088	1315.2		978.5		6.989	7.044	
Hillsborough	27.93473	-82.46378	8/25/19	4:30	0.2132	28.3398	1312.1		982.1		6.863	6.933	6.843
Hillsborough	27.90693	-82.46378	8/25/19	6:30	0.1875	28.2367	1283.7		949.2		6.959	6.924	
Hillsborough	27.84805	-82.46378	8/25/19	7:30	0.1877	28.1543	1308.6	1310.2	966.0	979.3	6.813	6.866	6.855
Hillsborough	28.01933	-82.46378	8/25/19	8:30	0.1951	28.1818	1310.9		982.2				6.849
Hillsborough	28.01933	-82.46378	8/25/19	9:30	0.2114	28.2739	1336.5		983.7				
Hillsborough	28.01933	-82.46378	8/25/19	10:30	0.2343	28.3724	1352.8		998.8		7.024	6.950	6.972

Table A12.1. Continued

Hillsborough	28.01933	-82.46378	8/25/19	11:30	0.2076	28.5774	1333.1		988.0				7.010
Hillsborough	28.01933	-82.46378	8/25/19	12:30	0.2217	29.1012	1335.0		1013.7		7.040	7.073	6.965
Hillsborough	27.94583	-82.46038	8/25/19	13:08	1.3538	29.4200	1476.0		1169.0		7.045	6.969	
Hillsborough	27.93473	-82.40360	8/25/19	13:25	9.5899	29.8686	1732.8		1573.0		7.103	7.079	
Hillsborough	27.90693	-82.46324	8/25/19	14:45	13.2666	31.8196	1809.9	1805.2	1741.5	1743.5	7.361	7.352	
Alafia	27.84805	-82.43078	8/31/19	9:17	15.4030	29.4877	1825.8	1825.7	1831.4	1832.4	7.641	7.638	
Alafia	27.85183	-82.40969	8/31/19	9:45	10.2023	28.9473	1773.2		1677.5		7.318	7.319	7.312
Alafia	27.85340	-82.40148	8/31/19	10:05	4.3247	28.1389	1661.9		1508.4		7.244	7.253	
Alafia	27.85810	-82.37656	8/31/19	10:27	1.0338	27.9207	1637.4		1436.9		7.284	7.324	7.308
Alafia	27.87472	-82.31121	8/31/19	10:30	0.0152	27.5594	1678.0		(1467.0)		7.535	7.503	7.494
Alafia	27.88554	-82.30203	8/31/19	11:30	0.1489	27.5764	1679.1		1464.1		7.424	7.382	7.422
Alafia	27.88554	-82.30203	8/31/19	12:30	0.1496	27.6544	1675.3		1460.2		7.415	7.402	7.406
Alafia	27.88554	-82.30203	8/31/19	13:30	0.1502	27.6529	1689.6		1476.1		7.378	7.399	7.385
Alafia	27.88554	-82.30203	8/31/19	14:30	0.1519	27.8458	1703.8	1706.9	1503.0	1494.6	7.400	7.412	
Alafia	27.88554	-82.30203	8/31/19	15:30	0.1528	27.7091	1714.6		(1498.5)		7.386	7.441	
Alafia	27.88554	-82.30203	8/31/19	16:30	0.1535	27.7006	1720.2		1501.5		7.500	7.532	
Alafia	27.88554	-82.30203	8/31/19	17:30	0.1545	27.7303	1714.8		1501.1		7.376		
Alafia	27.88554	-82.30203	8/31/19	18:30	0.1549	27.7296	1709.6		1511.7				7.394
Alafia	27.88554	-82.30203	8/31/19	19:30	0.1549	27.6763	1711.5		1518.1		7.410	7.389	7.412
Alafia	27.88554	-82.30203	8/31/19	20:30	0.1551	27.6782	1715.1		1527.4		7.391	7.388	7.399
Alafia	27.88554	-82.30203	8/31/19	21:30	0.1558	27.6554	1721.9		1531.5		7.399	7.405	7.393
Alafia	27.88554	-82.30203	8/31/19	22:30	0.1526	27.6375	1737.2		(1548.4)			7.395	
Alafia	27.88554	-82.30203	8/31/19	23:30	0.1574	27.5932	1764.4		1554.7		7.392	7.387	7.375
Alafia	27.88554	-82.30203	9/1/19	2:30	0.1619	27.3979	1790.9		1637.6		7.427	7.430	7.401
Alafia	27.88554	-82.30203	9/1/19	4:30	0.1641	27.3134	1815.9		(1646.6)		7.454	7.426	7.406
Alafia	27.88554	-82.30203	9/1/19	5:30	0.1643	27.2921	1828.0		1647.4		7.457	7.427	
Alafia	27.88554	-82.30203	9/1/19	6:40	0.1656	27.2555	1839.2		1655.1		7.411	7.381	7.408

Table A12.1. Continued

Alafia	27.88554	-82.30203	9/1/19	7:30	0.1666	27.2289	1839.5		1662.8		7.408	7.402	7.424
Alafia	27.88554	-82.30203	9/1/19	8:30	0.1674	27.2287	1896.4		1690.0		7.438		7.430
Alafia	27.88554	-82.30203	9/1/19	9:30	0.1678	27.2749	1855.7		(1664.2)		7.419	7.425	7.433
Alafia	27.88554	-82.30203	9/1/19	10:30	0.1682	27.3628	1866.9		1676.9		7.460	7.437	
Alafia	27.88554	-82.30203	9/1/19	11:30	0.1684	27.5392	1860.3		1678.0		7.470	7.419	7.425
Alafia	27.85738	-82.35783	9/1/19	12:30	1.0505	29.4763	1770.5		1614.2		7.382	7.356	7.379
Alafia	27.85880	-82.38432	9/1/19	13:00	7.0632	30.2870	1799.8		1706.7		7.377	7.390	7.389
Alafia	27.84939	-82.42340	9/1/19	13:25	13.8084	31.4307	1808.8	1811.0	1830.2	1849.3	7.725	7.716	7.715
Li'l Manatee	27.74143	-82.48248	8/17/19	11:30	15.8379	28.1860	1727.4	1723.1	1736.6	1734.4	7.626	7.639	7.642
Li'l Manatee	27.74143	-82.48248	8/17/19	12:10	8.3390	27.0472	1345.6		1252.0		7.445		
Li'l Manatee	27.73108	-82.49009	8/17/19	12:45	3.5406	26.5479	1068.8		840.2				
Li'l Manatee	27.69024	-82.44967	8/17/19	14:30	0.0915	26.1166	824.9		496.8			6.648	6.746
Li'l Manatee	27.66344	-82.40760	8/17/19	15:30	0.0897	26.0784	832.1		501.2				
Li'l Manatee	27.66344	-82.40760	8/17/19	16:30	0.0897	26.0845	832.5		514.9		6.688		
Li'l Manatee	27.66344	-82.40760	8/17/19	17:30	0.0898	26.0692	858.1		517.8		6.801	6.783	
Li'l Manatee	27.66344	-82.40760	8/17/19	18:30	0.0902	26.0477	838.7		554.5		6.757	6.706	
Li'l Manatee	27.66344	-82.40760	8/17/19	19:30	0.0904	26.0019	845.4		542.4		6.711		
Li'l Manatee	27.66344	-82.40760	8/17/19	20:30	0.0912	25.9648	847.6		523.9		6.643	6.625	
Li'l Manatee	27.66344	-82.40760	8/17/19	22:30	0.0912	25.9024	848.5		554.7		6.654	6.603	
Li'l Manatee	27.66344	-82.40760	8/18/19	0:30	0.0918	25.8340	860.1		535.5		6.708	6.694	
Li'l Manatee	27.66344	-82.40760	8/18/19	1:30	0.0921	25.7976	866.7		(582.3)		6.768	6.877	
Li'l Manatee	27.66344	-82.40760	8/18/19	2:30	0.0923	25.7559	868.8		554.0			6.872	
Li'l Manatee	27.66344	-82.40760	8/18/19	3:30	0.0963	25.7292	864.6		538.4		6.806		
Li'l Manatee	27.66344	-82.40760	8/18/19	5:30	0.0930	25.6661	869.7		562.4		6.795		
Li'l Manatee	27.66344	-82.40760	8/18/19	6:30	0.0931	25.6346	868.0		542.2		6.740	6.683	
Li'l Manatee	27.66344	-82.40760	8/18/19	7:30	0.0934	25.6453	869.2		537.9		6.825		
Li'l Manatee	27.66344	-82.40760	8/18/19	8:30	0.0937	26.6945	872.9	875.9	538.9	557.8	6.939		6.934

Table A12.1. Continued

Li'l Manatee	27.66344	-82.40760	8/18/19	9:30	0.0939	25.8146	902.8		(700.0)		6.840	6.757	
Li'l Manatee	27.66344	-82.40760	8/18/19	10:30	0.0941	26.0285	880.5		560.8		6.717		
Li'l Manatee	27.66344	-82.40760	8/18/19	11:30	0.0945	26.2567	888.0		584.6		6.742		
Li'l Manatee	27.66344	-82.40760	8/18/19	12:30	0.0947	26.4939	891.4		577.6				
Li'l Manatee	27.66344	-82.40760	8/18/19	13:30	0.0950	26.5132	890.7		(553.7)				
Li'l Manatee	27.66344	-82.40760	8/18/19	14:30	0.0950	26.6704	890.0		(574.6)				
Li'l Manatee	27.66344	-82.40760	8/18/19	15:30	0.0952	26.6006	890.7		554.1		6.616		
Li'l Manatee	27.66791	-82.42923	8/18/19	16:30	0.1027	27.4208	909.3		575.9		6.765	6.668	6.741
Li'l Manatee	27.67063	-82.43944	8/18/19	17:30	1.0289	27.8257	1046.5		767.8		6.779		
Li'l Manatee	27.68898	-82.44465	8/18/19	18:00	9.3623	28.6152	1611.9		1537.8		7.246	7.231	7.269
Li'l Manatee	27.71455	-82.46677	8/18/19	18:30	13.4223	29.3274	1654.1	1663.5	1635.5	1641.0	7.507	7.493	7.498
Manatee	27.50881	-82.58923	8/10/19	11:15	19.0000	31.3970	1671.2	1666.8	1784.0	1774.8	7.968	7.960	
Manatee	27.53384	-82.66974	8/10/19	12:20	12.2266	31.1988	1499.3		1556.6		8.008	7.989	
Manatee	27.53116	-82.64210	8/10/19	13:40	5.1292	30.8315	1353.8		1244.9		7.383	7.356	
Manatee	27.50456	-82.57698	8/10/19	14:30	0.2155	30.2502	659.9		421.3		7.086		
Manatee	27.52764	-82.46000	8/10/19	16:00	0.0731	28.7716	488.6		279.8		6.760	6.773	
Manatee	27.52283	-82.41096	8/10/19	17:30	0.0667	28.5670	486.5		273.3				
Manatee	27.52279	-82.41097	8/10/19	18:30	0.0672	28.4058	494.9		278.3		6.745	6.764	
Manatee	27.52279	-82.41097	8/10/19	19:30	0.0677	28.2843	502.4		265.4		6.749	6.764	
Manatee	27.52279	-82.41097	8/10/19	20:30	0.0681	28.2717	509.9		247.2		6.623	6.609	
Manatee	27.52279	-82.41097	8/10/19	21:30	0.0684	28.3671	504.6		255.8		6.714	6.727	
Manatee	27.52279	-82.41097	8/10/19	22:30	0.0692	28.4632	505.9		286.7		6.664	6.707	
Manatee	27.52279	-82.41097	8/11/19	0:30	0.0693	28.5251	487.6	492.7	271.3	281.2	6.642	6.638	
Manatee	27.52279	-82.41097	8/11/19	1:30	0.0693	28.4407	502.5		298.4		6.700	6.722	
Manatee	27.52279	-82.41097	8/11/19	2:30	0.0692	28.3899	502.8		289.7		6.669	6.727	
Manatee	27.52279	-82.41097	8/11/19	5:30	0.0701	28.4704	497.1		275.2		6.640		
Manatee	27.52279	-82.41097	8/11/19	6:30	0.0710	28.4763	504.7		263.0		6.687	6.716	6.790

Table A12.1. Continued

Manatee	27.52279	-82.41097	8/11/19	7:30	0.0714	28.5413	506.0		278.3			6.695	
Manatee	27.52279	-82.41097	8/11/19	8:30	0.0715	28.6161	510.7		279.3			6.651	
Manatee	27.52279	-82.41097	8/11/19	9:30	0.0714	28.8118	513.5		278.0				
Manatee	27.52279	-82.41097	8/11/19	10:30	0.0713	29.1640	505.8		281.1				
Manatee	27.52279	-82.41097	8/11/19	11:30	0.0716	29.1151	503.9		259.9				
Manatee	27.52279	-82.41097	8/11/19	12:30	0.0723	29.4029	504.7		(268.3)		6.938		
Manatee	27.52279	-82.41097	8/11/19	13:30	0.0731	29.5864	523.1		300.0				
Manatee	27.52279	-82.41097	8/11/19	14:30	0.0734	29.9543	516.3	518.3	298.6	279.0		7.051	7.111
Manatee	27.52279	-82.41097	8/11/19	15:30	0.0747	29.9211	517.6		286.5				
Manatee	27.52279	-82.41097	8/11/19	16:00	0.0760	29.9601	525.3		305.4		7.082		
Manatee	27.51841	-82.42807	8/11/19	17:30	0.3438	29.9908	954.2		781.0		7.267		
Manatee	27.52646	-82.50118	8/11/19	18:15	2.0555	30.5681	1282.8		1170.8		7.323		
Manatee	27.50249	-82.56700	8/11/19	19:00	14.6925	30.9017	1616.7		1631.5		7.724		

Appendix A13: Measured dry season nutrient concentrations

Table A13.1: Dry season inorganic nutrients (µmol kg $^{-1}$). P_T is inorganic phosphate, Si_T is inorganic silica, N_T is (NO_3^{2-}+NO_2^-), and NH_4^- is inorganic ammonia.

River	Latitude	Longitude	Date	Time	P_T 1	P_T 2	Si_T 1	Si_T 2	N_T 1	N_T 2	NH_4^- 1	NH_4^- 2
Hillsborough	27.88373	-82.45227	3/9/19	11:20	2.18		6.92		0.01		0.00	
Hillsborough	27.92525	-82.46304	3/9/19	12:01	5.11		35.54		0.00		0.00	
Hillsborough	27.93692	-82.46198	3/9/19	12:35	4.52		39.12		1.57		0.27	
Hillsborough	27.96023	-82.46730	3/9/19	14:00	2.62		61.06		2.87		2.32	
Hillsborough	27.96966	-82.47891	3/9/19	14:30	4.27		68.60		5.31		1.85	
Hillsborough	27.99008	-82.46751	3/9/19	15:00	4.67		77.36		4.10		0.77	
Hillsborough	28.01319	-82.46454	3/9/19	15:30	4.78		86.83		6.83		0.46	
Hillsborough	28.01319	-82.46454	3/9/19	16:30	4.35		87.67		3.26		0.61	
Hillsborough	28.01319	-82.46454	3/9/19	17:30	4.92		87.28		7.28		0.58	
Hillsborough	28.01319	-82.46454	3/9/19	18:30	4.68		94.03		4.39		0.64	
Hillsborough	28.01319	-82.46454	3/9/19	19:30	4.96	4.87	90.75	91.23	5.62	7.04	0.90	1.07
Hillsborough	28.01319	-82.46454	3/9/19	20:30	5.06		86.88		6.04		1.24	
Hillsborough	28.01319	-82.46454	3/9/19	21:30	5.16		86.21		5.72		1.29	
Hillsborough	28.01319	-82.46454	3/9/19	22:35	5.03		87.01		5.82		1.41	
Hillsborough	28.01319	-82.46454	3/9/19	23:30	5.08		86.50		5.16		1.28	
Hillsborough	28.01319	-82.46454	3/10/19	0:30	5.09		85.72		5.48		1.37	
Hillsborough	28.01319	-82.46454	3/10/19	1:30	5.12		86.83		5.65		1.50	
Hillsborough	28.01319	-82.46454	3/10/19	3:30	5.12		88.35		5.31		1.46	
Hillsborough	28.01319	-82.46454	3/10/19	5:30	4.74		84.28		4.15		1.59	
Hillsborough	28.01319	-82.46454	3/10/19	8:30	4.33		66.75		3.75		1.38	
Hillsborough	28.01319	-82.46454	3/10/19	9:30	4.90	5.02	92.43	88.80	5.25	7.52	1.45	1.57
Hillsborough	28.01319	-82.46454	3/10/19	10:30	5.13		86.01		7.91		1.57	
Hillsborough	28.01319	-82.46454	3/10/19	11:30	5.22		83.05		8.27		1.66	

Table A13.1. Continued.

Hillsborough	28.01319	-82.46454	3/10/19	12:30	5.20		88.91		8.35		1.43	
Hillsborough	28.01319	-82.46454	3/10/19	13:30	5.20		86.31		8.58		1.35	
Hillsborough	28.01319	-82.46454	3/10/19	14:30	4.43		72.03		6.51		0.80	
Hillsborough	28.01297	-82.46462	3/10/19	15:30	5.09		84.96		9.39		0.91	
Hillsborough	27.95804	-82.46435	3/10/19	16:30	4.79		87.91		5.44		0.57	
Hillsborough	27.92776	-82.46279	3/10/19	17:30	4.78		58.04		7.33		3.23	
Hillsborough	27.90787	-82.46072	3/10/19	17:45	4.91		55.65		5.78		3.30	
Hillsborough	27.93866	-82.46068	3/10/19	18:10	4.61		42.04		1.30		0.27	
Hillsborough	27.90319	-82.47176	3/10/19	18:55	3.55		16.54		0.29		0.30	
Alafia	27.85055	-82.41062	3/16/19	10:49	3.57		27.87		0.09		0.00	
Alafia	27.85735	-82.36939	3/16/19	11:30	5.61		46.07		4.19		0.11	
Alafia	27.86728	-82.31995	3/16/19	12:27	7.27		67.79		8.65		0.25	
Alafia	27.88565	-82.30304	3/16/19	13:11	14.90		82.83		42.04		1.66	
Alafia	27.88546	-82.30204	3/16/19	14:30	20.94		131.86		51.69		1.93	
Alafia	27.88548	-82.30208	3/16/19	15:30	22.78		126.37		46.06		2.76	
Alafia	27.88548	-82.30208	3/16/19	16:30	23.49		131.87		53.53		2.15	
Alafia	27.88548	-82.30208	3/16/19	17:30	23.29		128.48		53.59		2.16	
Alafia	27.88548	-82.30208	3/16/19	18:30	23.37		127.14		51.61		2.03	
Alafia	27.88548	-82.30208	3/16/19	19:30								
Alafia	27.88548	-82.30208	3/16/19	20:30	20.28		(80.04)		(32.45)		1.65	
Alafia	27.88548	-82.30208	3/16/19	21:30	23.02		130.26		46.94		1.88	
Alafia	27.88548	-82.30208	3/16/19	22:30	22.68		130.06		44.52		1.96	
Alafia	27.88548	-82.30208	3/16/19	23:30	20.46		129.80		53.70		2.03	
Alafia	27.88548	-82.30208	3/17/19	0:30	20.71		127.60		51.65		2.07	
Alafia	27.88548	-82.30208	3/17/19	1:30	(12.37)		127.94		35.27		1.75	
Alafia	27.88548	-82.30208	3/17/19	2:30	21.39		129.93		52.42		2.17	
Alafia	27.88548	-82.30208	3/17/19	3:30	22.72		133.89		38.90		1.96	

Table A13.1. Continued.

Alafia	27.88548	-82.30208	3/17/19	7:30	22.67		132.68		43.25		1.89	
Alafia	27.88548	-82.30208	3/17/19	8:30	22.16		133.56		40.18		0.45	
Alafia	27.88548	-82.30208	3/17/19	9:30	23.00		131.40		55.57		0.60	
Alafia	27.88548	-82.30208	3/17/19	10:30	22.50		137.57		55.06		0.51	
Alafia	27.88548	-82.30208	3/17/19	11:30	22.18		135.73		38.58		0.28	
Alafia	27.88548	-82.30208	3/17/19	12:30	22.62		134.07		49.33		1.13	
Alafia	27.88548	-82.30208	3/17/19	13:30	22.52		134.80		45.45		0.66	
Alafia	27.86943	-82.32525	3/17/19	14:30	23.21		132.93		54.61		0.60	
Alafia	27.85616	-82.39030	3/17/19	15:30	16.58		126.89		10.87		0.00	
Alafia	27.85267	-82.40451	3/17/19	16:00	10.38		83.89		10.02		0.33	
Alafia	27.85736	-82.36226	3/17/19	16:30	7.67		48.63		8.51		1.66	
Alafia	27.86575	-82.31980	3/17/19	16:50	4.85		38.82		0.09		0.00	
Li'l Manatee	27.72762	-82.51127	3/2/19	11:10	1.57		9.22		0.55		0.25	
Li'l Manatee	27.73072	-82.48123	3/2/19	11:47	1.57		10.09		0.09		0.00	
Li'l Manatee	27.71463	-82.46835	3/2/19	12:32	1.31		6.31		0.08		0.00	
Li'l Manatee	27.70172	-82.45079	3/2/19	13:28	2.34		13.21		0.99		0.22	
Li'l Manatee	27.68389	-82.43142	3/2/19	14:04	4.16		19.78		0.29		0.00	
Li'l Manatee	27.67125	-82.41526	3/2/19	14:44	6.55		34.59		8.99		0.06	
Li'l Manatee	27.66341	-82.40749	3/2/19	15:45	6.66		43.44		12.27		1.00	
Li'l Manatee	27.66340	-82.40750	3/2/19	16:30	6.63		25.76		12.09		0.63	
Li'l Manatee	27.66340	-82.40750	3/2/19	17:30	6.45		40.32		12.26		0.85	
Li'l Manatee	27.66340	-82.40750	3/2/19	18:30	6.63	6.49	33.21	42.57	12.20	12.47	0.85	0.89
Li'l Manatee	27.66340	-82.40750	3/2/19	19:30	6.15		35.98		12.45		0.88	
Li'l Manatee	27.66340	-82.40750	3/2/19	20:26	6.44		39.52		12.40		0.68	
Li'l Manatee	27.66340	-82.40750	3/2/19	21:30	6.52		43.30		11.87		1.25	
Li'l Manatee	27.66340	-82.40750	3/2/19	22:30	6.42		44.06		12.89		1.65	
Li'l Manatee	27.66340	-82.40750	3/2/19	23:30	6.33		44.74		12.80		1.90	

Table A13.1. Continued.

Li'l Manatee	27.66340	-82.40750	3/3/19	0:30	6.59		37.87		12.54		1.37	
Li'l Manatee	27.66340	-82.40750	3/3/19	1:30	6.22		43.75		11.64		1.48	
Li'l Manatee	27.66340	-82.40750	3/3/19	3:30								
Li'l Manatee	27.66340	-82.40750	3/3/19	6:30	6.44		48.51		12.27		1.58	
Li'l Manatee	27.66340	-82.40750	3/3/19	7:30	6.56		46.33		12.71		1.62	
Li'l Manatee	27.66340	-82.40750	3/3/19	8:30	5.57		33.10		9.81		1.31	
Li'l Manatee	27.66340	-82.40750	3/3/19	9:30	6.35		32.91		11.92		1.69	
Li'l Manatee	27.66340	-82.40750	3/3/19	10:30	6.32		45.41		11.90		1.59	
Li'l Manatee	27.66340	-82.40750	3/3/19	11:30	6.71		39.73		12.09		1.65	
Li'l Manatee	27.66340	-82.40750	3/3/19	12:30	6.48		40.48		11.92		1.67	
Li'l Manatee	27.66340	-82.40750	3/3/19	13:30	6.05		35.82		11.55		2.51	
Li'l Manatee	27.66340	-82.40750	3/3/19	14:30	5.96		43.02		10.82		2.07	
Li'l Manatee	27.66340	-82.40750	3/3/19	15:50	5.88		41.26		9.86		1.72	
Li'l Manatee	27.68657	-82.43480	3/3/19	16:47	5.18		25.56		0.00		1.30	
Li'l Manatee	27.70199	-82.45015	3/3/19	17:12	1.93		13.16		0.15		0.92	
Li'l Manatee	27.71486	-82.46831	3/3/19	17:34	2.21		12.29		0.00		1.09	
Li'l Manatee	27.71769	-82.48064	3/3/19	17:48	1.97		13.69		0.00		1.27	
Li'l Manatee	27.73262	-82.48608	3/3/19	18:15	1.60		12.66		0.00		1.40	
Manatee	27.55127	-82.67073	2/22/19	11:30	1.61		11.91		0.11		0.00	
Manatee	27.53934	-82.67202	2/22/19	12:30	1.30		10.53		0.10		0.00	
Manatee	27.52409	-82.62958	2/22/19	13:30	1.83		14.48		0.05		0.00	
Manatee	27.50675	-82.54318	2/22/19	14:30	3.08		21.33		1.10		0.21	
Manatee	27.52177	-82.44903	2/22/19	15:30								
Manatee	27.52281	-82.41085	2/22/19	16:30	7.63		25.95		0.34		0.28	
Manatee	27.52279	-82.41082	2/22/19	17:30	7.41		21.07		0.06		0.13	
Manatee	27.52277	-82.41087	2/22/19	18:30	7.02		20.29		0.05		0.74	
Manatee	27.52277	-82.41087	2/22/19	19:30	7.78		22.19		0.00		0.13	

Table A13.1. Continued.

Manatee	27.52277	-82.41087	2/22/19	20:30	7.77		19.78		0.00		0.19	
Manatee	27.52277	-82.41087	2/22/19	22:00	8.79		24.42		0.19		0.31	
Manatee	27.52277	-82.41087	2/22/19	23:40	8.99		24.00		0.52		0.46	
Manatee	27.52277	-82.41087	2/23/19	0:30	8.86		25.64		0.53		0.59	
Manatee	27.52277	-82.41087	2/23/19	2:35	8.22		28.61		0.16		0.37	
Manatee	27.52277	-82.41087	2/23/19	4:30	7.40		23.81		0.31		0.42	
Manatee	27.52277	-82.41087	2/23/19	6:30	7.81		28.71		0.38		0.49	
Manatee	27.52277	-82.41087	2/23/19	7:43	8.60		23.72		0.13		0.33	
Manatee	27.52277	-82.41087	2/23/19	8:30	7.99		21.14		0.15		0.24	
Manatee	27.52277	-82.41087	2/23/19	9:30	8.59		24.00		0.14		0.19	
Manatee	27.52277	-82.41087	2/23/19	10:30	8.91		24.42		0.20		0.39	
Manatee	27.52277	-82.41087	2/23/19	11:30	9.15		19.53		0.21		0.41	
Manatee	27.52277	-82.41087	2/23/19	12:30	9.09		17.78		0.21		0.41	
Manatee	27.52277	-82.41087	2/23/19	13:32	9.12		18.31		0.33		0.50	
Manatee	27.52277	-82.41087	2/23/19	14:30	8.66		23.66		0.26		0.46	
Manatee	27.52277	-82.41087	2/23/19	15:30	6.57		20.88		0.24		0.32	
Manatee	27.52277	-82.41087	2/23/19	16:30	7.51		34.43		0.00		0.00	
Manatee	27.51951	-82.44710	2/23/19	17:30	5.87		21.84		1.79		0.41	

Appendix A14: Measured wet season nutrient concentrations

Table A14.1: Wet season inorganic nutrients (µmol kg $^{-1}$). P_T is inorganic phosphate, Si_T is inorganic silica, N_T is (NO_3^{2-}+NO_2^-), and NH_4^- is inorganic ammonia.

River	Latitude	Longitude	Date	Time	P_T 1	P_T 2	Si_T 1	Si_T 2	N_T 1	N_T 2	NH_4^- 1	NH_4^- 2
Hillsborough	27.90807	-82.45410	8/24/19	9:00	8.8		56.3		6.9		0.3	
Hillsborough	27.93988	-82.45991	8/24/19	9:49	5.7		45.2		8.0		3.9	
Hillsborough	27.95732	-82.46418	8/24/19	10:19	6.3		59.2		4.6		3.7	
Hillsborough	28.01933	-82.46378	8/24/19	11:48	6.5		49.5		5.6		3.4	
Hillsborough	28.01933	-82.46378	8/24/19	12:31								
Hillsborough	28.01933	-82.46378	8/24/19	13:29	7.1		67.9		7.5		3.5	
Hillsborough	28.01933	-82.46378	8/24/19	14:28								
Hillsborough	28.01933	-82.46378	8/24/19	15:30	6.9		62.7		7.5		4.0	
Hillsborough	28.01933	-82.46378	8/24/19	16:30								
Hillsborough	28.01933	-82.46378	8/24/19	17:30	7.3		69.0		8.5		3.6	
Hillsborough	28.01933	-82.46378	8/24/19	18:30								
Hillsborough	28.01933	-82.46378	8/24/19	19:30	7.2		49.5		5.2		3.3	
Hillsborough	28.01933	-82.46378	8/24/19	20:30								
Hillsborough	28.01933	-82.46378	8/24/19	21:30	7.1		71.6		8.7		3.8	
Hillsborough	28.01933	-82.46378	8/24/19	22:30								
Hillsborough	28.01933	-82.46378	8/24/19	23:30	7.0		78.9		8.2		3.5	
Hillsborough	27.94583	-82.46378	8/25/19	2:30								
Hillsborough	27.93473	-82.46378	8/25/19	4:30	7.7		69.2		7.6		3.1	
Hillsborough	27.90693	-82.46378	8/25/19	6:30								
Hillsborough	27.84805	-82.46378	8/25/19	7:30	7.7		55.2		6.2		3.3	
Hillsborough	28.01933	-82.46378	8/25/19	8:30								
Hillsborough	28.01933	-82.46378	8/25/19	9:30	6.9		78.0		6.9		3.3	
Hillsborough	28.01933	-82.46378	8/25/19	10:30								

Table A14.1. Continued.

Hillsborough	28.01933	-82.46378	8/25/19	11:30	7.4		69.7		7.7		3.2	
Hillsborough	28.01933	-82.46378	8/25/19	12:30	7.7		65.1		8.7		3.2	
Hillsborough	27.94583	-82.46038	8/25/19	13:08	6.1		55.4		5.7		3.0	
Hillsborough	27.93473	-82.40360	8/25/19	13:25	2.6		26.1		3.8		3.0	
Hillsborough	27.90693	-82.46324	8/25/19	14:45	4.6		40.8		4.4		0.4	
Alafia	27.84805	-82.43078	8/31/19	9:17	6.6		53.1		1.9		0.4	
Alafia	27.85183	-82.40969	8/31/19	9:45	16.3		76.7		2.0		1.5	
Alafia	27.85340	-82.40148	8/31/19	10:05	20.5		58.4		12.1		2.9	
Alafia	27.85810	-82.37656	8/31/19	10:27	27.5		86.1		6.9		3.0	
Alafia	27.87472	-82.31121	8/31/19	10:30	28.3		101.0		11.9		3.0	
Alafia	27.88554	-82.30203	8/31/19	11:30	31.1		103.3		18.8		2.7	
Alafia	27.88554	-82.30203	8/31/19	12:30								
Alafia	27.88554	-82.30203	8/31/19	13:30	27.6		88.8		14.5		2.0	
Alafia	27.88554	-82.30203	8/31/19	14:30	27.1		102.3		17.6		2.0	
Alafia	27.88554	-82.30203	8/31/19	15:30								
Alafia	27.88554	-82.30203	8/31/19	16:30	31.5		104.5		19.9		2.3	
Alafia	27.88554	-82.30203	8/31/19	17:30								
Alafia	27.88554	-82.30203	8/31/19	18:30	32.5		90.4		20.6		3.4	
Alafia	27.88554	-82.30203	8/31/19	19:30								
Alafia	27.88554	-82.30203	8/31/19	20:30	26.9		107.0		20.6		2.1	
Alafia	27.88554	-82.30203	8/31/19	21:30								
Alafia	27.88554	-82.30203	8/31/19	22:30								
Alafia	27.88554	-82.30203	8/31/19	23:30	26.8		84.5		14.1		1.8	
Alafia	27.88554	-82.30203	9/1/19	2:30	33.2		99.6		22.0		1.9	
Alafia	27.88554	-82.30203	9/1/19	4:30								
Alafia	27.88554	-82.30203	9/1/19	5:30	29.8		113.9		20.9		1.5	
Alafia	27.88554	-82.30203	9/1/19	6:40								

Table A14.1. Continued.

Alafia	27.88554	-82.30203	9/1/19	7:30	32.5		115.1		21.5		1.5	
Alafia	27.88554	-82.30203	9/1/19	8:30								
Alafia	27.88554	-82.30203	9/1/19	9:30								
Alafia	27.88554	-82.30203	9/1/19	10:30	33.8		109.9		23.3		2.0	
Alafia	27.88554	-82.30203	9/1/19	11:30								
Alafia	27.85738	-82.35783	9/1/19	12:30	27.3		94.1		9.7		2.4	
Alafia	27.85880	-82.38432	9/1/19	13:00	16.1		69.2		15.3		1.8	
Alafia	27.84939	-82.42340	9/1/19	13:25	8.2		66.5		3.9		0.0	
Li'l Manatee	27.74143	-82.48248	8/17/19	11:30	6.8	5.8	53.9	46.8	2.1	2.0	9.8	8.8
Li'l Manatee	27.74143	-82.48248	8/17/19	12:10	9.0		33.8		3.4		7.8	
Li'l Manatee	27.73108	-82.49009	8/17/19	12:45	9.2		21.3		1.9		3.6	
Li'l Manatee	27.69024	-82.44967	8/17/19	14:30	(9.4)		(7.2)		(4.9)		1.7	
Li'l Manatee	27.66344	-82.40760	8/17/19	15:30	12.5		17.1		9.2		1.7	
Li'l Manatee	27.66344	-82.40760	8/17/19	16:30	12.7		17.4		9.6		1.8	
Li'l Manatee	27.66344	-82.40760	8/17/19	17:30	13.0		20.0		9.6		2.0	
Li'l Manatee	27.66344	-82.40760	8/17/19	18:30	13.0		17.9		9.7		1.9	
Li'l Manatee	27.66344	-82.40760	8/17/19	19:30	13.2		16.1		9.8		2.1	
Li'l Manatee	27.66344	-82.40760	8/17/19	20:30	13.0		28.5		9.7		1.8	
Li'l Manatee	27.66344	-82.40760	8/17/19	22:30	12.5		26.4		11.9		(6.0)	
Li'l Manatee	27.66344	-82.40760	8/18/19	0:30	12.6		15.9		8.8		2.4	
Li'l Manatee	27.66344	-82.40760	8/18/19	1:30	12.8		11.7		10.0		2.6	
Li'l Manatee	27.66344	-82.40760	8/18/19	2:30	13.1		21.4		10.0		2.3	
Li'l Manatee	27.66344	-82.40760	8/18/19	3:30	13.2		22.4		10.4		2.2	
Li'l Manatee	27.66344	-82.40760	8/18/19	5:30	13.1		18.8		10.3		1.9	
Li'l Manatee	27.66344	-82.40760	8/18/19	6:30	12.9		24.3		10.7		1.8	
Li'l Manatee	27.66344	-82.40760	8/18/19	7:30	12.7		25.3		10.7		1.7	
Li'l Manatee	27.66344	-82.40760	8/18/19	8:30	13.0	12.6	28.4	17.5	11.0	11.0	1.9	1.8

Table A14.1. Continued.

Li'l Manatee	27.66344	-82.40760	8/18/19	9:30	12.3		24.1		11.1		1.8	
Li'l Manatee	27.66344	-82.40760	8/18/19	10:30	12.4		32.6		10.7		1.6	
Li'l Manatee	27.66344	-82.40760	8/18/19	11:30	12.7		20.4		10.8		1.7	
Li'l Manatee	27.66344	-82.40760	8/18/19	12:30	12.5		24.7		10.9		1.3	
Li'l Manatee	27.66344	-82.40760	8/18/19	13:30	11.6		32.1		11.1		1.4	
Li'l Manatee	27.66344	-82.40760	8/18/19	14:30	12.2		20.8		8.6		1.6	
Li'l Manatee	27.66344	-82.40760	8/18/19	15:30	11.9		18.6		8.2		1.4	
Li'l Manatee	27.66791	-82.42923	8/18/19	16:30	14.0		19.3		7.3		1.5	
Li'l Manatee	27.67063	-82.43944	8/18/19	17:30	13.6		30.1		5.0		3.5	
Li'l Manatee	27.68898	-82.44465	8/18/19	18:00	8.5		45.6		3.1		11.7	
Li'l Manatee	27.71455	-82.46677	8/18/19	18:30	5.7	8.1	43.5	53.4	2.0	2.8	7.0	8.2
Manatee	27.50881	-82.58923	8/10/19	11:15	13.5		11.6		12.5		3.2	
Manatee	27.53384	-82.66974	8/10/19	12:20	8.5		44.6		0.3		0.0	
Manatee	27.53116	-82.64210	8/10/19	13:40	11.9		59.6		6.7		10.5	
Manatee	27.50456	-82.57698	8/10/19	14:30	14.2		16.6		13.5		3.5	
Manatee	27.52764	-82.46000	8/10/19	16:00	12.1		11.0		13.3		4.3	
Manatee	27.52283	-82.41096	8/10/19	17:30	12.0		14.6		12.0		4.0	
Manatee	27.52279	-82.41097	8/10/19	18:30	12.3		16.3		12.3		4.2	
Manatee	27.52279	-82.41097	8/10/19	19:30	12.1		10.3		11.3		4.4	
Manatee	27.52279	-82.41097	8/10/19	20:30	11.6		7.8		10.3		4.0	
Manatee	27.52279	-82.41097	8/10/19	21:30	12.3		9.1		12.5		3.9	
Manatee	27.52279	-82.41097	8/10/19	22:30	(4.9)		(23.6)		(0.0)		(0.2)	
Manatee	27.52279	-82.41097	8/11/19	0:30	11.9	12.2	9.2	9.3	10.3	13.2	3.4	3.4
Manatee	27.52279	-82.41097	8/11/19	1:30	12.4		10.4		13.2		3.7	
Manatee	27.52279	-82.41097	8/11/19	2:30	11.9		12.2		13.1		3.5	
Manatee	27.52279	-82.41097	8/11/19	5:30	11.9		20.6		13.7		3.2	
Manatee	27.52279	-82.41097	8/11/19	6:30	11.9		14.0		13.3		3.3	

Table A14.1. Continued.

Manatee	27.52279	-82.41097	8/11/19	7:30	11.8		16.0		13.2		3.2	
Manatee	27.52279	-82.41097	8/11/19	8:30	11.9		17.8		13.2		3.3	
Manatee	27.52279	-82.41097	8/11/19	9:30	11.8		14.8		13.4		3.2	
Manatee	27.52279	-82.41097	8/11/19	10:30	11.8		23.8		13.6		3.1	
Manatee	27.52279	-82.41097	8/11/19	11:30	11.8		9.6		13.6		3.3	
Manatee	27.52279	-82.41097	8/11/19	12:30	11.8		27.7		13.6		2.8	
Manatee	27.52279	-82.41097	8/11/19	13:30	11.9		16.8		13.8		3.5	
Manatee	27.52279	-82.41097	8/11/19	14:30	12.2	11.5	14.7	13.6	13.9	12.0	3.6	3.1
Manatee	27.52279	-82.41097	8/11/19	15:30	11.9		14.3		13.6		2.9	
Manatee	27.52279	-82.41097	8/11/19	16:00	11.9		27.6		13.9		2.8	
Manatee	27.51841	-82.42807	8/11/19	17:30	11.6		31.7		9.6		2.9	
Manatee	27.52646	-82.50118	8/11/19	18:15	11.1		60.9		6.4		6.1	
Manatee	27.50249	-82.56700	8/11/19	19:00	7.7		43.4		2.7		6.6	

Appendix A15: Seasonal river discharge for 24-hour measurement times on each river

Table A15.1. Seasonal river discharge data corresponding to 24-hour measurements on each river (U.S. Geological Survey (USGS) National Water Information System (NWIS) stream gauge stations, 2019).

Dry Season					Wet Season			
River	**Date**	**TIME**	**Discharge (ft^3/s)**		**River**	**Date**	**TIME**	**Discharge (ft^3/s)**
Hillsborough	3/9/2019	15:30	320		Hillsborough	8/24/2019	11:48	889
Hillsborough	3/9/2019	16:30	320		Hillsborough	8/24/2019	12:31	888
Hillsborough	3/9/2019	17:30	320		Hillsborough	8/24/2019	13:29	888
Hillsborough	3/9/2019	18:30	320		Hillsborough	8/24/2019	14:28	888
Hillsborough	3/9/2019	19:30	319		Hillsborough	8/24/2019	15:30	888
Hillsborough	3/9/2019	20:30	319		Hillsborough	8/24/2019	16:30	888
Hillsborough	3/9/2019	21:30	318		Hillsborough	8/24/2019	17:30	888
Hillsborough	3/9/2019	22:35	318		Hillsborough	8/24/2019	18:30	888
Hillsborough	3/9/2019	23:30	317		Hillsborough	8/24/2019	19:30	888
Hillsborough	3/10/2019	0:30	316		Hillsborough	8/24/2019	20:30	888
Hillsborough	3/10/2019	1:30	315		Hillsborough	8/24/2019	21:30	887
Hillsborough	3/10/2019	3:30	313		Hillsborough	8/24/2019	22:30	887
Hillsborough	3/10/2019	5:30	311		Hillsborough	8/24/2019	23:30	887
Hillsborough	3/10/2019	8:30	308		Hillsborough	8/25/2019	2:30	885
Hillsborough	3/10/2019	9:30	305		Hillsborough	8/25/2019	4:30	884
Hillsborough	3/10/2019	10:30	302		Hillsborough	8/25/2019	6:30	881
Hillsborough	3/10/2019	11:30	301		Hillsborough	8/25/2019	7:30	880
Hillsborough	3/10/2019	12:30	299		Hillsborough	8/25/2019	8:30	878
Hillsborough	3/10/2019	13:30	298		Hillsborough	8/25/2019	9:30	876
Hillsborough	3/10/2019	14:30	296		Hillsborough	8/25/2019	10:30	874
Hillsborough	3/10/2019	15:30	294		Hillsborough	8/25/2019	11:30	872
Hillsborough	3/10/2019	16:30	292		Hillsborough	8/25/2019	12:30	870
Alafia	3/16/2019	14:30	240		Alafia	8/31/2019	10:30	979
Alafia	3/16/2019	15:30	238		Alafia	8/31/2019	11:30	969
Alafia	3/16/2019	16:30	237		Alafia	8/31/2019	12:30	963
Alafia	3/16/2019	17:30	235		Alafia	8/31/2019	13:30	957
Alafia	3/16/2019	18:30	235		Alafia	8/31/2019	14:30	949
Alafia	3/16/2019	19:30	233		Alafia	8/31/2019	15:30	942
Alafia	3/16/2019	20:30	234		Alafia	8/31/2019	16:30	936
Alafia	3/16/2019	21:30	233		Alafia	8/31/2019	17:30	930
Alafia	3/16/2019	22:30	232		Alafia	8/31/2019	18:30	925
Alafia	3/16/2019	23:30	232		Alafia	8/31/2019	19:30	919

Table A15.1. Continued

Alafia	3/17/2019	0:30	231		Alafia	8/31/2019	20:30	915
Alafia	3/17/2019	1:30	227		Alafia	8/31/2019	21:30	910
Alafia	3/17/2019	2:30	228		Alafia	8/31/2019	22:30	906
Alafia	3/17/2019	3:30	228		Alafia	8/31/2019	23:30	901
Alafia	3/17/2019	7:30	227		Alafia	9/1/2019	2:30	888
Alafia	3/17/2019	8:30	227		Alafia	9/1/2019	4:30	881
Alafia	3/17/2019	9:30	226		Alafia	9/1/2019	5:30	878
Alafia	3/17/2019	10:30	225		Alafia	9/1/2019	6:40	875
Alafia	3/17/2019	11:30	224		Alafia	9/1/2019	7:30	872
Alafia	3/17/2019	12:30	224		Alafia	9/1/2019	8:30	869
Alafia	3/17/2019	13:30	221		Alafia	9/1/2019	9:30	868
Alafia	3/17/2019	14:30	224		Alafia	9/1/2019	10:30	866
					Alafia	9/1/2019	11:30	863
Little Manatee	3/2/2019	14:44	203		Little Manatee	8/17/2019	14:30	1120
Little Manatee	3/2/2019	15:45	203		Little Manatee	8/17/2019	15:30	1110
Little Manatee	3/2/2019	16:30	201		Little Manatee	8/17/2019	16:30	1110
Little Manatee	3/2/2019	17:30	202		Little Manatee	8/17/2019	17:30	1100
Little Manatee	3/2/2019	18:30	201		Little Manatee	8/17/2019	18:30	1100
Little Manatee	3/2/2019	19:30	201		Little Manatee	8/17/2019	19:30	1090
Little Manatee	3/2/2019	20:26	200		Little Manatee	8/17/2019	20:30	1080
Little Manatee	3/2/2019	21:30	199		Little Manatee	8/17/2019	22:30	1070
Little Manatee	3/2/2019	22:30	198		Little Manatee	8/18/2019	0:30	1050
Little Manatee	3/2/2019	23:30	197		Little Manatee	8/18/2019	1:30	1040
Little Manatee	3/3/2019	0:30	196		Little Manatee	8/18/2019	2:30	1040
Little Manatee	3/3/2019	1:30	195		Little Manatee	8/18/2019	3:30	1030
Little Manatee	3/3/2019	3:30	196		Little Manatee	8/18/2019	5:30	1010
Little Manatee	3/3/2019	6:30	194		Little Manatee	8/18/2019	6:30	999
Little Manatee	3/3/2019	7:30	193		Little Manatee	8/18/2019	7:30	992
Little Manatee	3/3/2019	8:30	192		Little Manatee	8/18/2019	8:30	981
Little Manatee	3/3/2019	9:30	191		Little Manatee	8/18/2019	9:30	973
Little Manatee	3/3/2019	10:30	190		Little Manatee	8/18/2019	10:30	965
Little Manatee	3/3/2019	11:30	189		Little Manatee	8/18/2019	11:30	955
Little Manatee	3/3/2019	12:30	189		Little Manatee	8/18/2019	12:30	947
Little Manatee	3/3/2019	13:30	188		Little Manatee	8/18/2019	13:30	938
Little Manatee	3/3/2019	14:30	188		Little Manatee	8/18/2019	14:30	929
Little Manatee	3/3/2019	15:50	187		Little Manatee	8/18/2019	15:30	920
Manatee	2/22/2019	16:30	20.5		Manatee	8/10/2019	16:00	506
Manatee	2/22/2019	17:30	20.5		Manatee	8/10/2019	17:30	495

Table A15.1. Continued

Manatee	2/22/2019	18:30	20.7		Manatee	8/10/2019	18:30	486
Manatee	2/22/2019	19:30	21		Manatee	8/10/2019	19:30	477
Manatee	2/22/2019	20:30	21		Manatee	8/10/2019	20:30	468
Manatee	2/22/2019	22:00	21		Manatee	8/10/2019	21:30	459
Manatee	2/22/2019	23:40	21		Manatee	8/10/2019	22:30	451
Manatee	2/23/2019	0:30	21		Manatee	8/11/2019	0:30	436
Manatee	2/23/2019	2:35	21.5		Manatee	8/11/2019	1:30	429
Manatee	2/23/2019	4:30	22		Manatee	8/11/2019	2:30	422
Manatee	2/23/2019	6:30	22.5		Manatee	8/11/2019	5:30	404
Manatee	2/23/2019	7:43	22.5		Manatee	8/11/2019	6:30	398
Manatee	2/23/2019	8:30	22.7		Manatee	8/11/2019	7:30	393
Manatee	2/23/2019	9:30	23.2		Manatee	8/11/2019	8:30	387
Manatee	2/23/2019	10:30	23.2		Manatee	8/11/2019	9:30	380
Manatee	2/23/2019	11:30	23.2		Manatee	8/11/2019	10:30	375
Manatee	2/23/2019	12:30	23.2		Manatee	8/11/2019	11:30	370
Manatee	2/23/2019	13:32	23.2		Manatee	8/11/2019	12:30	365
Manatee	2/23/2019	14:30	23.2		Manatee	8/11/2019	13:30	360
Manatee	2/23/2019	15:30	23.2		Manatee	8/11/2019	14:30	355
Manatee	2/23/2019	16:30	23.2		Manatee	8/11/2019	15:30	352
					Manatee	8/11/2019	16:00	350

Appendix B:

Supplemental Information for Chapter Three

Appendix B1. Initial (Field) pH_T measurement results

Table B1.1. Measured initial (field) pH_T results from each Niskin prior to bottle collection. pH_T data are temperature corrected to 20°C. TEMP stands for temperature, SAL stands for salinity, AVG stands for average, and SD stands for standard deviation.

Analysis Date	Analysis Time	TEMP °C	SAL	pH_T Niskin 1					pH_T Niskin 2				
				pH_T 1	pH_T 2	pH_T 3	AVG	SD	pH_T 1	pH_T 2	pH_T 3	AVG	SD
1/26/2021	13:00	21.4684	3.4385	7.300	7.284	7.296	7.294	0.008	7.299	7.326	7.314	7.313	0.014
1/26/2021	14:45	21.4684	3.4385	7.295	7.305	7.299	7.299	0.005	7.328	7.321	7.352	7.334	0.017

Appendix B2: Measured Hg^{II} poisoned and unpoisoned sample results

Table B2.1. Measured Hg^{II}-poisoned sample results where pH_T data are corrected to 20°C, SAL stands for salinity, AVG stands for average, and SD stands for standard deviation.

Date of Analysis	Days after Collection	SAL	pH_T					C_T (µmol kg^{-1})					A_T (µmol kg^{-1})					
			pH_T 1	pH_T 2	pH_T 3	AVG	SD	C_T 1	C_T 2	C_T 3	AVG	SD	A_T 1	A_T 2	A_T 3	AVG	SD	Calculated AVG
1/26/2021	0.25	3.4385						3099.6	3092.9		3096.3	4.8	2900.7			2900.7		
1/26/2021	0.5	3.4385	7.290	7.318		7.304	0.020	(3085.2)	(3083.7)		(3084.5)	1.1	2899.2			2899.2		2893.3
1/27/2021	1	3.4385	7.304	7.302		7.303	0.001	3092.6	3095.2		3093.9	1.8	2901.3	2899.3		2900.3	1.4	2901.6
1/29/2021	3	3.4385	7.294	7.334		7.314	0.029	3088.4	3092.9		3090.7	3.2	2894.9	2898.3		2896.6	2.4	2903.8
1/31/2021	5	3.4385	7.293	7.299		7.296	0.004	3091.0	3090.5		3090.8	0.4	2892.5	2892.6		2892.6	0.1	2895.4
2/2/2021	7	3.4385	7.298	7.311		7.304	0.009	3094.6	3094.1		3094.3	0.4	2891.8	2899.4		2895.6	5.4	2902.5
2/9/2021	14	3.4385	7.277	7.280		7.278	0.002	3101.9	3100.2		3101.1	1.2		2897.5		2897.5		2896.2
2/16/2021	21	3.4385	7.334	7.290		7.312	0.032	3096.3	3096.7		3096.5	0.3	2890.7	2889.8		2890.2	0.6	2897.8
2/23/2021	28	3.4385	7.277	7.277		7.277	0.000	3098.2	3098.9		3098.6	0.5	2885.3	2886.9		2886.1	1.1	2893.4
3/2/2021	35	3.4385	7.298	7.264		7.281	0.024	3094.6	3096.7		3095.7	1.5	2886.3	2882.3		2884.3	2.8	2892.6
3/9/2021	42	3.4385	7.299	7.244	7.294	7.279	0.030	3099.4	3096.6	3096.8	3097.6	1.6	2884.2	2884.1	2882.4	2883.6	1.0	2893.4
3/16/2021	49	3.4385	7.247	7.318		7.282	0.050	3092.6	3091.9		3092.3	0.5	2887.4	2892.6		2890.0	3.7	2890.0
3/23/2021	56	3.4385	7.261	7.258		7.259	0.002	3096.6	3096.2		3096.4	0.3	2881.4	2882.7		2882.0	1.0	2882.2
3/30/2021	63	3.4385	7.248	7.271		7.260	0.016	3099.3	3100.0		3099.7	0.5	2882.4	2880.6		2881.5	1.3	2885.8
4/7/2021	71	3.4385	7.256	7.264		7.260	0.005	3098.0	3092.7		3095.3	3.8	2873.9	2870.2		2872.0	2.6	2881.7
4/13/2021	77	3.4385	7.291	7.274		7.282	0.012	3097.7	3093.0		3095.4	3.3	2882.1	2874.6		2878.4	5.3	2892.9
4/20/2021	84	3.4385	7.278	7.288		7.283	0.007	3094.9	3091.1		3093.0	2.7	2874.5	2873.2		2873.8	0.9	2891.1
4/27/2021	91	3.4385	7.281	7.298		7.290	0.012	3093.0	3098.0		3143.1	3.6	2872.6	2872.3		2872.4	0.2	2896.9

Table B2.2. Measured unpoisoned sample results where pH_T data are corrected to 20°C, SAL stands for salinity, AVG stands for average, and SD stands for standard deviation.

Date of Analysis	Days After Collection	SAL	pH_T					C_T (µmol kg^{-1})					A_T (µmol kg^{-1})					
			pH_T 1	pH_T 2	pH_T 3	AVG	SD	C_T 1	C_T 2	C_T 3	AVG	SD	A_T 1	A_T 2	A_T 3	AVG	SD	Calculated AVG
1/26/2021	0.25	3.4385						3101.2	3101.2		3101.2	0.0	2920.4			2920.4		2915.1
1/26/2021	0.5	3.4385	7.334	7.397		7.365	0.045	(3082.4)	(3082.4)		(3082.4)	0.0	2925.7			2925.7		2932.1
1/27/2021	1	3.4385	7.403	7.399		7.401	0.003	3097.9	3096.1		3097.0	1.3	2925.0	2922.4		2923.7	1.9	2947.6
1/29/2021	3	3.4385	7.379			7.379		3101.2	3096.8		3099.0	3.1	2924.1	2922.5		2923.3	1.1	2940.4
1/31/2021	5	3.4385	7.356	7.386		7.371	0.021	3099.4	3107.6		3103.5	5.8	2920.1	2923.8		2921.9	2.6	2941.3
2/2/2021	7	3.4385	7.354	7.349		7.351	0.004	3103.2	3101.2		3102.2	1.4	2922.1	2920.4		2921.3	1.2	2931.4
2/9/2021	14	3.4385	7.383	7.379		7.381	0.003	3103.3	3109.0		3106.1	4.0	2924.8	2920.5		2922.6	3.0	2948.0
2/16/2021	21	3.4385	7.399	7.386		7.392	0.010	3102.5	3104.1		3103.3	1.1	2928.4	2925.7		2927.1	1.9	2949.9
2/23/2021	28	3.4385	7.357			7.357		3107.8	3113.0		3110.4	3.7	2925.8	2927.8		2926.8	1.4	2941.8
3/2/2021	35	3.4385	7.380	7.332	7.310	7.340	0.036	3111.3	3133.5	3123.3	3122.7	11.1	2921.1	2925.2	2924.6	2923.6	2.2	2945.9
3/9/2021	42	3.4385		7.324		7.324		3130.4	3127.6		3129.0	2.0		2926.6		2926.6		2944.5
3/16/2021	49	3.4385	7.324	7.312		7.312	0.008	3119.1	3121.6		3120.3	1.7	2922.3	2924.4		2923.3	1.5	2933.5
3/23/2021	56	3.4385	7.287	7.304		7.304	0.012	3125.2	3124.7		3125.0	0.3	2917.4	2917.1		2917.3	0.2	2926.9
3/30/2021	63	3.4385	7.284	7.306		7.306	0.015	3125.0	3123.1		3124.1	1.3	2917.7	2915.5		2916.6	1.6	2926.1
4/7/2021	71	3.4385	7.320	7.314		7.314	0.004	3122.1	3128.1		3125.1	4.2	2918.8	2916.6		2917.7	1.5	2937.5
4/13/2021	77	3.4385	7.288	7.297		7.297	0.006	3127.7	3128.0		3127.9	0.2	2915.1	2915.2		2915.2	0.1	2928.2
4/20/2021	84	3.4385	7.303	7.322		7.322	0.013	3128.1	3134.7		3131.4	4.6	2913.3	2915.5		2914.4	1.6	2945.8
4/27/2021	91	3.4385	7.312	7.344		7.344	0.023	3143.1	3137.7		3140.4	3.8	2923.8	2916.2		2964.3	5.3	2964.4